

Cryo-electron microscopy of vitrified specimens

JACQUES DUBOCHE¹, MARC ADRIAN², JIIN-JU CHANG³,
JEAN-CLAUDE HOMO⁴, JEAN LEPAULT⁵,
ALASDAIR W. McDOWALL⁶ AND PATRICK SCHULTZ⁴

European Molecular Biology Laboratory (EMBL), Postfach 10. 2209, D-6900 Heidelberg, FRG

1. FOREWORD	130
2. INTRODUCTION	132
3. WATER	135
3.1 Water and its bonds	136
3.2 The water molecule	137
3.3 Ice	137
3.4 Liquid water	139
3.5 Aqueous solution	140
3.6 Water in the electron microscope	141
4. FREEZING	145
4.1 Nucleation and growth	145
4.2 Hexagonal ice in solution	147
4.3 Cubic ice	150
4.4 Vitrification	151
4.5 Cryofixation	152
5. SECTIONS	155
5.1 Vitrified sections	155
5.2 Cryo-ultramicrotomy	158
5.3 Cutting artifacts	160
5.4 The sectioning process	163
6. SUSPENSION	165
6.1 Surface tension	165
6.2 Diffusion	167
6.3 Preparation on a supporting film	167
6.4 The bare-grid method	168
6.5 Evaporation	169
6.6 Surface effects	171

Present addresses: ¹ Centre de Microscopie Electronique (CME), 27 Rue du Bugnon, CH-105 Lausanne; ² Laboratoire Européen de Biologie Moléculaire, I.L.L. 156X; F-38042 Grenoble Cédex; ³ The Institute of Biophysics, Academica Sinica, Peking, China; ⁴ Institut de Biochimie, 11 Rue Humann, F-67000 Strasbourg; ⁵ Centre de Génétique Moléculaire, C.N.R.S., F-91190 Gif/Yvette; ⁶ Howard Hughes Medical Institute, Health Science Centre, 5323 Harry Hines Blvd. MY5-310, Dallas, Texas 75235-9050, USA.

7. CRYOSPECIMEN HOLDER	176
7.1 Heat transfer	176
7.2 Electron-beam heating	178
7.3 Quantitative estimation	179
7.4 Contamination	179
7.5 Anticontaminator	182
7.6 Stability	182
7.7 Other side-entry cryospecimen holders	184
7.8 Top entry	185
8. IMAGE FORMATION	186
8.1 Amplitude contrast	186
8.2 Phase contrast	188
8.3 Real image	190
9. BEAM DAMAGE	191
9.1 Electron scattering	192
9.2 The forms of beam damage	192
9.3 Mechanisms of beam damage	195
9.4 Structural damage	196
10. HOW TO OPERATE	197
10.1 Safety	197
10.2 Bulk specimens	198
10.2.1 Freezing	198
10.2.2 Sectioning	200
10.3 Thin layer of vitrified suspension	202
10.4 Transfer and observation	207
11. SOME RESULTS	218
12. REFERENCES	218

I. FOREWORD

Cryo-electron microscopy of vitrified specimens was just emerging as a practical method when Richard Henderson proposed that we should teach an EMBO course on the new technique. The request seemed to come too early because at that moment the method looked more like a laboratory game than a useful tool. However, during the months which ellapsed before the start of the course, several of the major difficulties associated with electron microscopy of vitrified specimens found surprisingly elegant solutions or simply became non-existent. The course could therefore take place under favourable circumstances in the summer of 1983. It was repeated the following years and cryo-electron microscopy spread rapidly. Since that time, water, which was once the arch enemy of all electron-microscopists, became what it always was in nature – an integral part of biological matter and a beautiful substance.

Obviously, the early eighties was the right time for the final development of

methods for the observation of frozen hydrated specimens. Freeze fracture, freeze drying or freeze substitution had become very successful and popular in the seventies. With these methods, however, freezing is used at the beginning of the preparation process, but at the end it is always a dry specimen which is observed in the electron microscope. The direct observation of frozen hydrated specimens had long been advocated by Fernandez Moran. It required, however, the decisive work of Bob Glaeser and Ken Taylor in Berkeley and of Nigel Unwin in Cambridge to make it ready for final development. The beginning of the eighties was also the time when instrument manufacturers succeeded in producing stable and handy cryo-specimen holders and cryo-ultramicrotomes.

Cryo-electron microscopy of thin vitrified films of suspension is now widely used for high-resolution observation of biological suspensions. Altogether, the results compare favourably with those obtained by classical methods. This, at least, can be said for those particles which give good results with classical methods, as, for example, small viruses and their components, or compact macromolecular complexes. The comparison favours vitrified specimens in many cases where the classical methods are in trouble or are difficult to practice, as is, for example, the case when observing lipid vesicles. Finally, there is a whole class of structures which cannot be visualized in dry specimens because they only exist under the action of forces which are acting in the liquid water. They represent a new field of observation for the vitrified state. Besides its advantages in terms of structure preservation, the thin vitrified film preparation method is easy, rapid and inexpensive. It seems therefore that there is really every reason for it to be used systematically in all electron-microscopy laboratories. This, indeed, is our opinion and also the working idea of our laboratory. In practice this means, for example that, when a colleague asks us to make a quick observation of some biological solution, we first look at it in the vitrified state. Sometimes it is found useful to complement the observation on a negatively stained specimen.

The present section is based on this point of view. It is built on the experience of the EMBO course of 1983 and of the following years. It is addressed to every electron microscopist who wants to use the method as we practice it at the European Molecular Biology Laboratory. It does not require previous knowledge with cryotechniques and it is intended to provide all the necessary information to implement the method and to practice it in the daily operation of an electron microscopy laboratory. Besides this, experience has shown that the preparation, observation and interpretation of vitrified specimens requires some knowledge about water, aqueous solutions and freezing, as well as about beam damage and image formation. The present article gives a concise presentation of these topics in a form which, we hope, will be useful to newcomers in cryo-electron microscopy.

This article is not intended to be a complete review of cryo-electron microscopy, and even less a course on water or aqueous material, but we hope that it will be a guide for those who want to learn how to work with vitrified specimens. It may also be useful for experienced cryo-electron microscopists who want to compare their views with those developed in our laboratory during the last nine

years. In order to bridge the gap with the rest of the literature, we have tried, at the beginning of each section, to cite authoritative references where detailed coverage of the various subjects can be found. We apologize to all of those whose important contribution seems to be neglected in our presentation.

It is a special pleasure to express our thanks to Sir John Kendrew, who made our work on cryo-electron microscopy at EMBL possible. We have a deep gratitude for the support he gave us at the beginning of the project, when we were learning to deal with water and when the results were meagre, to say the least. We also express our thanks to all those – and they are too numerous to be cited here individually – who helped, from close or far, during this research. This article would not have existed without the suggestion of Richard Henderson. It is not certain that we should be grateful to him for that, but we can definitely express to him our thankfulness for the friendly support he gave us all through our work. We also express our gratitude to Max Haider for useful comments and suggestions on the manuscript and to Christine Barber for her competence and legendary patience in typing and in dealing with the authors. Finally, we thank colleagues who provided us with documents or unpublished information used in this article. In particular, we thank R. Milligan and G. Vigers for splendid micrographs.

2. INTRODUCTION

Water is a beautiful substance. Its action is everywhere around us and in us. It has moulded the earth during geological times and it was the cradle of life. Even now, it is by far the most abundant constituent of living matter. Our body contains 65 % water and the most ‘intelligent’ part of it, our brain, is all water, except for a fifth of its mass. At the molecular level also, life works in, and with water. The liquid medium participates directly in many reactions and it provides the necessary mobility for the dynamics which is the essence of life.

However, water has long been neglected in molecular biology. There are good reasons for this. The two most powerful methods of ultrastructural analysis, X-ray diffraction and electron microscopy, have both neglected water: the first because the mobility of water molecules makes them invisible by diffraction of crystalline structure; the second because liquid water evaporates in the vacuum of the microscope. The consequence of this systematic bias could well be that our present understanding of biological ultrastructure is focused on rigid structures and under-emphasizes the dynamics of the biological matter.

In spite of their difficulties with water, electron microscopists have not been indifferent to it. On the contrary, it even seems probable that during their first fifty years of investigation they put more effort into finding out how to deal with water than into any other electron-microscopical problem. As we know, the results are remarkable. Biological specimens can now be observed in a surprisingly good state of preservation even though all their water has been removed. Plastic embedding or negative staining are, in this respect, admirable methods.

A number of researchers have also tried to overcome evaporation and thus preserve the hydrated state in the electron microscope. Hydration chambers, in which the specimen can be kept in an environment saturated with water vapour,

have been designed. With their help, and using electron diffraction on catalase crystals as a test, Parsons and collaborators could show, for the first time, that the atomic structure of biological objects can be preserved in an electron microscope (Parsons, 1974). Unfortunately, the method requires a physical separation between the specimen and the rest of the column. This is difficult to realize without a severe loss of resolution. In spite of all the efforts, the method has not yet become routine.

Cooling the specimen to a temperature where the evaporation rate of water becomes negligible is the other obvious avenue to preserve the hydrated state in the electron microscope. For nearly thirty years Fernandez-Moran was the active advocate of cryo-electron microscopy (Fernandez-Moran, 1960, 1985). In practice the results were mediocre. It required the work of Nigel Unwin and his colleagues at Cambridge, who introduced a whole new way of thinking towards electron microscopy, and which resulted in the now historical article on catalase and purple membrane (Unwin & Henderson, 1975), and that by Bob Glaeser and the Berkeley group who first quantified beam damage (Glaeser, 1971), to put cryo-electron microscopy on its tracks. The break-through came in 1974, only a few months after Parsons' group publication on catalase in water. Taylor & Glaeser (1974) showed that, in the frozen state, the structure of catalase crystals can be preserved to atomic resolution. In the following years they succeeded further in obtaining a number of remarkable micrographs showing good contrast and resolution in ice (Taylor & Glaeser, 1976). Nevertheless, cryo-electron microscopy was limited by a number of severe technical difficulties and it was constantly facing a basic problem, common to all aspects of cryobiology: water crystallizes upon cooling and ice is very different from liquid water; freezing kills cells and organisms and causes severe damage to most biological structures.

The problem of freezing damage is not new, nor is the idea of vitrification (Luyet & Gehenio, 1940), which has now been applied to overcome freezing damage in cryo-electron microscopy. The idea was proposed by the late Father B. Luyet, one of the founders of modern cryobiology, towards the end of the thirties. It consists of cooling a liquid so rapidly that its molecules become immobilized before they have time to crystallize. During his whole scientific career, Luyet and his excellent collaborators worked towards this goal. They did not succeed in reaching it, but they accumulated an enormous amount of valuable data which, till this day, forms the basis for modern cryobiology. With time, their approach lost favour because the alternative method, which consists of allowing ice crystals to grow, but under controlled conditions, became much more successful after the fortunate discovery of the cryoprotecting effect of glycerol (Polge *et al.* 1949; historical account in: Wilson, 1979). The result was the enormous development of cryobiology, with its known consequences for stock-farming, food technology and surgery. Perhaps it also had the effect of crediting the belief that vitrification of pure water or dilute solutions is fundamentally impossible. Theoretical arguments were also found in support of this belief (Rasmussen, 1982; Johari, 1977). The abandonment of the vitrification concept was also expressed in electron-microscopy literature, where the definition of vitrification was changed: vitreous became the state in which ice crystals are no

longer perceptible (Riehle, 1968). This is a distressing definition because it turns the worst observer into the best vitrifier.

Obviously, Brüggeller and Mayer in Innsbruck and ourselves in Heidelberg were not sufficiently informed about the difficulty of vitrifying water. The former found that micrometre-sized water microdroplets are readily vitrified if they are violently projected into cryogen (Brüggeller & Mayer, 1980), and we vitrified thin water layers, obtained by spreading on a support, by immersion in liquid ethane (Dubochet & McDowall, 1981). The vitreous water obtained could be characterized unambiguously by X-ray diffraction and differential thermal analysis for the first group and by direct imaging and electron diffraction for the second. The reason for this success, when all previous attempts had failed, is simple: cooling speed increases with decreasing sample size and vitrification becomes easy when the dimension of the sample reaches the size required for observation in transmission electron microscopy.

One piece of luck rarely comes alone, but seldom do they come as readily as they did just after the discovery of vitrification. Within a year, a number of decisive observations could be made. In particular it was noticed that a thin uniform layer of solution can be prepared on a carbon support pretreated by glow discharge in amyl amine (Dubochet *et al.* 1982c). Some time later it was even found that supporting film can be avoided altogether (Adrian *et al.* 1984). The low contrast inherent to unstained biological specimens in water was thought to represent a severe limitation for cryo-electron microscopy. It turns out that optimal use of phase contrast overcomes much of this difficulty (Adrian *et al.* 1984; Lepault & Pitt, 1984). Beam damage is also significantly reduced at low temperature, and water, which was thought to influence unfavourably the resistance of the specimen to the electron beam, was found to have no harmful effect, at least in the range of electron dose compatible with high-resolution observations (Glaeser & Taylor, 1978; Lepault *et al.* 1983a). Finally, it was found that among all the cryo-specimen holders and all the devices for manipulating and transferring the vitrified specimens which have been designed, the simplest and least expensive give the best results (Dubochet *et al.* 1982c).

Put together, these findings resulted in a simple and powerful method for high-resolution observation of aqueous solution, provided it does not contain too many large particles and is not too viscous. With some variations it is now used in many laboratories for the observation of a large number of specimens. Two recent reviews focusing on the applications of the method have already been published (Chiu, 1986; Stewart & Vigers, 1986). Other published works include studies on micro-emulsions (Dubochet *et al.* 1984), on clathrin cages and coated vesicles (Vigers *et al.* 1986a, b), on enveloped viruses (Vogel *et al.* 1986; Fuller, 1987; Fuller & Argos, 1987), on the packaging of DNA in bacteriophage heads (Lepault *et al.* 1987), on assembly of microtubules (Mandelkow *et al.* 1986), on actin (Trinick *et al.* 1986) and myosin filaments (Milligan & Flicker, 1987), and on the structure of chromosomes and chromatin (Dubochet *et al.* 1986; McDowall *et al.* 1986).

After the rapid development of 1980–3, the method itself was not significantly

improved during the next few years. This is perhaps because it provides so many possibilities for exploring biological structures that most microscopists choose to exploit the method instead of perfecting it. It is certainly not because it is now complete and cannot be further improved. In particular, the fact that in the thin-film method, the particles are always close to a surface has significant consequences that have hardly been investigated. Image formation in strongly defocused images and with inelastically scattered electrons is another field that requires much more work.

The study of thin films of suspension is not the end of cryo-electron microscopy. Sometimes the structure to be observed is damaged when it is prepared in a thin liquid layer. More frequently, the specimen is bulky and impossible to spread into a thin layer. The only solution in such cases is cryo-ultramicrotomy. It consists in vitrifying the specimen in order to cut it into thin sections and to observe it in the vitrified state. The method exists (McDowall *et al.* 1983; Dubochet & McDowall, 1984*a*). It has been applied with success to a number of specimens including bacteria (Dubochet *et al.* 1983*b*), muscle (McDowall *et al.* 1984) and culture cells (McDowall *et al.* 1986). Unfortunately it is still limited by severe cutting artifacts (Chang *et al.* 1983) and by the technical difficulty of obtaining good sections. Much more work is needed before it will also become a powerful method in routine use for ultrastructural investigations.

3. WATER

In order to interpret his micrographs and understand how water provides support and mobility to biological structures, the electron-microscopist needs to know about the water molecule, the way it interacts with its neighbours and the structures they can form all together. This is a difficult subject. It is outlined in the present chapter, where it is shown how the water molecule defines the tetrahedron which is the basic structure for any further associations. The rich possibilities of arranging this more-or-less deformed tetrahedron are illustrated by the numerous forms of ice and of water clathrates which become valuable didactical examples. They help one to understand what the much-more-complex structure of liquid water and aqueous solution could be. More detailed descriptions are found in the prolific literature in which the newcomer is faced with the difficulty of a choice. The series, edited by Felix Franks (1972–82), gives a voluminous description of the whole field in a form which is easily accessible to non-specialists. The shorter book by Eisenberg & Kauzmann (1969) is an old classic. Simple, but very valuable, are the chapters on water in the famous textbook of L. Pauling, *General Chemistry* (1970). Recent points of view can be found in conference proceedings (Neilson & Enderby, 1986). Four articles, published in *Science* by different authors (Narten & Levy, 1969; Frank, 1970; Stillinger, 1980; Stillinger & Weber, 1984) represent an excellent compendium. They give an impressive view of the evolution of the concepts during the last two decades.

3.1 Water and its bonds

Water is an exceptional substance with strange properties, differing significantly from most other substances. Some of these properties are: (a) A negative volume of melting, meaning that the ordered crystalline state is less dense than the more disordered liquid. (b) The highest density under normal pressure is reached at 4 °C, in the normal liquid range. (c) As compared to its molecular weight, water has a high freezing, melting and critical temperature. (d) It has a high surface tension and a high dielectric constant. (e) Its viscosity increases with pressure. (f) It forms at least ten solid polymorphs, including those existing under high pressure. All these properties are more or less directly related to the strong dipole moment and the hydrogen bonding properties of the molecule.

The hydrogen bond is that specific attraction that exists between electro-negative elements such as nitrogen, oxygen or fluorine and hydrogen when the latter is covalently bonded to another electro-negative atom. It is strongly directional in the prolongation of covalent bond joining the hydrogen atom and its electro-negative neighbour. Its energy is of some 10–20 kJ/mol, which makes it 'strong among the weak bonds' of chemistry. Table 1 summarizes this situation. In practice, this means that one hydrogen bond is strong enough to hold two particles together, but in the human time-scale it is frequently broken by thermal agitation.

For most molecular biologists, van der Waals forces are strong repulsive forces acting at very short distances. For physical chemists, however, they are weak attractive forces acting over long distances. The former view is correct if all the interactions of the order of kT are neglected. This approximation may work well for describing solid structures, but it renders an understanding of the liquid state or of the equilibrium of colloid solutions very difficult. By definition, van der Waals forces are dipolar interactions (Parsegian, 1975). They include the dispersion forces due to quantum fluctuation of atomic charges and therefore can also act on molecules which are non-polar *per se*. At short range a small dipole is generally represented by a Lennard-Jones potential of the form $V = ar^{-12}-br^{-6}$, in which r is the distance and a and b are adjustable parameters. When the effect of many dipoles is added, they may result in attractive forces acting over long distances between surfaces or particles. For example, on two parallel surfaces separated by a distance in the range of 10 nm, the potential has the form $r^{-\gamma}$ with γ not equal to 6 as for a small dipole but between 2 and 3. Its effect may therefore extend over a relatively long distance.

Table 1. *Typical energy involved in some bonds and in thermal agitation at room temperature*

Covalent	≈ 400 kJ/mol	van der Waals	≈ 1.5 kJ/mol
Ionic	≈ 100 kJ/mol	RT	≈ 2.5 kJ/mol
Hydrogen	≈ 20 kJ/mol		

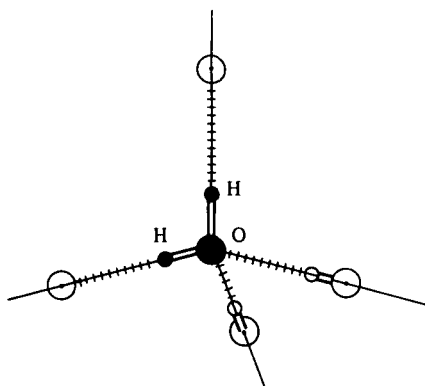


Fig. 1. Tetrahedral structure of the fully hydrogen-bonded water molecule.

3.2 The water molecule

The water molecule is a V-shaped arrangement of one oxygen between two hydrogen atoms. The O-H distance is approximately 0.1 nm. The bond angle of the free water molecule is 104.5° , which is only 5° less than the perfect tetrahedral angle. As illustrated in Fig. 1, the shape of the molecule is ideal to participate in four hydrogen bonds. When this is done with minimal constraints, the fully hydrogen-bonded water molecule is the centre of a tetrahedron. Starting from one oxygen atom, there are four symmetric ways to leave the molecule: one can follow one of the two covalent bonds to the hydrogen atoms and from there leave the molecule along the *ca.* 0.18 nm long hydrogen bond, or one could start by leaving the oxygen atom along one of the two hydrogen bonds, and reach the hydrogen of the neighbouring molecule. This tetrahedral structure is the basic feature of water structure. More or less distorted, it gives rise to all the various forms of solid, liquid, amorphous water or aqueous solution.

The water molecule is also a dipole. This originates from the V-shape of the molecule and from the displacement of the average position of the electrons with respect to their nuclei. The oxygen atom is slightly negative whereas both hydrogens have a net positive charge. The resulting dipolar moment has the relatively large value of 1.8 Debye (1 Debye corresponds to one electron displaced by 0.02 nm from the centre of charge). It causes a tendency in the water molecule to align in an electric field, as, for example, that surrounding an ion, and makes it especially sensitive to all kinds of van de Waals effects.

3.3 Ice

Common ice, or hexagonal ice, is obtained when other water molecules are attached at each summit of the tetrahedron and the structure is extended *ad infinitum*. This forms a space-filling hexagonal lattice of nearly undistorted hydrogen-bonded water molecules schematized in Fig. 2. Jumping from close neighbour to close neighbour, it is possible to describe closed paths in the crystal. They always include an even number of at least six molecules. The hexagonal

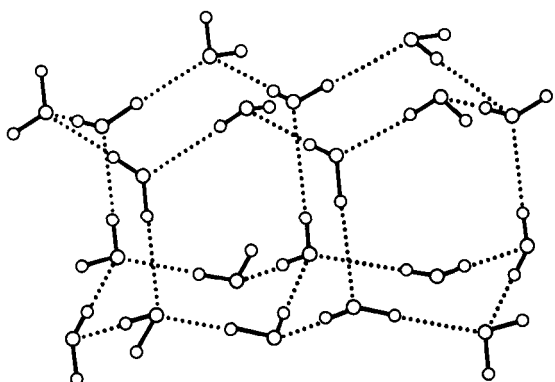


Fig. 2. Schematic view of a small part of a hexagonal ice crystal.

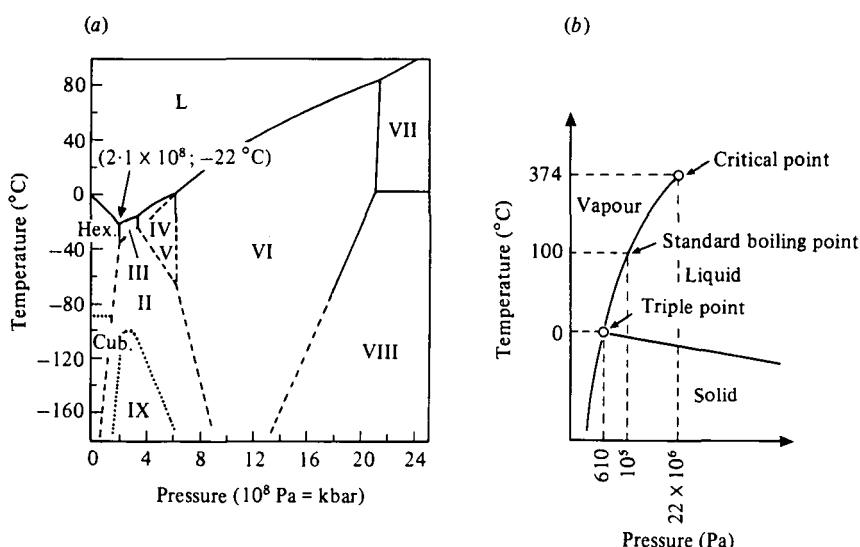


Fig. 3. (a) Part of the phase diagram of water. (b) Phase diagram around the triple point.

crystal is a very open structure; each molecule has only four nearest neighbours whereas the densest packaging of hard spheres leads to 12 nearest neighbours. In this sense the H bond in ice can be seen as holding the molecules firmly at a distance, instead of pulling them together. This also explains why the more ordered hexagonal crystal is less dense than the liquid.

Cubic ice is very similar to hexagonal ice but it is only stable below c. -70°C at normal pressure. Compared to hexagonal ice, the difference comes from the fact that, viewed from one molecule, its neighbour is rotated by 180° along the H bond. Besides this, the distortion of the H bond in the water molecule and the density of cubic ice is the same as in hexagonal ice.

Many more ice polymorphs exist at high pressure, when more distortion of the H-bond network becomes possible (Pauling, 1970; Hobbs, 1974). A phase diagram including most of these forms is shown in Fig. 3(a). Among them is ice II, where

the local tetrahedral symmetry is distorted by a fifth molecule approaching almost as closely as the 4 H-bonded neighbours. This distortion removes the degeneracy of the orientation of the molecules and therefore suppresses the residual oK entropy due, in hexagonal and cubic ice, to the several possible orientations that the water molecule can take in the lattice. In ice III and IX the distortion is strong enough to allow the formation of four member rings. The tetragonal symmetry is restored in ice VII and VIII, which are formed by two interpenetrating networks of cubic ice. The density is therefore close to double that of hexagonal ice. The highest conceived high-pressure form, sometimes called ice X, introduces a new level of symmetry: the H-bonded water molecules are pushed so close together that the hydrogen atom involved in the bond is at mid distance between the oxygens and is indifferently associated with both oxygens. This form seems to have been detected at a pressure above 44 GPa (Polian & Grimsditch, 1984).

3.4 *Liquid water*

Liquid water differs from the various solid forms in the great mobility of its molecules. The rotation or the exchange time at room temperature is of the order of 10^{-12} s. Furthermore, liquid water has the same global symmetry as the gas phase, since it is possible to transform the gas into the liquid without phase transition, provided the transformation is made at a high enough temperature and pressure to turn around the critical point (Fig. 3b). Since the work of Bernal (Bernal & Fowler, 1933) it has been known that the structure of liquid water is also based on the tetrahedral nature of the molecule. Some of the H-bonds are, however, broken and the others are more or less distorted. Some non-H-bonded molecules can therefore 'fall down' between H-bonded molecules, thus increasing the density of the liquid. With the oversimplified but nevertheless useful model that melting is just a matter of H-bond breaking, the comparison of the latent heat of fusion (333 J/g) and of vaporization (2255 J/g) suggests that only 13 % of the H-bonds are broken in the liquid.

The detailed structure of liquid water is still mysterious, but this is certainly not due to a lack of models. In fact, the history of the structure of water is a long list of models, made to fit some measured properties and generally giving a poor description of the others. Since the beginning of the seventies rapid progress has been made, thanks to the possibilities of molecular dynamics (MD) with high-speed computers. Nevertheless the quality of a simulation is never better than the choice of the molecular potential used for the calculation. An outsider is generally impressed by the coarse approximations made in these choices. For example, the well-known ST2 model (Rahman & Stillinger, 1971), which had, and still has an important role in MD development, simply describes the tetrahedral local symmetry of the water molecule by two positive and two equal negative charges placed at the vertices of a tetrahedron centred at the origin. The ST2 potential is the sum, limited to the next neighbour molecules, of the coulomb potential due to these four charges and the Lennart-Jones potential of neon, a spherical atom of the same charge as H_2O .

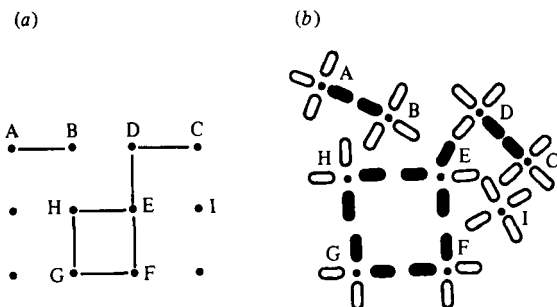


Fig. 4. Percolation model of liquid water. (a) Representation of the topological network of H-bonds between neighbouring molecules. (b) One possible schematic representation of the state presented in (a). (From Teixeira *et al.* (1983), with permission.)

At present it is generally accepted that liquid water is best described by some form of the random H-bond network. It is based on the local tetrahedral symmetry of the molecule, so much distorted that the spatial correlation is lost between more distant molecules. The disorder is thus spread everywhere in the liquid. This is the opposite of the iceberg model, in which ice-like domains are separated by disordered regions. The random H-bond network model is not easy to visualize, except for MD simulations, but the percolation model (Stanley & Teixeira, 1980) is an elegant way to represent it. In this topological model, each water molecule is represented by a point in a two-dimensional square lattice (Fig. 4a). As required by the basic tetrahedral symmetry, each molecule has four neighbours. The H-bonds are randomly distributed between all the possible nearest neighbours but some are left open. Each molecule therefore has a defined probability of being engaged in 1, 2, 3 or 4 bonds. The binding state of the molecules, as also the way they are clustered, can be represented by this model. Further MD calculations can then lead to a useful geometrical description (Geiger *et al.* 1986).

Clathrate is another arrangement of water molecules, of special didactical value for understanding the interaction of water with solutes and the so-called hydrophobic interaction (Pauling, 1970; Davidson, 1973). With little distortion, a small number of water molecules can form a cage such that all the H-bond possibilities of the involved molecules either participate in the formation of the cage or are directed towards the exterior. The smallest of these cages has the shape of an icosahedron at the vertices of which one more H-bond is pointed towards the outside. Other cages may be larger. They can therefore solubilize atoms or molecules which otherwise would be very hydrophobic. This is, for example, the case at high pressure, for rare gas and for several small hydrocarbon molecules. In some cases, many cages, containing, for example, one Argon atom, form an H-bonded crystalline network.

3.5 Aqueous solution

The understanding of aqueous solution requires a microscopic description of how the solute molecules are integrated in the H-bond water network. In general, we

are far away from reaching this level of knowledge. In particular, the question of the role of water in biological systems is still in its infancy and the problem could become even more difficult if, as suggested by much indirect evidence, the volume of water influenced by – and influencing – the solute is much larger than the few water molecules in direct contact with the solute (Clegg, 1982). Nevertheless, hard facts are emerging from molecular studies, in particular from X-ray data (Finney, 1986). Amazingly, it is more often when the solute molecules are not integrated into the water network that the system is best understood. Clathrate, mentioned above, is one such case.

The water dipole is the other feature of the molecule which plays a major role in aqueous solution. Microscopically, the water molecule tends to become aligned by an electric field and to be attracted towards the charge, where the field is maximum. Water dipoles are therefore associated with ions and they screen their field. In most cases the association is not strong enough to establish a fixed binding between the ion and a small number of water molecules, but a dynamic cloud of many slightly polarized water molecules is formed around the ion. In the case of dilute ionic solution, molecular dynamics gives a satisfactory description of the system. Macroscopically, the polar nature of the molecules causes water to have the high dielectric constant of $\epsilon_0 = 80$. The famous Debye-Hückel theory, which forms the basis for the understanding of ionic solutions, is not easy to understand in detail (Berry *et al.* 1980) but its basic principles and results are simple (Feynman *et al.* 1965). It is a semi-microscopic theory in the sense that it considers each ion separately but replaces the water dipoles by a continuous medium in which the magnitude of the electrostatic forces are decreased, and their range increased by ϵ_0 . The major conclusion is that each monovalent ion is surrounded by a counter-charge cloud of decreasing density extending over a distance characterized by the Debye length $D = \{\epsilon_0 kT / 2n_0 e^2\}^{1/2}$ in which n_0 represents the charge density and e the charge of an electron. This effect is of direct relevance for interpreting the effect of charged liquid interfaces or particles in aqueous solutions. For monovalent salt solution D is *c.* 10 nm for 1 mM solution. It would be *c.* 0.3 nm for 1 M solution, but at this high concentration the theory cannot be applied. More elaborate descriptions will be faced with even greater difficulties.

3.6 Water in the electron microscope

Three kinds of solid water exist at low pressure. They are all easily observed in the electron microscope. As illustrated in Fig. 5, they can be distinguished by their general appearance and by electron diffraction. Table 2 gives the position and the relative intensity of the main reflexions seen by electron diffraction. The most important properties of these three forms of ice are summarized in previous publications (Dowell & Rinfret, 1960; Dubochet *et al.* 1982*c*) and in the following paragraphs.

Hexagonal ice is obtained from cooled liquid water or by warming vitreous or cubic ice. The lattice parameters at -160°C are $a_0 = 0.449$ nm, $c_0 = 0.732$ nm, density $\rho = 933$ kg/m³, and the linear thermal expansion coefficient is

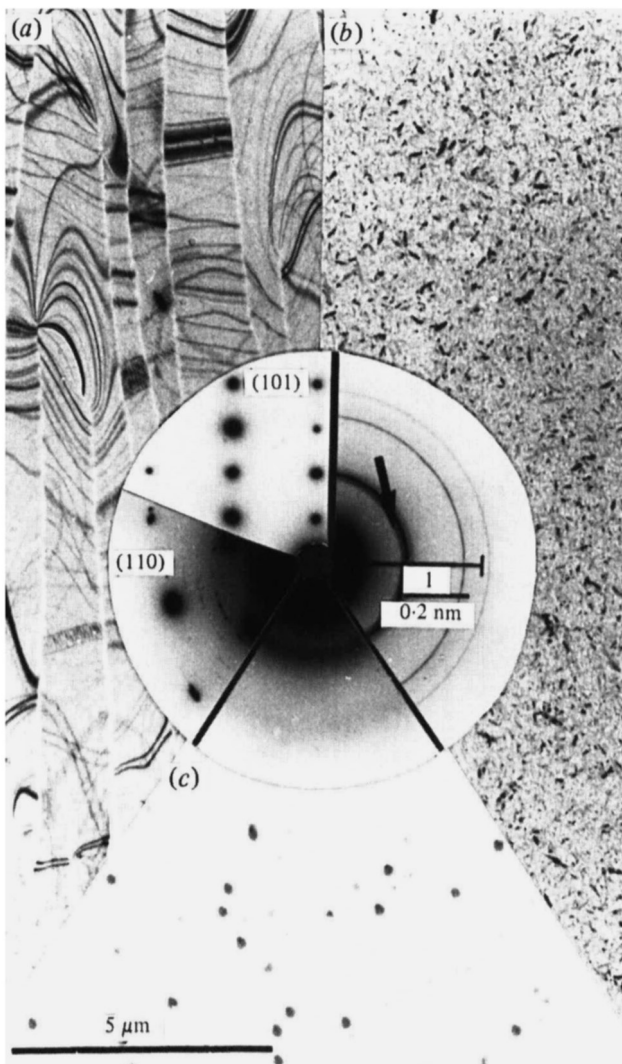


Fig. 5. Typical images and electron diffractograms of three forms of solid water observed in the electron microscope. The direct images and their diffractograms are all printed at the same scale. (a) Hexagonal ice obtained by rapid freezing of a water layer on a carbon film. The diffractograms, obtained from other specimens, show the (110) and (101) plane. (b) Cubic ice obtained by warming a layer of vitreous water obtained by condensation. The shoulder on the (111) reflection, possibly indicating the presence of a small amount of hexagonal ice, is marked by an arrow. (c) Vitreous water obtained in the microscope, by condensation of vapour on a cold carbon film supporting polystyrene spheres. The shadow effect demonstrates that the flux of water molecules was anisotropic. (From Dubochet *et al.* 1982c.)

approximately $2 \times 10^{-5} \text{ }^{\circ}\text{C}^{-1}$. The aspect of hexagonal crystals depends on their origin. They are always relatively large (μm) and are typically striated by bend contours when they originate from the freezing of liquid water. They appear as grains with more or less regular polygonal contours which can be as small as 20–30 nm, when they originate from the condensation of atmospheric water

Table 2. Main reflections in the electron diffractogram of the various forms of ice at -160°C

Hexagonal	Cubic	Vitreous	d (nm)	Intensity
100	—	—	0.389	Very strong
	—	First maximum	0.370	Very strong
002	111	—	0.366	Strong/very strong
101	—	—	0.343	Strong
102	—	—	0.266	Weak
110	220	—	0.224	Medium/medium
	—	Second maximum	0.214	
103	—	—	0.207	Medium
200	—	—	0.194	Very weak
112	311	—	0.191	Weak/weak
201	—	—	0.188	Very weak
202	—	—	0.172	Very weak

vapour on a cold specimen or in the cryogen. The hexagonal form of deuterated water has the same lattice parameters but a density of $\rho = 1040 \text{ kg/m}^3$.

Cubic ice is obtained by slow deposition of water vapour in vacuum at a temperature between approximately -135 and -100°C (König, 1943), by warming vitreous water above the devitrification temperature T_v or by very rapid cooling of liquid water (Dubochet & McDowall, 1981; Mayer & Hallbrucker, 1987). Once formed it is also stable below T_v . As seen in Fig. 5(b), the 111 reflexion always has a shoulder on its inner side. This may be due to the presence of a small amount of hexagonal ice appearing with its 100 reflexion. The lattice constant of cubic ice is 0.634 nm at -160°C . The spacing of the 111 reflexion is 0.366 nm. Its density is, within 0.2%, the same as that of hexagonal ice. Cubic ice appears as a mosaic of small crystals with dimensions in the $0.1 \mu\text{m}$ range, generally leading to an electron diffraction pattern characteristic for a powder. It should be noticed that all the reflexions of the diffractogram of cubic ice are superimposed with those of hexagonal ice. Consequently, the identification of one cubic crystal from its diffractogram cannot be done unambiguously.

Vitreous ice is obtained by slow deposition of water vapour on a cold substrate below T_v (Burton & Oliver, 1935) or by rapid cooling of liquid water (Brüggeller & Mayer, 1980; Dubochet & McDowall, 1981). It has the same density as cubic or hexagonal ice (Ghormley & Hochanadel, 1971; Dubochet *et al.* 1983a). Vitreous water appears as a smooth layer without internal structure. The electron diffractogram is characterized by diffuse rings of diameter corresponding to 0.37 and 0.21 nm with a full width at half maximum of $0.6-1.5 \text{ nm}^{-1}$. Recent observations suggest that vitreous water is polymorphous (Mayer & Brüggeller, 1983; Mishima *et al.* 1984) and that a second, low-temperature high-density form may have been observed by electron microscopy (Heide & Zeitler, 1985).

Phase transitions from vitreous water to cubic ice and from cubic to hexagonal

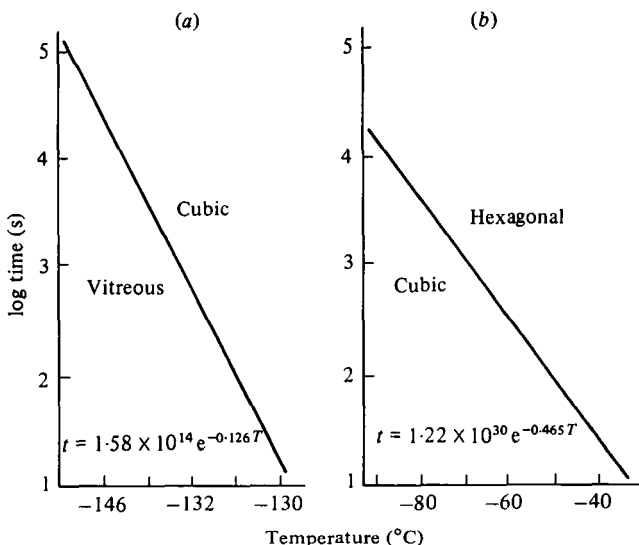


Fig. 6. Time t required, at the temperature T ($^{\circ}\text{C}$), for the phase transition from (a) vitreous water to cubic ice and (b) cubic to hexagonal ice to take place (Dowell & Rinfret, 1960). Recent results suggest that curve (a) should be displaced by 10–20 $^{\circ}\text{C}$ towards the higher values (see text).

ice are triggered by increased temperature. The time t (s) taken for the transition, rapidly decreases with increasing temperature T according to the equations (Dowell & Rinfret, 1960)

$$t = 1.22 \times 10^{30} \exp(-0.465 T)$$

for the vitreous-to-cubic transition and

$$t = 1.58 \times 10^{14} \exp(-0.126 T)$$

for the cubic-to-hexagonal transition. These two equations are represented in Fig. 6. According to these data, devitrification of vitreous ice should take place in c. 5 min at -137 $^{\circ}\text{C}$. Recent measurements in the electron microscope (Dubochet *et al.*, 1983a), by X-ray diffraction and by thermal analysis (Angell, 1983; Mayer & Brüggeller, 1983) seem, however, to demonstrate that devitrification of vitreous water takes place at a higher temperature, probably between -133 and -117 $^{\circ}\text{C}$, depending on the way the sample was vitrified. In the absence of a more precise determination the value $T_v = -120$ $^{\circ}\text{C}$ seems to be a usable approximation. It should be noticed that the vitreous-to-cubic transformation is truly a phase-transition and not a continuous extension of short-range order. This can be seen by the fact that the diffuse maxima of the vitreous state do not become sharper during the transition, eventually leading to the cubic ice pattern, but fade away while being replaced by the ring pattern of cubic ice. Under normal conditions the transition from cubic to hexagonal ice cannot be observed in the electron microscope because it takes place at a temperature at which ice evaporates too rapidly.

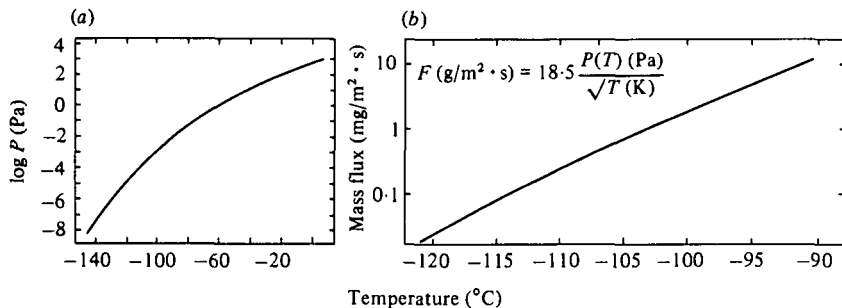


Fig. 7. (a) Vapour pressure P expressed in Pa ($133\text{ Pa} = 1\text{ Torr}$; $10^5\text{ Pa} = 1\text{ bar} = 0.987\text{ atm}$) as a function of the temperature in $^\circ\text{C}$. (b) Evaporation of water in perfect vacuum as a function of the temperature in $^\circ\text{C}$. One mg/m^2 corresponds to 1 nm thickness at a density of $1\text{ g}/\text{cm}^3$.

Evaporation and condensation of ice. In a perfect vacuum the mass flux of evaporating ice F (expressed in $\text{g}/\text{m}^2 \cdot \text{s}$) is

$$F = 18.5 P / \sqrt{T},$$

in which P (expressed in Pa) is the vapour pressure at the temperature T . (The factor becomes 2.47×10^3 if P is expressed in Torr). The curve $P(T)$ is given in Fig. 7(a) whereas Fig. 7(b) gives the $F(P, T)$ relation. It should be noticed that, in this latter equation, the sublimation rate is calculated on the assumption that the accommodation coefficient (the probability that a molecule hitting the surface will stick to it) is 1. This was found to be correct in some cases (Davy & Branton, 1970), but measurements made directly in the electron microscope lead to a slower sublimation rate (Dubochet *et al.* 1982*c*; Heide, 1982*a*). In any case the sublimation rate becomes very small at the devitrification temperature or below ($F < 0.03\text{ mg}/\text{m}^2 \cdot \text{s}$ corresponding to $< 0.03\text{ nm}/\text{s}$ at $-120\text{ }^\circ\text{C}$) and we have never observed its effect in the electron microscope. In practice this means that, for a cryo-microscopist, sublimation of vitreous water is negligible.

4. FREEZING

An excellent general introduction to the field of freezing can be found in Franks (1982), and the review by MacKenzie (1977) elaborates on the problem of rapid cooling of aqueous solutions. The wide range of literature on freezing to preserve viability is reviewed by Mazur (1970, 1984). The new developments resulting from the discovery of vitrification are discussed by Angell & Choi (1986) and by Fahy *et al.* (1984).

4.1 Nucleation and growth

The classical nucleation theory (Franks, 1982) is represented schematically in Fig. 8. It considers a spherical ice crystal of radius r in water below $0\text{ }^\circ\text{C}$. The free energy, ΔG , of the system has two components. The first, ΔG_v , favours the growth

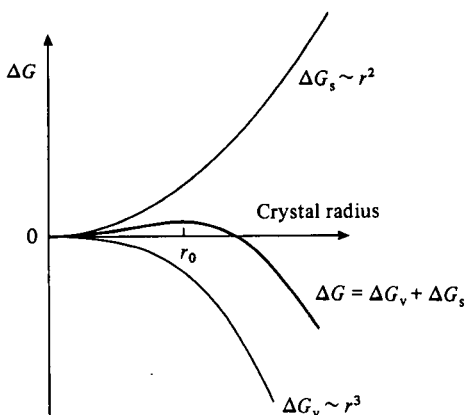


Fig. 8. Classical nucleation theory. The free energy, ΔG , of a spherical ice crystal of radius r in water below 0°C can be expressed as the sum of volume, ΔG_v , and surface, ΔG_s , contributions. Below r_0 the crystal is unstable.

of the crystal. It expresses the fact that water molecules are more stable in the crystal than in the liquid. It is proportional to the number of molecules in the crystal and hence to its volume. The second component, ΔG_s , expresses the instability of the liquid–solid interface and is therefore proportional to the surface of the sphere. It favours the dissolution of the crystal. Whatever the constants defining the magnitude of these two components, the total free energy always has the same general shape: ΔG increases first, with increasing radius, until it reaches a maximum for $r = r_0$, after which it decreases more and more rapidly. In other words, an ice crystal must be sufficiently large before it is thermodynamically favoured. A nucleation event resulting from the favourable but fortuitous arrangement of randomly fluctuating molecules must first take place before the crystal can grow independently.

The nucleation event in pure water is mysterious and will probably remain so for a long time. It is also a rare event – at least if it is estimated at the molecular scale. Indeed, the fact that vitrification is possible in cubic micrometre-sized volumes, demonstrates that the molecules did not have the time to produce a single nucleation event during cooling. As the number of molecules involved is more than 10^{10} and their average time for changing position is 10^{-12} s , the number of conformations that the system explores during the 10^{-4} s required for cooling is larger than 10^{18} ; a very large number indeed but still insufficient to produce a nucleation event.

In principle, nucleation begins as soon as the water reaches 0°C . However, thermal agitation counterbalances most of the thermodynamical potential favouring the ordered crystalline state over that of the liquid. A sample of pure water can therefore remain undercooled for a long period of time without crystallizing. At a still lower temperature, call *homogeneous nucleation temperature*, T_0 , crystallization becomes unavoidable. No absolute value can be attributed to T_0 as it depends on experimental conditions, including the time one is prepared to wait for the observation. In any case, it is very difficult to avoid crystallization

of pure liquid water below -35°C . At a still lower temperature the nucleation probability increases very rapidly unless the sample can be brought below the *glass temperature* T_G . This is when the viscosity of liquid water becomes so large that all rearrangements, including the formation of nuclei, are essentially stopped. This takes place when the viscosity is at least 10^{14} N s/m^2 . In practice, T_G can be identified with the devitrification temperature T_v and a sample which has not crystallized before it reaches T_G is vitrified.

In most real situations crystallization of macroscopic samples takes place long before T_0 because it is triggered by the phenomenon of *heterogeneous nucleation*, taking place at temperature T_E somewhere between the melting temperature T_M and T_0 . It can be understood as a catalytic-like formation of a nucleus by a seed contaminant. Seeds of this kind are omnipresent in nature except (a) in the purest water, (b) in the cleanest atmosphere (as in cloud chambers), (c) when the water volume is very small (micrometre-sized water droplets in oil; Rasmussen & Mackenzie, 1973) or, to a large extent, (d) in living cells.

Once nucleation has taken place the growth of an ice crystal occurs very rapidly. However, the process releases energy, causing a local heating of the sample. As complete crystallization would correspond to a temperature rise of 80°C , freezing cannot proceed to an end before the heat is dissipated. Crystal growth is therefore based on the dynamic equilibrium between heat production and dissipation at the crystal surface. Recent computer simulations have provided a better insight into this complicated process (Langer, 1980; Maddox, 1983; Nittmann & Stanley, 1986).

4.2 Hexagonal ice in solution

The presence of a solute changes the freezing conditions (Mackenzie, 1977). As shown in Fig. 9, T_M , T_E and T_0 are lowered and T_G is raised with increasing solute concentration. During crystal growth, the solute is rejected from the crystal, thus further increasing its concentration in the remaining liquid. The evolution of a slowly cooling liquid, frozen by heterogeneous nucleation, can then be represented by the heavy line in the graph of Fig. 9. In the case of extremely rapid cooling, the sample may reach T_G before crystallization starts, and become vitrified. This course of events is represented by the vertical dotted line. Most practical freezing conditions correspond to an intermediate situation, represented by the dashed line on the figure.

During the rapid growth of an ice crystal there is not enough time for the solute rejected from the crystal to equilibrate its concentration in the residual liquid volume. A gradient of concentration is built up in front of the ice surface, further increasing the resistance to crystal growth. As illustrated in Fig. 10, this situation favours the formation of ramified ice crystals which may extend over large volumes, though no molecules of the solute are displaced by more than the radius of each ramification. When the observation of frozen hydrated sections became possible, it was demonstrated that this crystal shape is usual in frozen biological materials (Chang *et al.* 1983; Dubochet & McDowall, 1984*b*). An example is

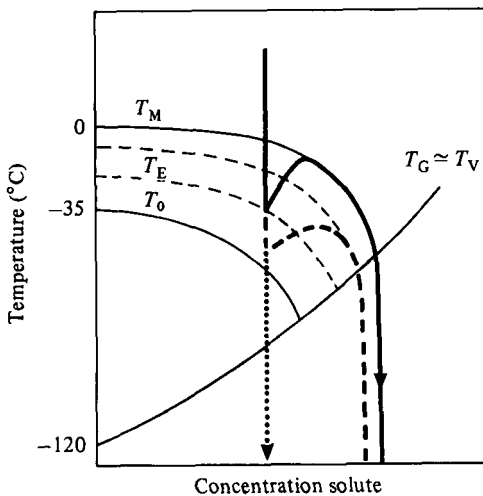


Fig. 9. Temperature of a binary solution where the solute does not crystallize during freezing. T_M , T_E , T_O , T_G and T_V , are melting, heterogeneous nucleation, homogeneous nucleation, glass and devitrification temperature, respectively. The heavy line represents the case of slow cooling; the dashed line a more rapid cooling; the dotted line represents the case in which vitrification is achieved.

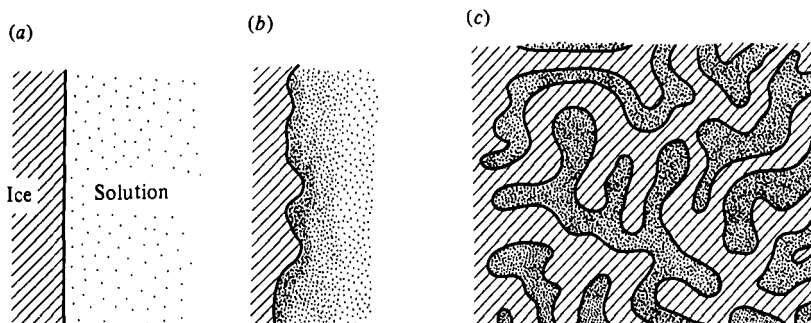


Fig. 10. Growth of an hexagonal ice crystal in an aqueous solution. Starting from a flat surface in a homogeneous solution (a), the rapid growth of the crystal makes the solute accumulate in front of the ice surface. This reduces the crystallization speed. Local statistical fluctuations in growth are amplified by the resistance of the concentrated solute layer (b). Finally, all the freezable volume may be filled by the ramified network of a single or a few crystals (c).

shown in Fig. 11. It represents a thin section of a frozen 15% gelatine solution. A large number of domains are clearly visible. However, electron diffraction demonstrates that there is only one, somewhat distorted, ice crystal in the observed field. Each domain therefore represents another ramification of the same crystal. This observation is reproduced each time water is frozen into hexagonal crystals in a biological sample. The crystals are then, at least, some micrometres in overall size. In most cases there is only one, or a few, of them per cell. Consequently their size does not depend very much on the cooling speed. What varies, however, is the size of the domains or of the ramifications in the crystal.

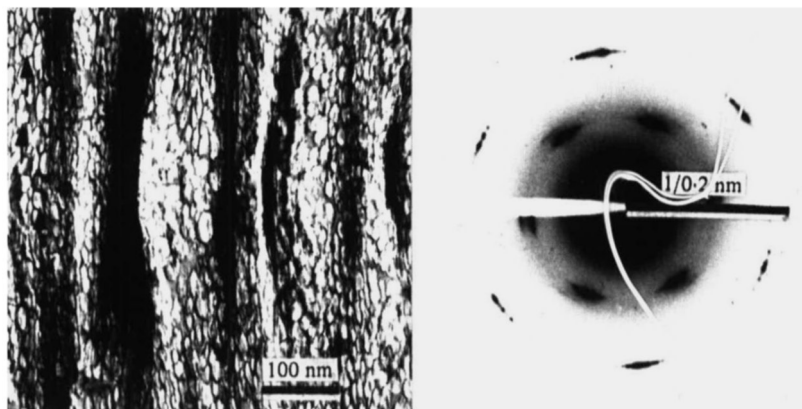


Fig. 11. (a) Cryosection of a frozen 15% gelatin solution in which severe freezing damage is obvious. Some domains from which the solute has been excluded by the growing ice crystal are marked by arrows. (b) Electron diffractogram of the whole field shown on the micrograph. It represents a single, though distorted hexagonal ice crystal.

They become smaller with increasing cooling speed, thus reducing the structural damage suffered by the specimen.

The above description of the freezing process differs from traditional explanations. The domains seen in frozen specimens were previously interpreted as being individual ice crystals instead of ramifications from a single large crystal. This misinterpretation is easily understandable because it was based on the observation of dry remnants of frozen samples in freeze-dried or freeze-substituted preparations. The new understanding allows a more satisfying interpretation of the image of frozen biological samples. As an example, we can consider the freeze-substituted specimen depicted in Fig. 12, which was originally presented as an illustration of a badly frozen sample (Handley *et al.* 1981). According to the above knowledge on freezing we can describe this micrograph as follows: The sample of erythrocytes in saline solution was frozen by projection on a cold surface situated at the upper border of the specimen. As soon the specimen reaches the cold block, its surface is cooled very rapidly and a temperature-gradient forms in the specimen. Shortly after, in a point of the solution, close to the surface and where the temperature is below zero (but above T_0), a nucleation event takes place by heterogeneous nucleation. The growth of the ice crystal in the interspace is rapid at first and the temperature rises to almost 0°C . Crystal growth continues more slowly deeper in the specimen because it takes longer to remove the heat of crystallization and the temperature, along the surface of the growing crystal remains close to 0°C . During all this time the cells remain unfrozen because they do not contain nucleation seed and because their dense cytoplasm serves as a cryoprotectant. They suffer some dehydration due to the osmotic effect of the increasing salt concentration of the liquid in the interspace. Some of them may burst. Once crystallization of the solution is terminated, the temperature begins to decrease again, from the surface towards the interior of the specimen. Sometimes, after the local temperature has reached T_0 , an homogeneous

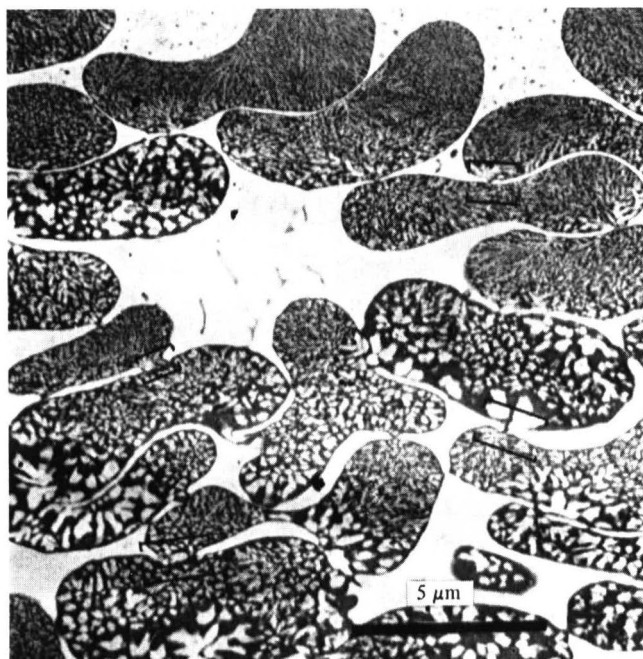


Fig. 12. Human erythrocyte suspension frozen by projection of a sample enveloped in a thin titanium foil into liquid cryogen. The part of the sample which is in contact with the metal foil is the most rapidly cooled. It corresponds to the upper part of the figure. For explanation: see text. (From Handley *et al.* (1981), with permission.)

nucleation event takes place in each cell where a single crystal starts to grow. Here again, growth is rapid at first but it becomes slower while the residual space is warming, and the solute concentration increases. Because of the original temperature gradient, the nucleation event is more likely to take place on the cell side which is proximal to the cooling surface. The domains are therefore smaller on this than on the distal side. The random time at which the initial nucleation event takes place in each cell influences the average domain size, which therefore appears to be uncorrelated between neighbouring cells.

4.3 Cubic ice

For a long time cubic ice has been known as a low-temperature ice modification, obtainable by condensation of the vapour around -100°C or by devitrification of vitreous water. As soon as it became possible to observe vitrified and crystallized aqueous samples directly in the microscope, it was found that cubic ice could also be obtained from the liquid (Dubochet & McDowall, 1981; Dubochet *et al.* 1982c), a fact which has recently been confirmed by X-ray of rapidly quenched aerosol droplets (Mayer & Hallbrucker, 1987). In order to produce cubic ice the cooling speed must be slightly lower than that required for vitrification, consequently a zone of cubic ice frequently forms the border between vitrified domains and regions where the water forms hexagonal crystals. In the practice of

cryo-electron microscopy, cubic ice is frequently obtained when vitrification is attempted under suboptimal conditions, either because the cryogen is not cold enough or because a less-efficient cryogen, as for example nitrogen slush, is used.

Cubic ice crystals are much smaller than hexagonal crystals. Their dimensions range from 30 nm to 1 μm but not smaller, at least as indicated by direct observations and from the width of the rings of the electron diffractogram. The formation of cubic ice crystals in solutions or in biological samples also seems to produce much less structural damage than during the formation of hexagonal ice. As seen in frozen sections, membranes seem to be unaffected when they are surrounded by cubic ice and, in solution, it does not seem to cause aggregation of biological particles. Only one clear case of freezing damage by cubic ice has been documented and that is in thick filaments of insect flight-muscle (McDowall *et al.* 1984).

4.4 Vitrification

Vitrification takes place at a still higher cooling rate. It is the state in which immobilization is achieved before nucleation. Consequently there is a clear discontinuity between the smallest ice crystals which are in the 30 nm range and the vitrified state, which does not have any crystals. In terms of thermodynamics, this discontinuity is referred to as phase transition. It is wrong to consider vitrification as the extreme case when the size of the ice crystals continuously decreases as the cooling speed increases. A scheme of the crystal size in relation to the estimated cooling speed is shown in Fig. 13.

A large amount of experimental data has been collected on the properties of vitreous water obtained by vapour condensation (Searns & Rice, 1982). Results on vitrified liquid water are now accumulating rapidly (Mayer & Brüggeller, 1982; Dubochet & Lepault, 1984; Mayer, 1985). The density of pure vitrified water has been measured by electron microscopy, in comparison with the known density of polystyrenes spheres (Dubochet *et al.* 1982a). The value found is 0.93 ± 0.02 g/cm³, which is close to that of ice at the same temperature. This low density implies that water expands linearly by 2–3 % during vitrification. However, according to size measurements on catalase crystals made in collaboration with N. Unwin, we found that the lattice parameters in vitrified samples do not differ by more than 0.5 % from those measured by X-ray at room temperature. This could indicate that water distribution in the crystal changes during cooling or that the density of vitreous water is not the same in the protein crystal as it is in its surroundings.

For an electron microscopist, the essential question about vitrification is whether it keeps the original biological structures intact. There is no simple answer to this question; the only thing known for sure is that vitrification avoids ice-crystal formation. Other transformations could well be induced during the cooling time, estimated to be equal to about 10^{-4} s in the most favourable case (thin-layer vitrification). In general, this time is short in respect to the time required for large rearrangements of biological structures. It is long, however,

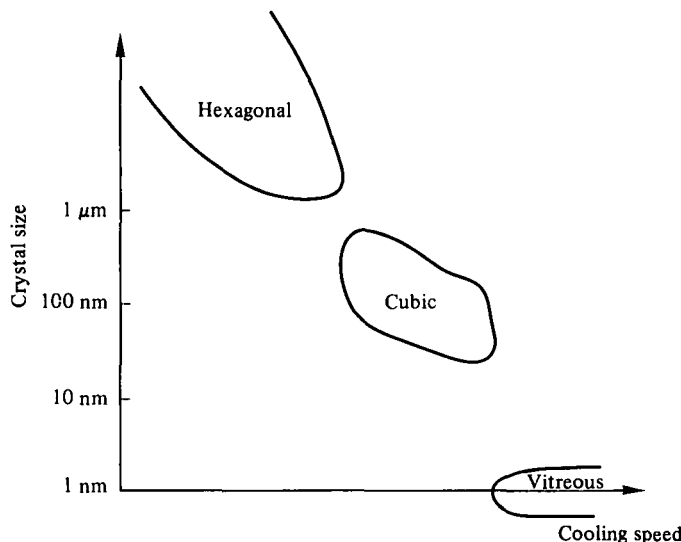


Fig. 13. Relationship between the cooling speed and the size of the ice crystals. The crystal size is measured by electron diffraction on frozen hydrated specimens. The width of the rings of the powder diffractogram gives an estimate of the minimum size of the cubic crystals. (From Dubochet & McDowall (1984b), with permission.)

when compared to rearrangements of the size of one macromolecule or, more so, if the diffusion speed of atoms or of small metabolites is being considered (Hiromi, 1979). In practice, however, all observations made up to now have confirmed the excellent preservation of vitrified specimens. As far as we know, only one case in which a rearrangement takes place during vitrification has been documented (Lepault *et al.* 1985). It concerns lipid vesicles, vitrified from a starting temperature at which the lipids are in their liquid state (α conformation). This conformation is not conserved during vitrification but is transformed into a crystalline β conformation, still different from β' , the low-temperature equilibrium conformation.

4.5 Cryofixation

Recommendable reviews about cryofixation have been prepared by Plattner & Bachmann (1982), Robards & Sleytr (1985) or Menco (1986). They give a good picture of the enormous amount of work which has been devoted to developing methods for rapid cooling and for obtaining quantitative data on the achieved cooling rate. Most of this work, however, is of limited value for our purpose because it concerns samples of much larger volumes than those considered for vitrification. Furthermore, the indicator for the quality of cryofixation is, in most cases, the size of the 'ice crystals', in freeze-substituted, freeze-etched or freeze-dried specimens, which, of course, is inadequate for deciding if a specimen has been vitrified during cooling. The review by Sitte *et al.* (1987) keeps the need for vitrification closer in view.

Determining directly whether a sample is vitrified or not is an unambiguous indicator of cooling efficiency. Of course, it is not a very differentiated indicator but it tells if a sample is optimally frozen or not, which is ultimately the most relevant question that the electron microscopist can ask. No quantitative data on the cooling speed required for vitrification of pure water is available yet but some extrapolations can be made from measurements made with thin thermocouples at a known distance from the sample surface (Escaig, 1982*a, b*). It was found, for example, that a tissue block cooled by projection on to a cold metal surface reaches a cooling rate of 50000 °C/s at *c.* 20 µm depth. It seems therefore that a cooling speed of the order of 10⁶ °C/s could be achieved in a 1 µm thick water layer. This value probably gives an order of magnitude for the minimum cooling speed required for vitrification of pure water. Other lines of thought lead to a comparable result (Mayer, 1985).

The requirements for vitrifying aqueous solutions or biological suspensions are not as severe because most solutes play the role of a cryo-protectant. The size of a sample that can be vitrified can be increased accordingly. For example, a fragment of liver or a pellet of typical mammal culture cells can be vitrified to a depth of 10–20 µm. Similar values are obtained with pure 20% sugar solution. Higher sugar concentration is of little use for cryo-electron microscopy because it reduces too much the contrast of most biological structures. However, it is useful for other techniques, such as cryosectioning for immunolabelling, where saturated sucrose solution allows easy sectioning of millimetre-size blocks of vitrified tissues (Tokuyasu, 1980; Griffiths *et al.* 1983).

In our experience the rapid immersion of a small sample in an efficient cryogen easily gives good and rapid results (see § 10 below, 'How to operate'). The immersion can be done with a plunger, and liquid ethane or propane can be used as a cryogen. In most cases we do not obtain vitrification if immersion is carried out directly by hand, though some people seem to be successful (U. Aebi, personal communication). We are also unsuccessful when nitrogen slush is used as a cryogen, but here again others do not seem to have this limitation (Fujiyoshi *et al.* 1986, personal communication). The cooling efficiency of liquid propane or ethane at their melting points seems to be similar. In practice they differ in the way a small amount of cryogen, left on the grid after vitrification, evaporates during transfer and in the microscope; ethane (boiling point = -89 °C) rapidly sublimates in the cold specimen holder whereas propane (boiling point = -42 °C) may remain longer and disturb observation.

It is possible to draw some conclusions on the cooling mechanism by considering the conditions giving best results and by comparing the effects of various cryogens. In order to be efficient, cooling should take place by direct conduction from the liquid cryogen to the liquid film. Liquid ethane or propane at their fusion temperature are therefore excellent because they can be warmed by nearly 100 °C and can absorb a large enthalpy before significant evaporation takes place. The process of calefaction, in which a layer of gas prevents good thermal contact between the sample and the cryogen, is therefore avoided. On the contrary, the whole cooling effect of liquid nitrogen at its boiling point takes place through

evaporation. Calefaction is therefore unavoidable. Nitrogen slush can only be warmed by 14°C before it reaches its boiling point. This is apparently insufficient for best cooling efficiency. Another consequence of the poor cooling efficiency through a gas layer is that no significant cooling takes place during plunging, before the sample reaches the liquid cryogen.

From the estimated vitrification rate for pure water ($10^6\text{ }^{\circ}\text{C/s}$) the vitrification time can be deduced to be of about 10^{-4} s . During this time the specimen, falling with the plunger described below, moves by only $100\text{ }\mu\text{m}$. This may seem to be a short distance but it is nevertheless 1000 times more than the thickness of a typical vitrified thin film. At this scale it seems probable that convection of the cryogen on the moving specimen produces an excellent heat exchange.

The cooling process involving direct contact of the liquid cryogen with the liquid film of solution raises the question whether some mixing taking place between the two fluids could result in a new solution with more favourable properties for vitrification. A mixture resembling clathrate hydrate of hydrocarbons could be considered here (Davidson, 1973). One could even argue that the vitrified sample is of a different nature to that of the liquid solution and observations made on the former are not relevant for the latter; fortunately all the practical experiments with biological specimens refute this argument. Furthermore the similarity between the electron diffractogram of vitrified water obtained from the liquid and that obtained by vapour condensation suggests that the liquid cryogen does not seriously influence the structure of the vitreous film (Dubochet *et al.* 1983a). Finally, the presence of liquid cryogen is not a requirement for achieving vitrification of pure liquid water. Cooling on a solid cold surface is equally possible and leads to vitrified water with identical properties (Mayer, 1985).

Jet freezing is another method for cooling with liquid cryogen (Müller *et al.* 1980; Plattner & Knoll, 1984). The advantage is that the specimen is kept out of direct contact with the air or with the cryogen. However, the thin metal foil which encloses the specimen forms a thermal barrier between the specimen and the cryogen. As a result the preparation is also somewhat more demanding. Whether vitrification of dilute solution can also be obtained with this method has not yet been established.

Slam freezing, which consists in projecting the specimen directly on to a metal block cooled by liquid helium or liquid nitrogen (Harreveld *et al.* 1974; Christensen, 1971; Escaig, 1982a; Sitte *et al.* 1987), almost immediately brings the very top surface of the sample close to the block temperature. The value of the method for achieving excellent cryoprotection of the surface has been amply demonstrated (Heuser *et al.* 1979). How it compares with the effects of liquid cryogen for deeper cooling is not yet known quantitatively. In our experience, it can give excellent results and some of the very best specimens we have ever obtained were produced by this method. However, it requires adequate solving of some technical difficulties. In particular the specimen should not be severely squeezed by the slammer, and bouncing must be avoided. Contamination of the cold metal surface also prevents good thermal contact, especially around the

liquid-helium temperature, where air can also condense on the block. Whether the use of liquid helium instead of liquid nitrogen offers a real practical advantage is dubious, in view of the minor improvement in cooling speed which has to be compensated by a large increase in cost and in difficulty of operation.

High-pressure cooling (Riehle & Hochli, 1973; Müller & Moor, 1984; Moor, 1987) is based on the attractive theoretical idea that T_M , T_O and T_E decrease with increasing pressure. The lowest values are reached at 2100 atm, where T_M and T_O are at -21 and -90 °C respectively. The onset of crystallization during cooling could be delayed accordingly, though the fact that viscosity of water decreases with increasing pressure could have an unfavourable influence. An instrument for jet freezing at this pressure is now commercially available. Results obtained up to now are promising, though only with poorly defined indicators. The method will probably also be useful for vitrifying larger samples, but this remains to be tested.

5. SECTIONS

5.1 Vitrified sections

In his most enjoyable dream the electron microscopist may imagine cryo-ultramicrotomy: a biological sample is vitrified, cut into thin sections and observed in a cryo-electron microscope where it reveals all its most subtle structures. As surprising as it may be, this dream, sometimes, becomes truth. One of the first examples is illustrated in Fig. 14 (McDowall *et al.* 1983). It shows a vitrified section from rat liver. The specimen is neither chemically fixed, nor stained nor infused by cryoprotectant. Many internal structures of the cell are visible. On the whole they resemble those observed in conventionally prepared specimens – a fact which is reassuring for cryo-ultramicrotomists as also for those used to conventional embedding methods. The image becomes even more interesting when the section is observed closer. An example taken from a muscle sample is shown in Fig. 15. The method has been applied with success on a number of specimens and valuable new results have been obtained (Dubochet *et al.* 1983b; McDowall *et al.* 1984, 1986). The practical aspects of the method are described below and in § 10.

Unfortunately it may also happen that an experienced cryo-ultramicrotomist dreams, on the same theme, the most dreadful nightmare. He would see a specimen without consistency refusing to behave decently for vitrification; he would see a knife scratching the specimen into unshaped fragments which fly away as soon he tries to catch one; the climax would arise in the microscope, where contamination, charging and bubbling add to create chaos. This dream, also, is part of the cryo-ultramicrotomy experience.

Cryo-ultramicrotomy was developed a long time ago (Bernhard, 1965) and it is now in standard use for several techniques, as for example immunolabelling (Tokuyasu, 1973, 1980; Griffiths *et al.* 1983) or elemental analysis (Gupta & Hall, 1981), but, as for many other cryo-electron microscopy methods, it is dry specimens that are finally observed in the electron microscope. In spite of

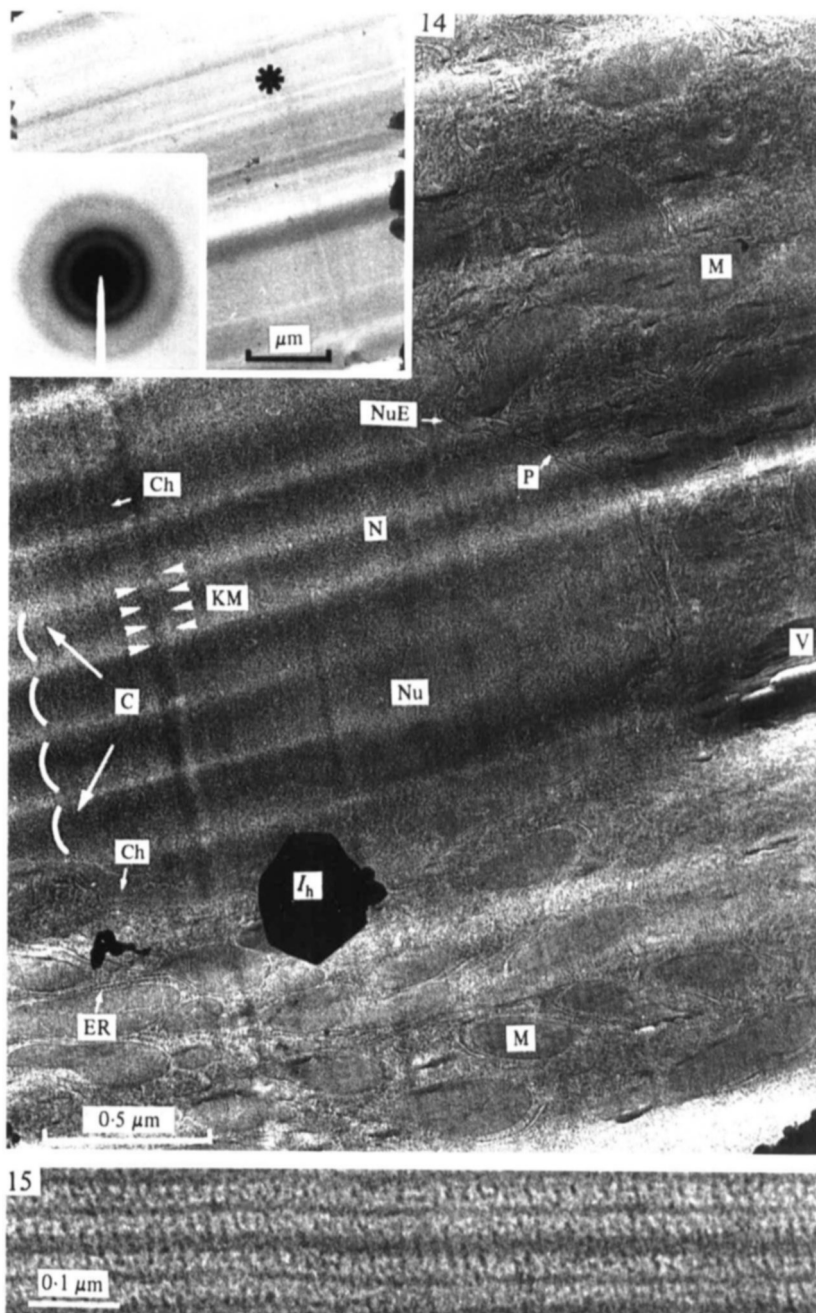


Fig. 14. Section from an untreated fragment of rat liver, vitrified by projection on a cold metal block. Sectioning temperature: -160°C . Thickness: 180 nm. N, nucleus; Nu, nucleolus; NuE, nuclear envelope; P, nuclear pore; Ch, chromatin; M, mitochondria; ER, endoplasmic reticulum with ribosomes; V, vacuole; I_h, contaminating hexagonal ice crystals; KM, knife marks; C, chatter. Insert: section from a block of vitreous ice with its electron diffractogram. The block was obtained by condensation of water vapour at -10^{-1} Pa for 2 hours on a specimen holder kept at liquid nitrogen temperature. Sectioning temperature: -160°C . The thickness at the point marked by a star is 120 nm. The first separated ring in the diffractogram corresponds to 0.37 nm (From: McDowall *et al.* (1983), with permission.)

Fig. 15. Longitudinal cryosection in a vitrified unfixed fibril of glycerinated insect flight muscle in the relaxed state. Section thickness: 80 nm. (From McDowall *et al.* (1984), with permission.)

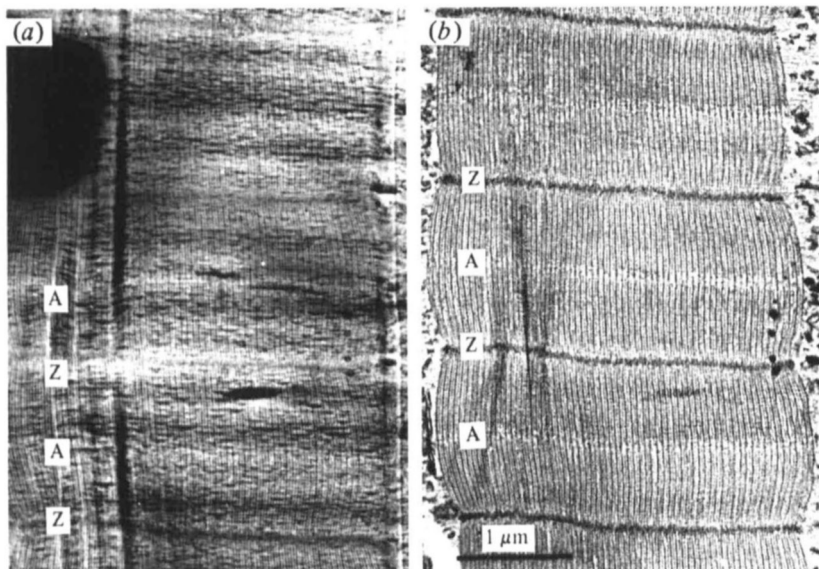


Fig. 16. Longitudinal cryosection of glycerinated insect flight muscle washed in 20% sucrose buffer. This region of the sample was not vitrified, but water was crystallized into cubic ice. (a) Fully hydrated section. (b) Same region as in (a) after freeze drying in the microscope. A and Z: A and Z bands. (From Dubochet & McDowall, 1984.)

numerous trials, ultrastructural observations on fully hydrated sections had given few results (Hutchinson *et al.* 1974; Gupta & Hall, 1981) until vitrification was discovered. It could then be developed into a practical method (McDowall *et al.* 1983; Dubochet & McDowall, 1984*a*) which has since been applied to a number of specimens (Dubochet *et al.* 1983*b*; McDowall *et al.* 1984, 1986). In spite of the break-through that vitrified sections could be for ultrastructural research, the method is not yet in general use. The reason is unfortunately quite clear; the method is still technically difficult, the yield of good micrographs is low and, in most sections, the severity of the cutting artifacts is discouraging for many. Much effort has been put into understanding and overcoming these difficulties (Chang *et al.* 1983; Frederik *et al.* 1982, 1984; Griffiths *et al.* 1984; Zierold, 1982, 1984) but a lot remains to be done.

The cleanest demonstration that cryo-ultramicrotomy of vitrified specimens is possible is reproduced in insert of Fig. 14. It shows a thin section made from a block of pure vitreous water, obtained by condensation from the vapour. Its electron diffractogram confirms that the section is still vitrified. Obviously, sectioning was possible, the sample did not dry during preparation and the vitreous state was conserved during the whole process. The merit of hydrated sections, as compared to freeze-dried or freeze-substituted ones, has also been a matter of debate. As illustrated in Fig. 16, for a sample of washed, glycerinated insect flight-muscle the freeze-dried section may at first give a better impression than the hydrated specimen because it is more contrasted. Careful observation shows, however, that all the valuable features observed in the freeze-dried section

are also visible in the hydrated one, but many details, present in the hydrated specimen, are lost during the dehydration process. This effect is common to many preparations. It was carefully tested on various specimens, including insect flight-muscle (McDowall *et al.* 1984), collagen (McDowall & Lepault, personnel communication) and chromatin (J. M. Smith, personal communication), by comparing the results from electron and optical diffraction on vitrified sections with those from X-ray diffraction of hydrated samples at room temperature. Except for the cutting artifacts, vitrified sections seem to be identical to the native sample whereas any other preparation method leads to obvious transformations. It must, however, be kept in mind that, if the advantage of vitrified over freeze-dried sections is obvious for ultrastructural observations in the range smaller than 100 nm, the situation may be different at lower resolution where a strong amplitude contrast is necessary, or for elemental analysis which may require an irradiation dose that a hydrated specimen cannot tolerate.

5.2 *Cryo-ultramicrotomy*

A good cryo-ultramicrotome should provide the same regularity of cut and advance as a microtome operating at room temperature and it should also allow reasonable ease for manipulation of the sample and the sections. These are severe requirements when they have to be fulfilled under conditions where the operating temperature is some 200 °C below room temperature. In fact, ultramicrotomes capable of producing good thin sections of vitrified samples have been commercially available only since 1980 (Sitte *et al.* 1980). Their construction principles and operation modes are reviewed in Sitte & Neumann (1983). They are directly derived from the standard instrument by placing the specimen and the knife in a thermally isolated chamber cooled by liquid nitrogen. The isolation of the chamber is most difficult along the moving arm, where strength and rigidity cannot be reduced, and above the specimen, where a large window is required for manipulation and observation. For technical reasons the primary cooling of the chamber (flow of liquid nitrogen) is not continuous. The chamber is therefore designed in such a way as to minimize temperature variations of the knife and of the specimen during the cooling cycle. In practice, this stabilization is not perfect. Sufficient cutting regularity is obtained during only part of the cycle. Another major difficulty is to conciliate the requirement for easy access to the specimen chamber with a good protection against contamination by ice crystals formed where the humid air of the room comes in contact with the cold air of the specimen chamber. If this is not done correctly the freshly prepared sections rapidly become unusable. For this reason the specimen chamber is designed to be protected by a laminar flow of cold gas, pushing away all the ice crystals formed above it. This system is reasonably efficient, though it does not provide full protection. Furthermore, it is perturbed each time the operator carries out a manipulation in the specimen chamber. As a consequence, optimum sections of vitrified samples can only be obtained if the operator acts rapidly and minimizes manipulations in the chamber. This requires skill and experience.

Mounting the specimen. Specimens used for cryo-ultramicrotomy are small and only part of them may be vitrified. It is this part that must be correctly positioned and cut. The specimen must be mounted in a secure manner and with good thermal contact. The operation should be easy and rapid in order to avoid unnecessary manipulation in the cold chamber. After having tried several devices we found that the most practical one consists of two jaws, tightly clamped by a screw. A platelet of indium, a soft metal which deforms under pressure, guarantees a good thermal and rigid mechanical contact between the specimen and the holder. The jaws are well adapted for receiving fragments of the flattened frozen specimen obtained from projection on the cold metal block or the pin supporting the specimen frozen with the plunger.

Sectioning. Sectioning can be carried out with a diamond or a good glass knife. Normal diamond knives designed for room temperature operation must be used with caution because the cement holding the diamond is not always made to withstand large temperature variations. Special cryo-knives are commercially available for cryo-ultramicrotomy. Glass knives of adequate quality can be obtained with the procedure originated by Tokuyasu & Okamura (1959) and described in detail by Griffiths *et al.* (1983). Their longevity and cutting quality is improved when they are coated with a thin layer (*c.* 1 nm) of tungsten (Roberts, 1975). The cutting parameters such as knife and clearance angle, cutting speed and stroke time, temperature of the specimen, of the knife and of the surrounding gas all play a role in the cutting conditions but none of them has been found to have a systematic and decisive influence on the section quality.

Picking up the sections. A major difference between cryo-ultramicrotomy of vitrified specimens and conventional sectioning is that the cryosections are not floated on water. They accumulate at the cutting edge, from where they must be removed before they form an inextractable heap of fragments. This is done manually, by touching the section with an eyelash and moving it to the grid. It requires great skill and unusually favourable cutting conditions to pick up the sections one by one at each successive stroke. In most cases it is only some scratched fragment of several sections which can be picked up. They are transferred on to the grid, which is held on a special support in the immediate vicinity of the cutting edge. Because of the small size of the section it is helpful to use grids with a small mesh size coated with a sufficiently resistant carbon supporting film. The transfer of the section may be helped by the effect of an antistatic pistol. Grids carrying sections are placed on a cooled polished metal block on which a similar block is pressed by a screw. This helps to flatten the sections and keep them uniformly cooled and protected. They can then be stored indefinitely by keeping the blocks in liquid nitrogen or they can be transferred directly to the microscope as for grids prepared from suspensions.

Observation. The sections are generally agglomerated in a few regions of the grid. They must therefore first be located and selected at low magnification. The sections also tend to aggregate contaminating ice crystals, in the preparation chamber of the microtome and during transfer. Beginners frequently find that the sections are completely hidden under the ice crystals. These, however, are not

tightly bound and most of them can be removed by the electrostatic effects of a short and strong local illumination. The sections are generally not flat. The irregularity of the topography is not evident on a single micrograph but it is revealed on stereo pairs. This effect has to be taken into account when recording images with minimum irradiation because it may introduce excessive focus change between the focusing and the recording area.

5.3 Cutting artifacts

Most cutting artifacts observed in vitrified sections are well documented from conventional work with plastic (Hayat, 1970). They are, however, more pronounced. They will be described separately before conclusions on the cutting mechanism and possible ways of improving section quality are discussed.

Deformation. All sections are deformed by the cutting process. In general, this corresponds to 30–60% reduction of the original dimension along the cutting direction whereas the dimensions are conserved in the perpendicular direction, in the plane of the section. As the volume of an hydrated biological specimen does not vary when it is deformed, the reduction of the length along the cutting direction must correspond to an increase in the section thickness. The amount of deformation varies from place to place and it also depends on the material. It is, for example, more severe than average in lipid droplets and less than average along muscle fibres. Deformation does not depend significantly on the sectioning speed and temperature. Some observations have shown that it is less severe in specimens in which the water is in cubic crystals than when it is vitrified. It is also strongly influenced by the thickness of the section; the thinnest sections being the most deformed. This effect probably limits the possibility of obtaining ultra-thin sections.

Crevasses. The term ‘crevasse’ comes from the similarity of the characteristic microripple observed on most cryosections and the surface of some glaciers. An example is shown in Fig. 17(a), Crevasses appear as a network of lines, approximately parallel to the knife edge – even when the cutting direction is not perpendicular to it. They are found on every non-vitrified section and, to a variable extent, also on vitrified samples. Some materials are more prone to crevasses than others. Pure water or lipid droplets are among the worst. Regions rich in soluble biological material are generally crevasse-free. The most heavily crevassed regions are in the thicker part of the sections. As can be seen in Fig. 17(b), when the section is shadowed with a heavy metal, the surface of the section is very irregular in the crevassed area. Fig. 17(c) shows that the crevasses produce discontinuity in the image of biological structures and therefore must correspond to deep fractures in the sections. We have generally found that crevasses are only on one side of the section, probably on the side which was inside the block before the section was cut. Zierold has shown that, in some cases at least, the crevasses are on the other side (Zierold, 1984) or on both sides (Zierold, 1987).

Chatter. Chatter is a more or less regular variation of the section thickness due to vibration of the specimen in respect to the knife. Its period ranges from less

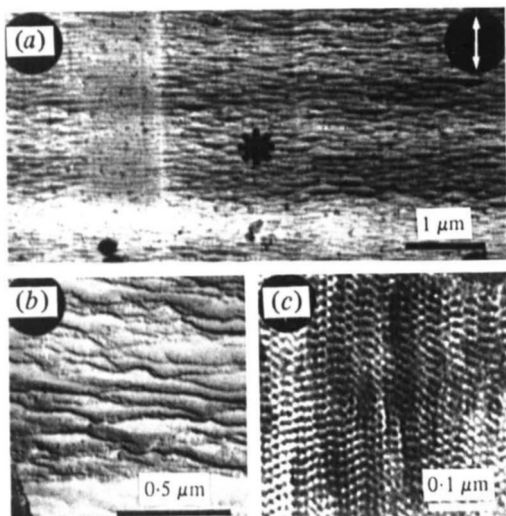


Fig. 17. Crevasses. (a) Cryosection of a 40 % polyethyleneglycol solution. (b) Shadowed section of the same specimen as in (a). Sectioning temperature: -160°C . Section speed: 0.2 mm/s . (c) Section of an unstained catalase crystal. The crystal structure is discontinuous because it is fractured by crevasses. (From Chang *et al.* 1983.)

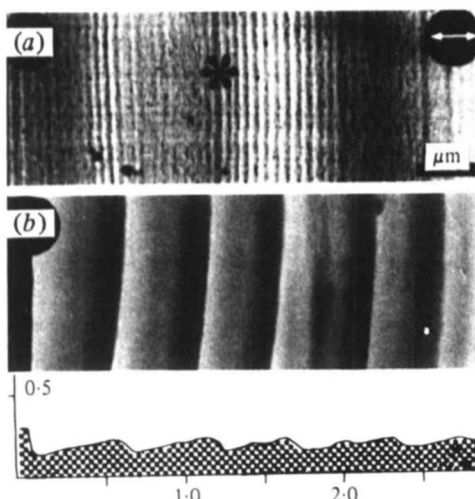


Fig. 18. Chatter in vitrified sections. (a) Solution of 40 % bovine serum albumin. Two modes of vibration with periods of 0.2 and $4 \mu\text{m}$ are superimposed. Sectioning temperature: -160°C . Sectioning speed: 6 mm/s . Thickness: $\geq 120 \text{ nm}$. (b) Saw tooth in a section of pure vitreous water. Sectioning speed: 0.2 mm/s . (c) Representation at the same scale of the thickness of the section shown in (b).

than $0.1 \mu\text{m}$ to several micrometres. Examples are shown in Fig. 18. Chatter is due to an insufficiently tight mounting of the specimen in the holder or to some other instrumental vibration around the specimen. In some cases, as for example in Fig. 18(b), it is the consequence of the irregular progression of the knife in the specimen; the knife does not move until the accumulated energy allows a sudden

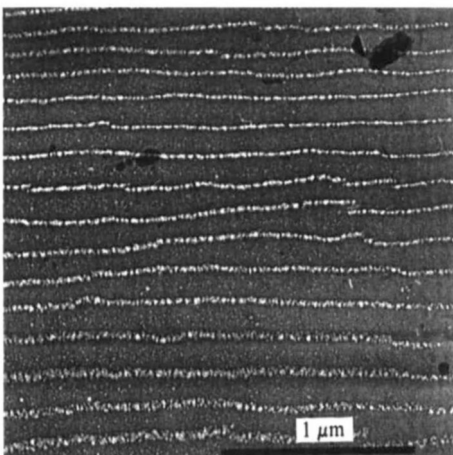


Fig. 19. Cutting induced beam damage in a section of a 35% gelatin solution. Sectioning temperature: -160°C . Sectioning speed: 0.2 mm/s. Thickness: < 100 nm. Electron dose: c. $10^4 \text{ e}/\text{nm}^2$.

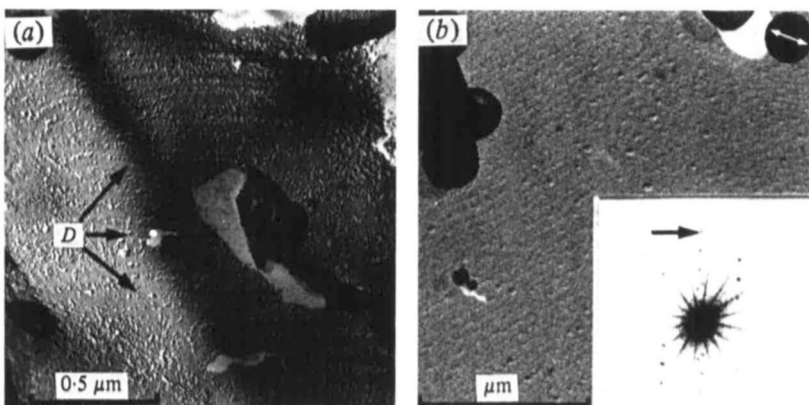


Fig. 20. Surface deformation (*D*) during cutting of a catalase crystal pellet. (a) Shadowed section. (b) Replica of the surface of the freshly cut block. The optical diffractogram shows that the surface deformation reproduces the periodic structure of the catalase crystal down to c. 7 nm (arrow). Cutting temperature: -160°C . Cutting speed: 0.2 mm/s.

jump. This mode of advance produces the frequent but remarkable artifact of *cutting dependent beam damage*, illustrated in Fig. 19. It is characterized by a local sensitivity to the electron beam, which causes bubbling to appear along well-defined lines, always parallel to the cutting edge and with a distribution akin to chatter. In general, the latent effect is not detected before the onset of bubbling. This artifact is probably due to a local transformation of the vitrified sample, making it more prone to bubbling. It is frequently observed in small regions with concentrated biological material and one should be aware not to attribute a biological significance to it.

Surface deformation. The surface of the section, as also that of the block, is

deformed by the cutting process. This effect resembles the plastic deformation in freeze-fracture (Sleytr & Robards, 1977; Lepault & Dubochet, 1980). It is made visible on shadowed replicas of the section or of the block, where the structure of the subjacent biological specimen is revealed. Examples are shown in Fig. 20. In other sections, or parts of them, the effect is not observed and the surface is smooth. *Knife marks* are another form of surface deformation. They are generally more pronounced than in conventional sections because, in most cases, they are only on one side of the section and therefore are not compensated by the complementary relief on the other side. The side on which they are most frequently found is that forming the surface of the block. There are also some occasions where the knife marks are symmetrical on both sides of the section. When this is the case, the two complementary marks appear with opposite contrast and are irregularly shifted, one in respect to the other, thus revealing how much shift and deformation takes place during sectioning.

5.4 The sectioning process

The cutting artifacts are the most conspicuous features of vitrified sections. At first sight they may seem incomparable with those formed in conventional plastic sections but a more careful examination reveals that they also exist in standard sections. They are, however, more severe in water, not so much because the cutting process produces more damage in frozen material, as because the damage suffered by conventionally prepared sections is cured by flotation. This fact can easily be tested when plastic embedded specimens are cut dry at room temperature. Their aspect is then not much different from cryosections (Griffiths *et al.* 1984). There is, however, one property in which sections of vitrified specimens differ fundamentally from other materials. Plastic embedded specimens, as ice crystals, are all elastic solids in the sense that they cannot deform indefinitely before breaking. Vitrified water, on the contrary, is a liquid of extremely high viscosity. If a strong enough force is applied for long enough, it can deform to any extent. This fact is probably reflected in the severe deformation observed in vitrified specimens.

Much has been said on the mechanism of cutting but little is known for sure. Three major theories reviewed in recent papers all have their supporters. (a) Cutting produces a local melting of the specimen. The knife therefore advances on a liquid layer (Thornbury & Mengers, 1957; Sitte *et al.* 1987). (b) The specimen is broken in front of the knife edge in a process similar to freeze-fracturing (Frederik *et al.* 1982). (c) The specimen is deformed and rearranged along the cutting edge as is the case in metal machining (Lickfeld, 1985). In addition to these three cases, the friction of the newly formed section on the knife face is considered to play an important role. The confrontation between these various theories and the observed section is easier in sections of vitrified samples than in conventional plastic embedded material because the former has not been subsequently rearranged by flotation. It then becomes evident that the true phenomenon of cutting involves something from each of these theories. The severe deformation is

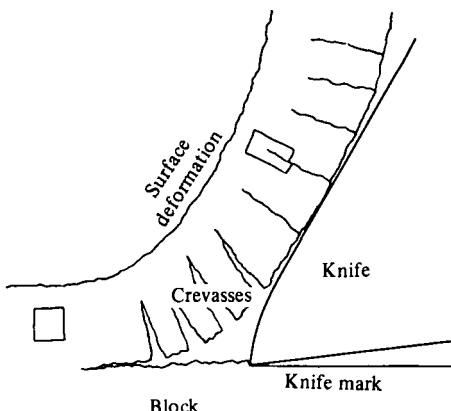


Fig. 21. Tentative schematic drawing of the cutting process during sectioning of vitrified samples.

best compatible with the description of machining. The surface deformation, as also the crevasses, resemble the effects of fracture. The quality and smoothness of some sections together with the fact that vitreous water is a liquid with high viscosity, favour the theory that the knife is gliding on a viscous surface, though the whole section thickness is certainly not liquefied in the common sense of the term. Also the phase diagram of water shows that, however high the applied pressure may be, crystalline ice cannot be liquefied below -22°C . All these data are incorporated in Fig. 21, leading to a schematic view of what the cutting process could be. Other schemes have also been proposed (Zierold, 1987). They certainly also contain a part of the truth.

Several avenues can be envisaged in order to improve ultracryomicrotomy of vitrified samples and reduce cutting artifacts. First of all there is a requirement for more systematic testing of the cutting parameters and, in particular, the role of the temperature. The domain of very low temperature (below -160°C) has not yet been explored. On the opposite side, the domain of the high temperature, just below the actual devitrification temperature of the specimen, has shown some promise.

Another approach consists of searching for substances which modify the properties of water, making it more suitable for good sections. It has already been observed that many substances make vitreous water more brittle and more prone to crevasses. On the contrary, sucrose has a favourable effect. Other substances could be even more beneficial.

We have also searched for a liquid, on which the section could be floated. However, those substances which are still liquid below -120°C cannot have strong molecular interaction and have therefore a low surface tension. In all cases tested the sections did not float on the liquid but sank in it. Here also we still see some chance of finding an adequate solution close to the devitrification temperature.

Decreasing the knife angle seems an obvious method of reducing deformation and some other artifacts. The method has been tested with success on plastic

sections at room temperature (Jesior, 1987). Preliminary tests on vitrified sections have not yet yielded encouraging results, even though the knife angle was as small as 26° (McDowall & Gnägi, private communication).

6. SUSPENSION

The phenomena which take place when liquid suspensions are made into thin films for electron-microscopical observation are dominated by surface tension and diffusion. These effects are very different in the micrometre range from those we are accustomed to observe at human size. A brief refresher could be useful for the cryo-electron microscopist. Some similar considerations are presented in other articles (Kellenberger & Kistler, 1979; Kellenberger *et al.* 1986*b*; Dubochet *et al.* 1982*b*) but the basic material can be found in any textbook on physical chemistry (Tanford, 1961; Eisenberg & Crothers, 1979; Cantor & Schimmel, 1980). The method for preparing thin vitrified films of suspension is described in Dubochet *et al.* (1982*c*), Lepault *et al.* (1983*a*), Adrian *et al.* (1984), Dubochet *et al.* (1985) and Lepault & Dubochet (1986*a*).

6.1 Surface tension

Water has a high surface tension because the strong and specific network of bonds established between molecules in liquid water is broken at the surface. More bonds must be broken when the surface area is increased and energy must be put into the system. This energy is called surface tension, γ . In order to minimize its surface energy, a liquid tends to reduce its surface-to-volume ratio. This is why water droplets are spherical or why their formation first requires a nucleation event. The interfacial tension between water and another substance depends on how water molecules combine to the other substance and this may be smaller than for the liquid alone. For example, the interfacial tension between water and octane is high, because no strong bonds can be established between the two species. Octane is therefore hydrophobic and insoluble whereas n-octyl alcohol, which can form hydrogen bonds with water, has a low interfacial tension and is miscible. Lipids reduce the surface tension of water because their polar heads bond with the water dipoles whereas their hydrophobic tails, which do not interact with water, tend to form a new surface layer. The interfacial tension between a liquid and a solid also depends on the molecular properties of both substances. The solid is said to be hydrophilic if water spreads on it, whereas it is hydrophobic if it does not. A more quantitative description is schematized in Fig. 22. It considers the surface tension of the liquid γ_l and of the solid γ_s , as also the interfacial tension γ_{sl} . The Young condition gives the equilibrium condition: $\gamma_{sl} + \gamma_l \cdot \cos \theta = \gamma_s$. Perfect wetting conditions are obtained when the wetting angle θ is zero. In fact, wetting is a much more complicated and interesting phenomenon than inferred from this simple equation. A very thin precursor film, which may be only a few molecules thick, rolls first on the surface, preparing the movement of the bulk liquid. The flow of the precursor film involves large relative velocities and strong

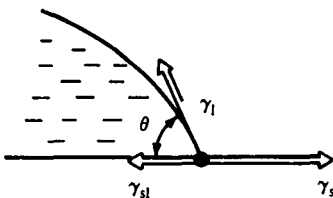


Fig. 22. Interfacial tension of a liquid on a solid. The Young condition states that, at equilibrium, the surface tension of the solid, γ_s , of the liquid, γ_l and of the interfacial tension, γ_{sl} , are related by the relation $\gamma_{sl} + \gamma_l \cos \theta = \gamma_s$, in which θ is the wetting angle.

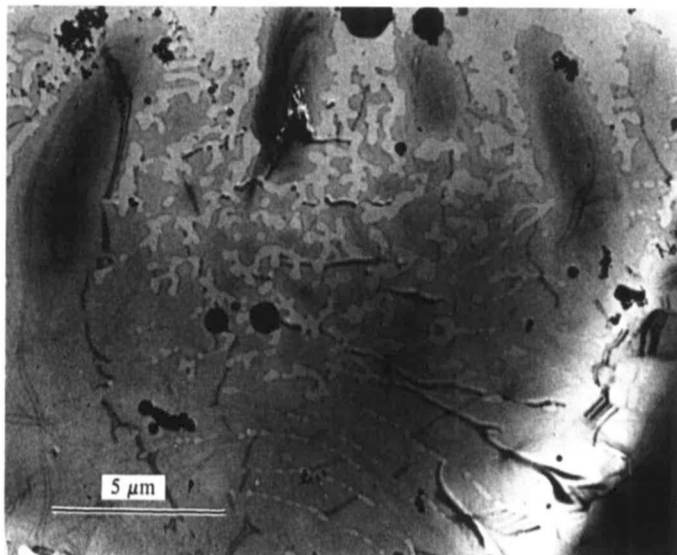


Fig. 23. Laborious spreading of a water microdroplet on a partially hydrophilic carbon supporting film. Microdroplets of pure water were produced in a nebulizer and the specimen was frozen by immersion in nitrogen slush, 0.12 s after deposition (From Dubochet *et al.* (1982c), with permission.)

effects of viscosity. As a consequence, the wetting edge does not advance in a straight line but has a complex progression, looking for the geometry of least resistance (De Gennes, 1984, 1985) in a manner similar of the growth of an ice crystal in a concentrated solution. An example is shown in Fig. 23.

Some quantitative values help to give an idea of the magnitude of the surface effects. The surface tension of water is $7.2 \times 10^{-2} \text{ J m}^{-2}$. The additional pressure, Δp , that surface tension produces in a spherical droplet of radius r is given by $\Delta p = 2\gamma/r$. For a 2 mm drop, Δp corresponds to a mere 14 cm water column, but it becomes 140 bar if the drop has a radius of 10 nm. Similarly, the forces involved in increasing the surface energy when a film 0.1 μm thick is formed correspond to a hydrostatic pressure of 14 bar in the film. The surface energy is also increased by the order of γS , when a hydrophilic particle of surface S is removed from its aqueous environment. For a 20 nm particle this corresponds to 13 Mcal/mol. It must be kept in mind that this large amount of energy is involved each time water is removed from a soluble particle, independently of the method used for drying;

the final energy balance is the same after air-drying, freeze drying or critical-point preparation and some form of collapse must also be expected with these methods (Kistler & Kellenberger, 1977).

As compared to surface tension, other forms of energy, which are important in everyday life, become negligible at microscopic scale. For example, the gravitation forces acting on a $0.1\text{ }\mu\text{m}$ film are 10^9 times smaller than those due to surface tension. Kinetic energy does not produce many effects either. We realized this when trying unsuccessfully to use the kinetic energy of microdroplets to help spread them on a carbon support (Dubochet *et al.* 1982c). We could have spared the experiment because a simple calculation shows that the kinetic energy in a water droplet of $2\text{ }\mu\text{m}$ diameter projected at 10 m/s in a nebulizer is only sufficient to increase its surface by 0.001% !

6.2 Diffusion

Brownian motion and stochastic particle diffusion can be estimated on the basis of diffusion theory. The average displacement x , during the time period Δt is given by the relation $X^2 = 6D\Delta t$, in which D is the diffusion coefficient. For spherical particles of radius r the diffusion coefficient has the value: $D = kT/6\pi\eta r$, where $k = 13.8 \times 10^{-24}\text{ J}/^\circ\text{C}$ is the Boltzmann constant, T is the temperature and η the viscosity, which has a value of around one centipoise (10^{-2} N s/m) for pure water. It can also be inferred from the sedimentation coefficient s using the relation $D = RTs/M(1-v\rho)$, where $R = 8.31\text{ J}/^\circ\text{C mol}$ is the gas constant, M is the molecular weight, v is the partial specific volume of the particle in solution and ρ is the solvent density. From this data the average time τ needed by a globular biological particle of radius r to move over its diameter, or to rotate on itself (relaxation time), can be estimated to be around $\tau = 4\pi\eta r^3/kT$, which corresponds to an order of 3 ns for glucose molecules, $1\text{ }\mu\text{s}$ for a small protein (BSA) and 1 ms for a small spherical virus. Similarly, these particles are likely to meet the surface of a $0.1\text{ }\mu\text{m}$ film within $5\text{ }\mu\text{s}$, $20\text{ }\mu\text{s}$ and 1 ms for the sugar molecule, the small protein and the virus respectively, if no other surface force is present.

6.3 Preparation on a supporting film

The preparation of the thin liquid film for vitrification is tricky because of the unfavourable surface-to-volume ratio and the rapid evaporation of the liquid. Inexperienced workers tend to obtain specimens which are either dry or too thick for observation. A good starting point is a perfectly hydrophilic supporting film (contact angle = 0°) allowing a regular, thin coverage of the surface. This requirement is, however, more severe than what is generally understood by the word hydrophilic. Spray freezing provides a good test. The method has been described previously (Dubochet *et al.* 1982c). It consists in spraying microdroplets from a nebulizer on a supporting film while it is falling towards the cryogen. Depending on the surface properties of the support, the droplets may remain compact or spread more or less rapidly. Freezing interrupts the

process after a time period ranging from 10^{-3} to 1 s. Perfect hydrophilicity leads to microdroplets without visible edge; the thickness of the liquid decreases uniformly towards zero. A somewhat less effective spreading results in the laborious development of the film depicted in Fig. 23. Without special precautions, most droplets spread even less, leaving a thick layer of useless aggregates after freezing or drying. Many methods are in current use for obtaining hydrophilic films for conventional preparations (Review in Dubochet *et al.* 1982*b*). They include treatment with surface-active agents, cleaning with a solvent, glow discharge in air, or simply using the films shortly after they have been prepared. The requirement for perfect hydrophilicity described above requires more caution. Glow discharge is the only practical method we know to achieve it simply and reproducibly. It requires a clean glow-discharge apparatus and its effect lasts only for a period of seconds.

Some of the solutions which have been tried with limited success for preparing thin frozen films of solutions include sandwiching the liquid layer between carbon films (Taylor & Glaeser, 1974, 1976; Jaffe & Glaeser, 1984), slowing down evaporation speed by preparing the specimen in a humid chamber (Taylor, 1978) or removing the water excess by partial freeze-drying in the microscope (Heide & Grund, 1974; Taylor *et al.* 1975). More practical success was obtained by forming the film under an oil layer (Hayward *et al.* 1978; Chang *et al.* 1985), which helps to keep the liquid film uniform and reduces its evaporation. It seems likely that the preparation on carbon films treated by glow discharge in alkylamine, which, in our hands, gives the best and most reproducible results (see below, How to Operate; Dubochet *et al.* 1982*c*; Lepault *et al.* 1983*a*), also rely on the sandwich principle. In fact, the film treated by glow discharge in alkylamine appears hydrophobic at first contact with the water but, after a drop has been forced on to it, it behaves in a hydrophilic manner. Glow discharge probably covers the carbon film with an amphiphilic layer and the water film is stabilized when it is sandwiched between it and the carbon film (Dubochet *et al.* 1982*b*).

6.4 *The bare-grid method*

It came as a surprise when it was found that the easiest way to obtain a thin water film is to stretch it, without any support, over the holes of a grid or those of a perforated film, otherwise used as support for ultra-thin carbon film (Adrian *et al.* 1984). Obviously, the unsupported water film is not stable. Surface tension and evaporation cause it to break. However, the last phase of the process, when the film thickness is in the $0.1 \mu\text{m}$ range, seems to last for the best part of a second. This leaves enough time to form and vitrify the uniform thin film, either by pipetting away the excess water or by removing it with blotting paper (see § 10, 'How to operate'). Unsupported films can be obtained with pure water on a clean grid but they are easier to prepare in the presence of additional substances such as detergents or lipids, probably because they reduce the surface tension at the liquid-air interface. In fact, it seems unlikely that a clean water surface can never be obtained in the usual environment of an electron-microscopy laboratory.

Similarly, most molecules in solution tend to react with the high-energy water surface. They influence the conditions under which the thin unsupported film can be prepared. It is not yet clear why the formation of a thin unsupported water film is at all possible. It has, perhaps, something to do with repulsion forces acting between the two surfaces. Furthermore, breaking starts with the fusion of the two opposing surfaces. The process may be difficult to initiate. It also requires the displacement of a relatively large amount of liquid in the thin film, against the resisting action of viscosity.

Biological particles observed in a thin vitrified film of solution are free of all the classical preparation artifacts, such as those due to chemical fixation, dehydratation, staining and adsorption on to a supporting film. Nevertheless the thin vitrified specimens cannot merely be considered as a faithful representation of the initial solution. Vitrification itself is hardly a disturbing factor but partial evaporation of water during preparation and surface effects can have a profound influence. As a matter of fact, surface effects have been responsible for the most intriguing observations we have made since the method has been working routinely.

6.5 Evaporation

Some evaporation always takes place during the preparation of the specimen. When the liquid film is thin, this leads to a significant increase in solute concentration. The water activity decreases accordingly, thus reducing evaporation rate and facilitating the preparation of a thin layer of suspension (Hayward *et al.* 1978; Jaffe & Glaeser, 1984). In principle, this method is analogous to that introduced in the now classical study of the purple membrane (Unwin & Henderson, 1975), further used with several biological crystals to preserve their 'hydrated state' by the presence of sugar or of other substances (Chiu, 1982; Rachel *et al.* 1986).

The thin film vitrification method, described in this section, consists in avoiding evaporation as much as possible, not only in order to keep the biological particles sustained by the surrounding water but also to preserve the physical-chemical properties of the medium. Some evaporation is, however, difficult to avoid and it produces an increase in solute concentration during the last phase of specimen preparation. The effect is important when the specimen is prepared by pipetting or blotting the excess water from the side of a supporting film. The formation of the thin film then takes several seconds and during this time the solute concentration in the thinnest parts of the film may reach any value including complete drying. Much better is the situation with unsupported liquid films prepared by direct blotting, because the total preparation time is only in the order of 1 s and the liquid layer is more mobile, thus partially avoiding build-up of local concentration.

Evaporation can be measured quantitatively. One method consists in comparing the mass of the thin vitrified layer of a known specimen before and after freeze-drying. The measurements are made from the optical density of the micrographs.

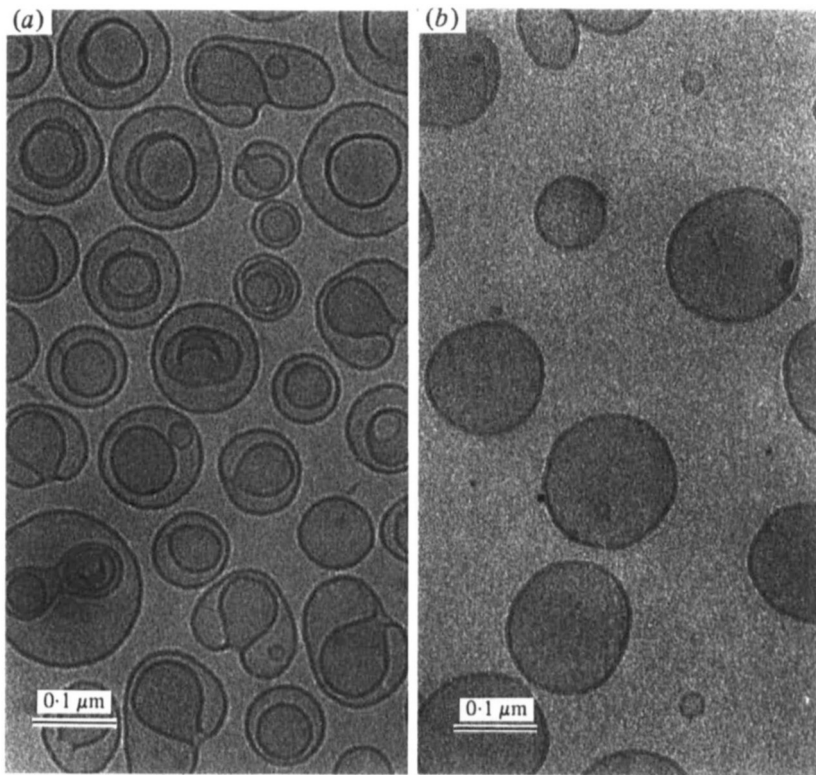


Fig. 24. Solution of lipid vesicles in 100 mM-NaCl. (a) The specimen has been prepared by the bare-grid method under conditions where part of the water evaporates before the thin film is vitrified. Invagination of the vesicles and formation of concentric vesicles reveal the osmotic effect due to the rapidly changing salt concentration in the liquid. (b) The same sample prepared in saturated humidity does not show osmotic effects.

The method is rapid and easy to perform (Euseman *et al.* 1982; Dubochet *et al.* 1983*b*). It can also be used with unsupported film, provided the concentration of solute is high enough to leave a continuous film after drying (around 5% in most cases). An alternative method consists in measuring the contrast of known particles in a known solution of heavy salt. For example, polystyrene spheres ($\rho = 1.05 \text{ g cm}^{-3}$) have no contrast in a 17% (w/w) solution of caesium chloride ($\rho = 1.12 \text{ g cm}^{-3}$ at room temperature, corresponding to 1.05 g cm^{-3} in vitreous water). They can nevertheless be detected *a posteriori* by beam-induced bubbling. Deviation of the expected contrast is a measure of the change in concentration. An alternative method consists in using small lipid vesicles as osmometers. When the salt concentration is rapidly changing in the thin film, just before vitrification, the lipid vesicles adjust by losing water, while practically no salt has time to cross the bilayer. The volume of the vesicle decreases while its surface remains constant. An invagination results which may develop into two concentric vesicles. A typical case is shown in Fig. 24. Using these methods it was found (Cyrclaff *et al.*, in preparation) that evaporation varies from place to place on a specimen, and that it can easily result in a twofold increase in the concentration of a solution prepared

on perforated grids as described below (see 'How to Operate'). Evaporation can be reduced in every case to less than 30% by simple measures, as for example a shower of humid air flowing along the guillotine or a device holding blotting-papers against both sides of the specimen until shortly before immersion in the cryogen (Cyrclaff *et al.*, in preparation). A humid chamber has also been tested with success by Bellare *et al.* (1986).

6.6 Surface effects

The most severe surface effect takes place when the water surface crosses the biological particle during drying in conventional specimen preparations. As discussed above, the energy involved is considerable. It corresponds to many MJ/mole for an average-sized protein. The result, which has been abundantly documented, is that dry biological particles are severely flattened and collapsed (Kistler & Kellenberger, 1977; Kellenberger & Kistler, 1979; Kellenberger *et al.* 1982; Kellenberger, 1987). This effect does not exist in vitrified specimens. No dehydration energy is involved and the water matrix is preserved. All experiments confirm the expectation that the shape of the particles is well preserved in the water film (Stewart & Vigers, 1986). This has been tested quantitatively in several cases. For example, no flattening was detected by three-dimensional reconstruction of spherical viruses (Vogel *et al.* 1986) or of T4 bacteriophages (Dubochet & Adrian, unpublished). The cylindrical symmetry of the delicate empty polyheads of the T4 bacteriophage, as also some other helical structure, are unaltered (Lepault, 1985). Of course, this only holds true where the liquid film is thicker than the particles. In the example shown in Fig. 25 the T4 polyheads have a well-preserved cylindrical symmetry except where they overlap, at which point the thickness of the film is insufficient.

The fact that the aqueous environment is preserved in vitrified specimens does not mean that there are no surface effects. Particles in water can interact either with the air/water interface or with the supporting film, should there be one. These effects are known from conventional electron microscopy and they have also been used for a long time. For example, in negatively stained preparations, some particles adhere more readily than others to the supporting film (Dubochet & Kellenberger, 1972) and others are adsorbed with preferential orientations (van Heel, 1981). The famous Kleinschmidt method for visualizing nucleic acids (Kleinschmidt & Zahn, 1959) and its successors (Brack, 1981) also relies on specific adsorption on to a layer of surface-denatured proteins. The surface effects taking place in the liquid are frequently conspicuous in vitrified specimens because they are not hidden by more brutal forces. In particular, the possibility of preparing specimens in absence of a supporting film, allows much more subtle rearrangements of the mobile particles under the action of the surface forces. Some examples are given below.

The micrograph reproduced in Fig. 26 is an unsupported preparation of partially dissociated adenovirus, showing a large number of groups of nine (G9) which, in the virus, form the central part of each face. Depending on their

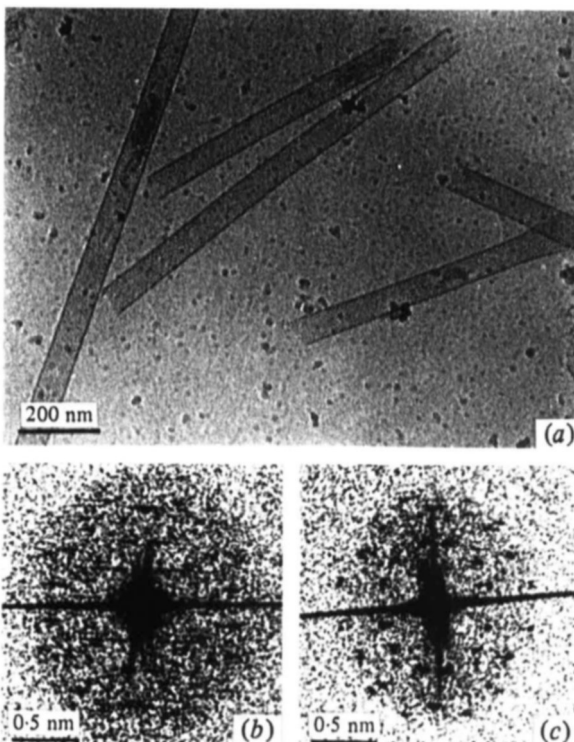


Fig. 25. Polyheads of the T4 bacteriophage. (a) Prepared in a c. 100 nm thick layer of vitrified solution. Two particles are flattened at the point where they are superimposed. (b) Optical diffractogram of a particle shown in (a). It is characteristic for a cylindrical particle. (c) Optical diffractogram of a particle embedded in a vitrified layer, much thinner than the particle diameter. It is characteristic of a flattened particle. (From Lepault (1985), with permission.)

orientation, the G9 should appear right- or left-handed. Surprisingly enough, only left-handed are visible in the figure. Why is this the case when, at first sight, one would guess that they are in a symmetrical situation between the two surfaces of the thin film? The only explanation we can propose is schematized in Fig. 27. It implies that the specimen observed in Fig. 26 is not a faithful representation of the bulk solution but only of its surface. A similar surface-effect takes place with most suspensions. As a result the density of particles in the vitrified thin film does not correspond to the concentration in the bulk solution. It may be higher if the particles tend to adsorb to the surface or lower in the opposite case. Discrepancies by two orders of magnitude are not infrequent. In this respect, lipid vesicles are remarkable. It may be observed, for example, that a high concentration of lipid vesicles are observed in a thin film made from a 10 mg/ml solution but that practically no particles are observed at half this concentration. One possible explanation is that the vesicles left in the thin film fuse with the freshly formed air/water interface until a monolayer is formed on the surface. Vesicles observed in the specimen are only those left in the liquid after the surface is fully covered or after vitrification has put an end on the phenomenon.

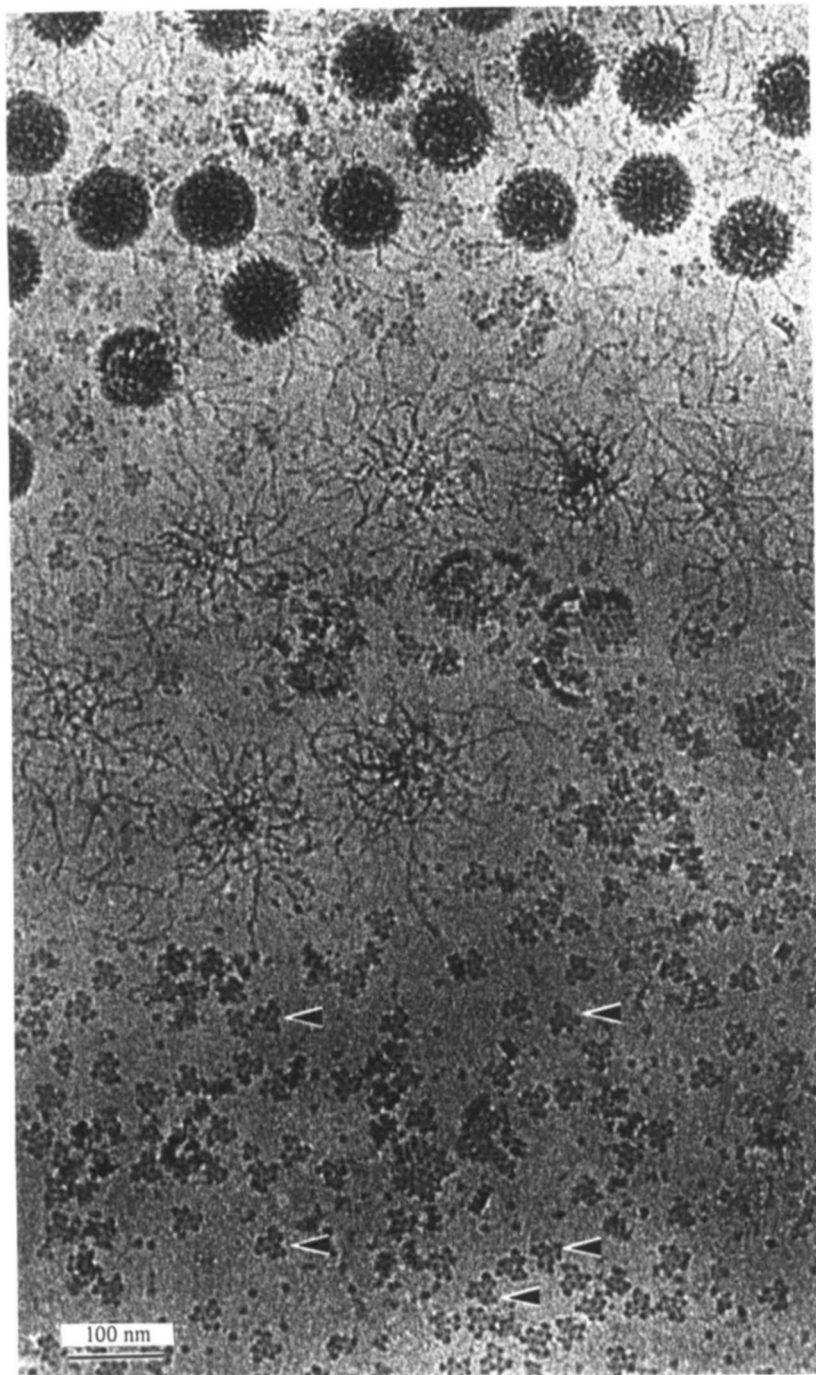


Fig. 26. Thin vitrified layer of a solution of partially disrupted adenovirus. Many groups of nine (G9) are visible; some have been marked by an arrow. (From Dubochet *et al.* 1985.)

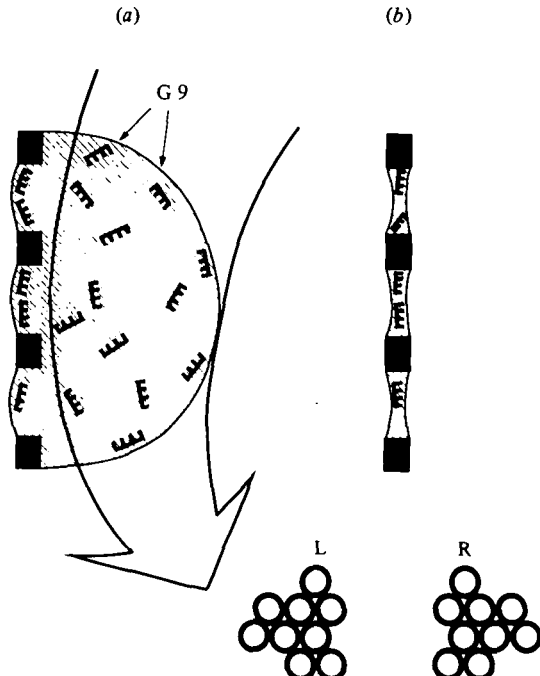


Fig. 27. Schematic explanation for the asymmetry of the G9 observed in Fig. 26. Depending from which side they are observed, the G9 are seen as L or R. When the drop of suspension is put on the grid, those G9 which are close to the surface take a fixed orientation (a). Removing most of the drop from one side leaves a sample which only represents the left-side of the bulk sample (b). (From Dubochet *et al.* 1985.)

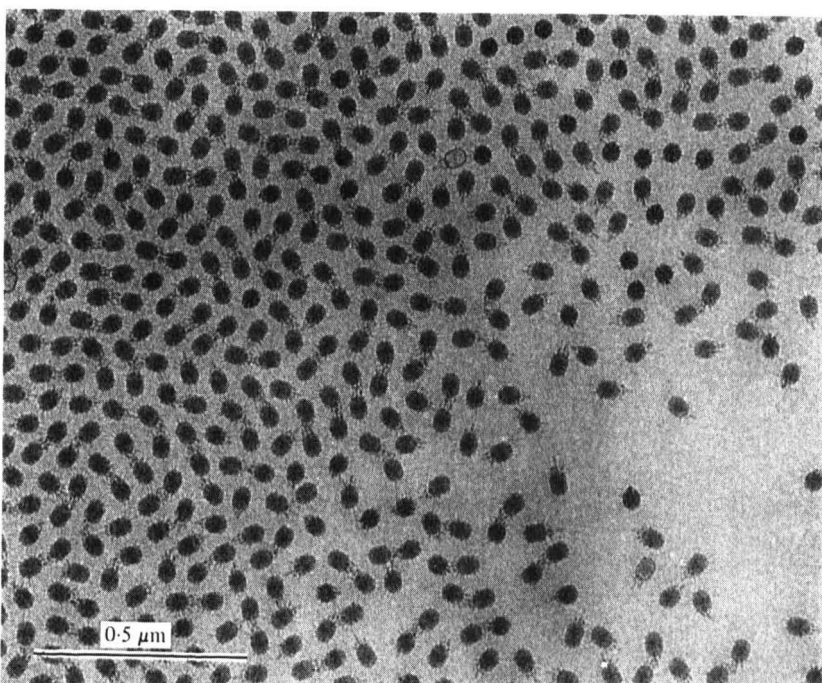


Fig. 28. Thin vitrified layer of $\phi 29$ bacteriophages, prepared on a perforated carbon film. The viruses, rejected from the thinnest central part of the grid hole (above right corner), are concentrated at the edge where they form a loose hexagonal packing.

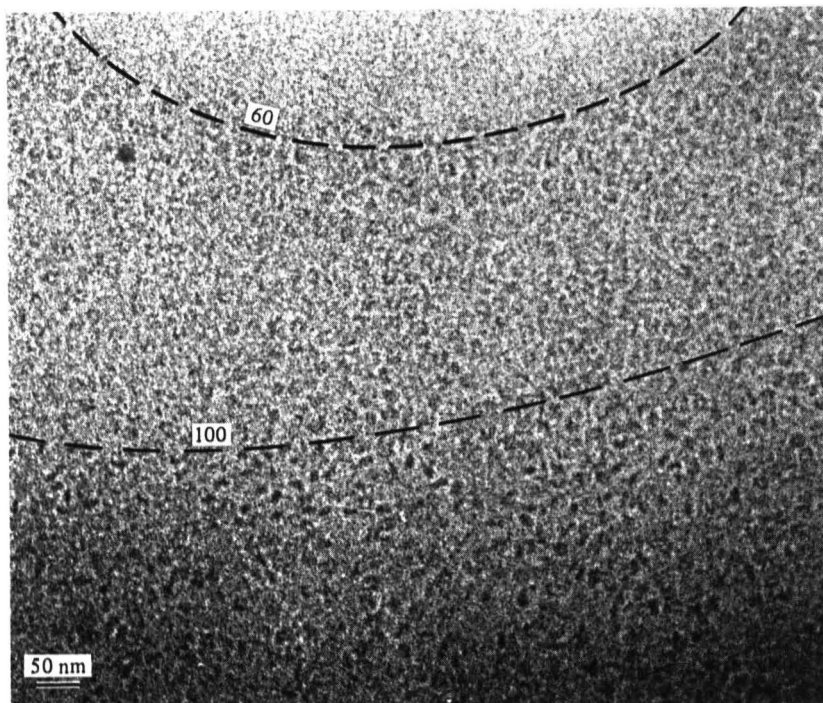


Fig. 29. Isolated nucleosomes prepared in presence of negatively charged lipids in 100 mM-NaCl. The repulsive effect of the negatively charged surface layer has expelled the nucleosomes from regions where the film is thinner than c. 60 nm. The nucleosomes are all aligned parallel to the surface where the thickness is between 60 and 100 nm. They seem to be randomly orientated and unaffected by the surface in thicker regions.

In the bare-grid method the particles are not uniformly distributed over the surface of a hole. They are repelled from the centre, where the film is generally the thinnest, and are concentrated at the edge, where they frequently rearrange into ordered structures. An example is shown in Fig. 28.

In the examples given above it is the concentration and the orientation of the particles which are influenced by surface effects, but the structure of each individual particle remains apparently unaltered. This suggests that the forces involved in the interaction with the surface are small compared to those defining the structure of the particle itself. One notable exception has been observed with chromatin and with nucleosomes. Under some conditions, chromatin fragments fuse into a 'sea of nucleosomes' when they are squeezed in thin regions of the liquid film. In other cases isolated nucleosomes which otherwise appear as small disks c. 10 nm in diameter (Dubochet *et al.* 1986), are unwrapped into short, c. 4 nm wide filaments (Schultz *et al.*, in preparation).

Recently it became possible to control the surface effects by the addition of surface-active agents to the solution (Schultz *et al.*, in preparation). The most reproducible results have been obtained with lipid vesicles. They fuse with the surface of the specimen, thus forming a layer of controlled charge, reducing surface tension. It is then possible to preserve the delicate structure of 30 nm

chromatin filaments and of nucleosomes by preparing them in the presence of neutral lipids. Isolated nucleosomes also remain intact when they are prepared between two negatively charged surfaces. They are, however, repelled away from the surface and are concentrated in the middle of the film. An example is shown in Fig. 29. The nucleosomes have been rejected from the central region of the hole, where the film is the thinnest. In intermediate regions, where the film is 60–100 nm thick, the interaction with the surface is still strong enough to orientate all the nucleosomes in the plane of the film. In still thicker regions the nucleosomes are randomly orientated, showing that the energy involved in the interaction with the surface is not sufficient to hold the nucleosomes in their random thermal motion.

7. CRYOSPECIMEN HOLDER

The devices for observing cold specimens by electron microscopy are as numerous as they are diverse. Since the first report was published in 1954 (Leisegang, 1954), new systems are presented at every major electron-microscopy conference. Some of them are only simple modifications of standard specimen holders, others are all new instruments of great cost and complexity (Fernandez-Moran, 1966). Among these profuse offers (Heide 1982*b*) the choice of the best system for practical work with vitrified biological specimens may seem difficult. This is, however, not so if the requirements are clearly set. They are: (*a*) operation temperature around -160°C , (*b*) good resolution, (*c*) possibility of transfer of vitrified specimens, (*d*) low contamination, (*e*) ease and speed of operation, (*f*) reasonable price.

Several designs of cryospecimen holders fulfil these requirements, others have been found unsuitable for the work with vitrified specimens. The choice of the best system and its optimal use requires a good knowledge of the working principle as also of the technical pitfalls encountered in their construction and use. This is the subject of the present chapter. The discussion is based on a side-entry holder cooled by metal conduction (Fig. 30) as is the case for the Gatan system (Gatan, Pittsburgh, USA). Other systems are discussed by comparison.

7.1 Heat transfer

The temperature of the specimen (T_2) in the cryo-specimen holder depicted in Fig. 30 results from the cooling effect of liquid nitrogen ($T_1 = -196^{\circ}\text{C}$) acting through a conductive metal rod and of the heat coming from the warm surrounding (T_3) through direct contact, through the surrounding gas or by thermal radiation. The electron beam can also bring a significant amount of heat. The various effects are discussed below.

Conduction through a solid. Heat conduction through a solid, w_c , is locally proportional to the section S and to the temperature gradient: $w_c = \lambda_c S(dT/dx)$. The proportionality factor, $\lambda_c(T)$, is the thermal conductivity. It depends on the temperature but for most solids it does not vary by more than a factor of two between room and liquid-nitrogen temperature. Some values are given in

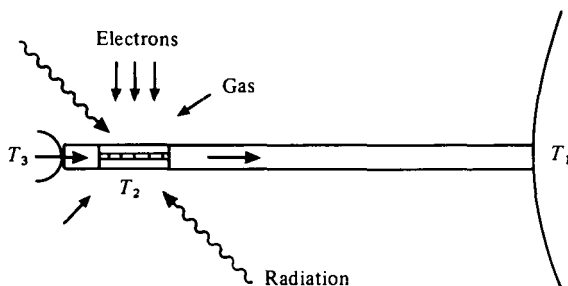


Fig. 30. Schematic representation of a side-entry cryospecimen holder cooled by conduction in a metal rod. The temperature T_2 of the specimen results from the balance between the cooling of the liquid nitrogen at temperature T_1 , -196°C , and the heating from the warm surrounding, acting by direct contact with surfaces at room temperature, T_3 , by gas conduction, by radiation and by the energy brought with the electron beam.

Table 3. Thermal conductivity λ_c , expressed in $\text{W}/\text{m} \cdot ^\circ\text{C}$, for some solids

	Temperature ($^\circ\text{C}$)		
	-269	-100	20
Stainless steel	0.24	9.50	15
Copper	240	450	400
Brass	2	47	90
Glass	0.1	0.5	1
Teflon	0.046	0.24	0.26
Nylon	0.012	0.31	0.35

Table 3. The heat flow through the rod of length L and of section S can then be approximated by: $w_c = S\lambda_c(T_2 - T_1)/L$.

Gas conduction. Gas transfers energy to the specimen by laminar or by free molecular conduction, depending on the pressure. At atmospheric pressure it can also act by convection, which is a form of forced diffusion due to gas movement (wind). This latter effect may be important and it should be avoided by preventing the flow of air on to the specimen. It is difficult to estimate and will therefore not be discussed further in this chapter. Laminar or molecular conduction depends on the mean free path Λ of the molecules. By definition, Λ is the average distance travelled by a molecule between two collisions with other gas molecules. It can easily be calculated from the perfect gas theory and, for air, it can be expressed by $\Lambda = 6 \times 10^{-8}/P$, in which Λ is expressed in metres and P in pascals (1 Torr = 133 Pa).

Laminar conduction takes place when the mean free path is much smaller than the geometric dimension of the system. This is the case when the specimen is at atmospheric pressure or in the prevacuum of the specimen airlock. The mechanism is illustrated in Fig. 31(a). In a first approximation this mode of conduction is independent of the pressure. It can be characterized by the

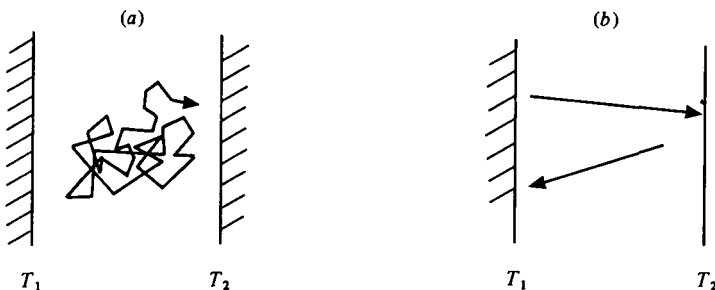


Fig. 31. Principle of thermal conduction by laminar (a) and molecular (b) conduction between the surfaces at temperature T_1 and T_2 .

coefficient of laminar conduction λ_l , which for air has the value $2.5 \times 10^{-2} \text{ W/m.}^\circ\text{C}$ at room temperature and $0.8 \times 10^{-2} \text{ W/m.}^\circ\text{C}$ at liquid-nitrogen temperature.

Molecular conduction takes place when A is larger than the geometrical dimension of the system and therefore when the molecules bounce directly between the warm and the cold surface (Fig. 31b). An important parameter is then the accommodation coefficient α , the ratio of the actual average energy deposited by a molecule hitting the cold surface to the energy it could deposit if all its energy were given. α describes therefore how a molecule is effectively cooled when it hits the cold surface. The heat transfer by the gas is then expressed by $w_m = S\alpha P(T_1 - T_2)/\sqrt{M}$, where M is the molecular weight of the gas. In air, between two fully accommodating surfaces at room and liquid-nitrogen temperature, the energy transfer is 6 W/m^2 at 10^{-2} Pa measured at room temperature. It decreases linearly with decreasing pressure.

Radiation. The heat transfer from a warm surface to a cold surface by radiation is governed by the T^4 relation of the Stefan–Boltzmann Law. For a small cold object on a large warm container it can be expressed by $w_r = S_2 \epsilon_2 \sigma (T_1^4 - T_2^4)$, where $\sigma = 5.67 \times 10^{-8} \text{ W/m}^2 \text{ K}^4$ is the Stefan–Boltzmann constant, S_2 the surface and ϵ_2 the emissivity of the cold surface, which corresponds to the proportion of radiation energy actually received by the surface. It depends sharply on the surface state; a realistic value for a carbon-coated copper grid at liquid-nitrogen temperature could be around 0.03.

Condensation. It has been observed that vitrified specimens crystallize sometime during the rapid condensation of a water layer. This is possibly due to the fact that the condensing water molecules come from warmer regions of the microscope column and bring more energy than can be removed by conduction through the specimen and the holder. For example, the immediate condensation of water molecules of energy corresponding to room temperature into a layer with a mass equal to that of a vitrified specimen at -160°C would raise the temperature of the specimen to -90°C —far above the devitrification temperature.

7.2 Electron-beam heating

Electrons lose energy when they are inelastically scattered in the specimen. On average, this represents about 20 eV each time an electron crosses 80 nm of

biological material and this energy appears as heat in the specimen (see below, beam damage). The warming of a thin film has been calculated and the results tested for various irradiation conditions. It is found to be at most a few degrees for normal working conditions with vitrified specimens around liquid-nitrogen temperature. The situation may, however, be different for large particles attached with bad thermal contact to the supporting film as is frequently the case for contaminating ice crystals or for the whole specimen grid if it is not well fixed in its holder.

7.3 Quantitative estimation

The system, schematically represented in Fig. 30, is used as an example. Further characteristics are: cryogen temperature, $T_1 = -196^\circ\text{C}$ (boiling nitrogen); specimen temperature, $T_2 = -183^\circ\text{C}$; length of the copper bar, $C = 25\text{ cm}$. The surface of the specimen holder is 5 cm^2 , its emissivity ϵ_2 is 0.03 and the accommodation coefficient α is 1 . The copper bar is surrounded by a stainless-steel shroud 20 cm long of 8 mm diameter and 0.1 mm thickness connecting the specimen holder to the microscope wall ($T_3 = 27^\circ\text{C}$). The heat transfer from the tip of the holder is negligible. Applying the data given above to this system leads to the following values:

- (1) heat conduction through the shroud: $W_c = 37 \times 10^{-3}\text{ W}$;
- (2) heat transfer by radiation: $W_r = 450\text{ W/m}^{-2}\cdot\text{S}$, $\epsilon_2 = 7 \times 10^{-3}\text{ W}$;
- (3) heat transfer by residual gas: $W_m = \sigma W/\text{m}^{-2}\cdot\text{S}$, $\alpha = 3 \times 10^{-3}\text{ W}$.

In this case the major part of the heat exchange takes place through the shroud. Heat exchange by radiation or by the electron beam is not negligible, however, if they act on the specimen grid alone as is approximately the case when it is isolated from the rest of the holder by ice crystals. Thus, a 100 kV electron beam of $5\text{ }\mu\text{m}$ diameter with a flux of $1000\text{ electrons/nm}^2\cdot\text{s}$ leaves $3 \times 10^{-4}\text{ W}$ on the grid if it is completely intercepted by a grid bar. The copper grid (diameter: 3 mm ; thickness: $30\text{ }\mu\text{m}$) would warm up at the rate of $c. 0.5^\circ\text{C/s}$. This would have important consequences. However, if the electron beam goes through a thin vitrified film, it loses only a small fraction of its total energy and beam-heating becomes negligible again. This calculation also shows that heat transfer by residual gas or radiation may be important if the grid is not in good thermal contact with the rest of the specimen holder. A radiation shield, as the anticontaminator may be, and an excellent vacuum are therefore important for optimal observation conditions.

7.4 Contamination

Contamination with water is a severe problem in cryo-electron microscopy. There are several reasons for this: Firstly, the cold specimen is an efficient cryopump for water and some other substances which are volatile at room temperature. Secondly, the introduction of hydrated specimens in the electron microscope cannot be done without also introducing some additional water in the specimen chamber. Thirdly, ionic pumps which are frequently used for the specimen

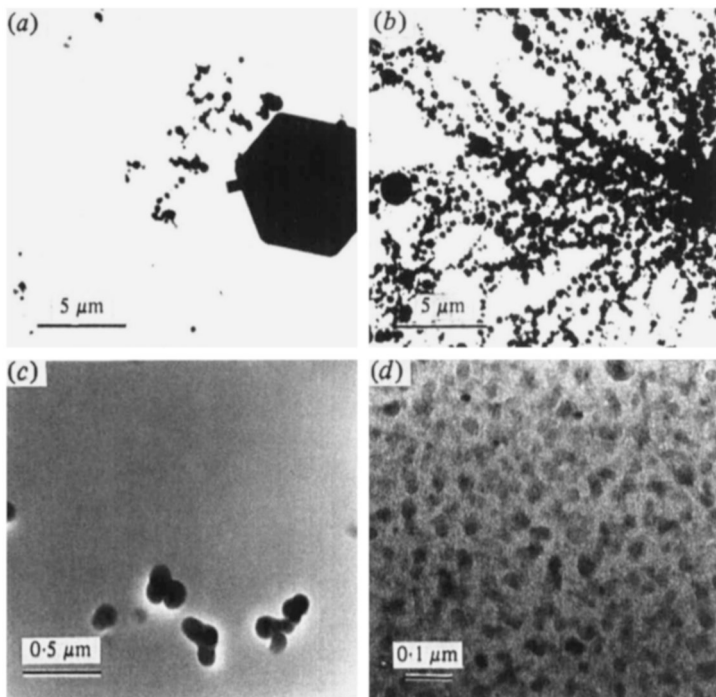


Fig. 32. Various forms of contamination on the specimen. (a) Hexagonal ice crystals formed in humid air and deposited during preparation of the specimen (in particular in the cryochamber of the microtome) and during transfer. (b) Agglomerate of hexagonal ice crystals formed by humid air condensing on liquid nitrogen. (c) Layer of vitreous water deposited in the microscope, on a thin vitrified film. Hexagonal ice crystals deposited on the specimen have been shadowed, thus revealing the contaminating layer and demonstrating that the water molecules came predominantly from one direction. (d) Crystals of cubic ice formed by deposition of water vapour in the microscope in a similar but more rapid way than in (c).

chamber are poisoned with water and may lose their efficiency. All this may result in various disturbing effects which are important to diagnose.

Hexagonal ice crystals are formed in the cold air of the preparation chamber or in the liquid nitrogen used for specimen preparation and transfer. They fall down in the air, like snow, and accumulate on the specimen (Fig. 32a). This effect may be severe in the cryochamber of the microtome where the grids are exposed for many minutes but it also takes place to a lesser extent, during transfer of the specimen into the electron microscope. The ice crystals formed in liquid ethane and liquid nitrogen are frequently smaller. As illustrated in Fig. 32b, they tend to form large agglomerates with the typical shape of diffusion-limited aggregates (Sander, 1986). The contamination formed during preparation and transfer cannot be completely suppressed, but the simple measures described below (see 'How to Operate') reduce it to a level where it causes no practical trouble.

More severe, and more difficult to prevent, is the contamination taking place in the electron microscope by condensation of water vapour. It may originate, in part, from the usual water source of the microscope and in particular from

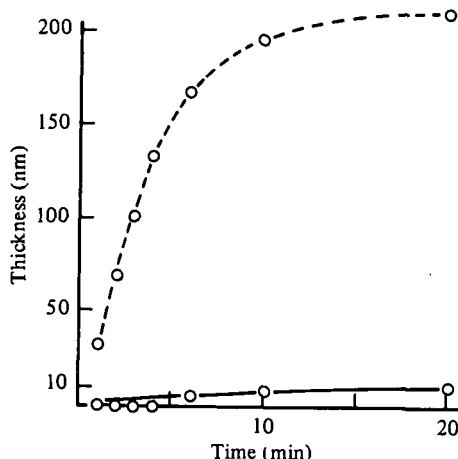


Fig. 33. Building up of a condensed layer of vitreous water on a carbon film transferred from liquid nitrogen into the electron microscope and kept at the lowest possible temperature. The time origin is the moment of insertion of the specimen in the specimen chamber. Temperature: c. -170°C . The dashed line corresponds to a measurement in absence of any anticontaminator. The heavy line was recorded in presence of a double blade anticontaminator as depicted in Fig. 35. (From Homo *et al.* 1984.)

photographic material, but more trouble is caused by the water brought into the microscope during transfer by the specimen holder itself. Typically this effect takes place as follows: During insertion of the specimen into the specimen holder and during transfer, some water of the air condenses on the holder and is introduced into the specimen chamber. This may represent a large amount of water, as, for example, when most of the specimen holder is covered with a visible layer of frost. This ice, however, does not evaporate significantly in the electron microscope as long as its temperature is below -120 or -130°C but, in every specimen holder, there are regions which are cooled at intermediate temperature or regions which were cooled during transfer but are warmed up in the electron microscope. This is the case, for example, for the shroud around the cooling rod of a side-entry specimen holder. The resulting contamination takes place during the first minute after introduction. Examples of contamination kinetics are shown in Fig. 33. Depending on the temperature and the partial pressure of water, the layer may be vitreous (Fig. 32c) or crystalline (Fig. 32d). When it is crystalline it is frequently cubic and the crystal size is in the 50 nm range. The specimen then has a characteristic rough appearance. A vitrified contamination layer is not easily visualized because it has no structure of its own. Nevertheless it increases the specimen thickness and reduces the image quality. The most frequent sign at which a vitrified contamination layer can be recognized is the shadowing effect due to the preferential direction of the contaminating water molecule. It has frequently happened that beginners believe they observe thin layers of vitrified suspension when they are in fact observing particles which have been dried on a supporting film and have been subsequently coated with a layer of condensed vitreous water. The results are accordingly disappointing.

7.5 Anticontaminator

Water cannot be completely removed from the microscope. In fact, every surface which is not very cold is a source of water. The worst is the immediate vicinity of the specimen, where large amounts of water are introduced at each transfer. The anticontaminators of most modern microscopes are designed to prevent molecules that condense at room temperature (as, for example, hydrocarbons from the diffusion pump or solvents used for cleaning) from reaching the specimen. In order to leave more space around the specimen they are generally placed at some distance from it. They are, however, not made to prevent water, originating from the specimen chamber, from reaching the specimen.

An adequate anticontaminator for protecting the specimen from water contamination is described in Figs. 34 and 35. The plans can be provided upon request. This device consists of a cold shroud surrounding the specimen in such a way that, from every point of the specimen, the solid angle through which warm parts of the microscope can be seen is as small as possible but still allows efficient pumping of non-condensing gas around the specimen. Assuming a sticking coefficient of 1 for the anticontaminator and a temperature low enough to make water evaporation negligible, only those molecules coming through the solid angle Ω will contribute to the contamination on one point of the specimen. Contamination is therefore reduced by the ratio $\Omega/2\pi$ (for one side). In fact, this simple description is not correct because the sticking coefficient, which depends on the temperature, is smaller than one. Molecules approaching with other directions may nevertheless reach the specimen after some rebounding. The temperature of the anticontaminator must therefore be below that at which water evaporation becomes negligible (*c.* -130°C), and also below that of the specimen itself. The system shown in Fig. 35 has been found to give good results (Homo *et al.* 1984). It reaches a temperature of -180°C . It is independent of the *X-Y* specimen movement, thus allowing the whole specimen to be observed, though not on one field. It is retractable in order to leave space for tilting the specimen. This can be done, some minutes after introduction, when the vacuum in the specimen chamber is restored.

Some manufacturers have added to the specimen holder a cold shutter just at the top and bottom of the specimen. It protects efficiently during transfer and until the vacuum is restored. It can be retracted from the outside for observation, but when this is done the specimen is no longer protected.

7.6 Stability

Most cryospecimen holders are less stable than the corresponding room-temperature holder. In particular they suffer from thermal drift and from vibration originating in the cryogen. Thermal drift arises from changes in dimension of the material when the temperature varies. This effect can be considerable, as illustrated by the following example: using the geometry of Fig. 30 and assuming that the fixed point at room temperature, T_3 , is at 15 mm from

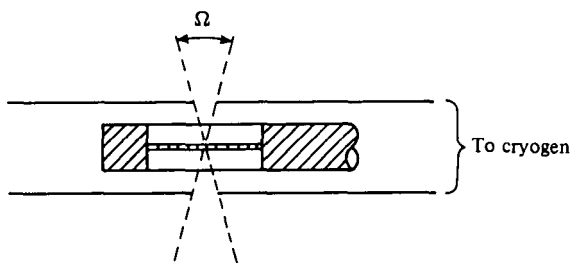


Fig. 34. Principle of a double-blade anticontaminator. Ω is the solid angle in which contaminating molecules can reach the specimen.

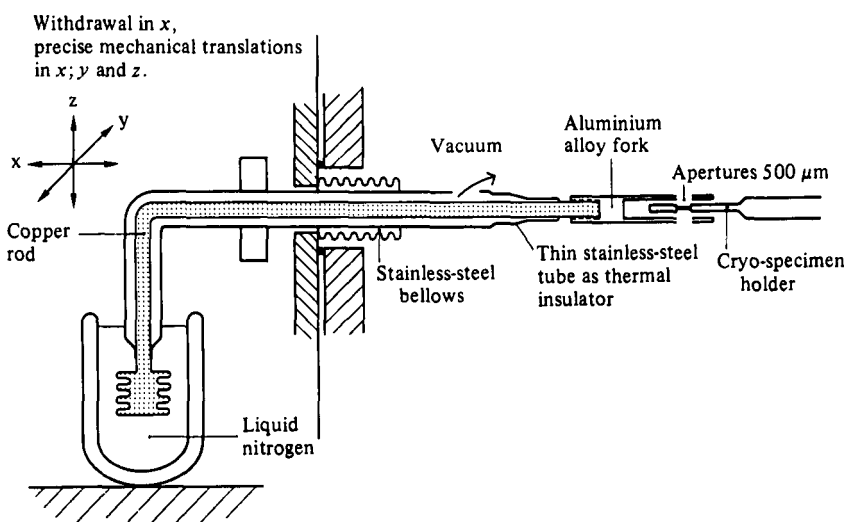


Fig. 35. Double-blade anticontaminator for reducing the condensation of water vapour produced in the vicinity of the specimen. (From Homo *et al.* 1984.)

the specimen, the thermal contraction during cooling of the holder will displace the specimen by *c.* 65 μm if the holder is made of aluminium. In order to reduce this effect, one manufacturer has replaced the connexion at the tip of the specimen holder by a quartz rod, which has a temperature dilatation coefficient 50 times smaller. Another approach consists of maintaining the specimen at a constant temperature during observation. This, however, is difficult because the temperature of the specimen depends on the heat flow coming from the punctual contact at the tip of the holder. This is a poorly defined thermal contact which may vary with each movement of the specimen, thus inducing short-term drift.

Vibration is frequently associated with the exchange of energy which is required for cooling the specimen. For example, in the system schematized in Fig. 30 any forces acting in or on the cryogen recipient, and in particular those due to boiling of the liquid cryogen, propagate along the cooling rod and make the specimen vibrate perpendicularly to the rod. This effect is difficult to suppress because, if the specimen holder is made to be more robust, the increased thickness of the

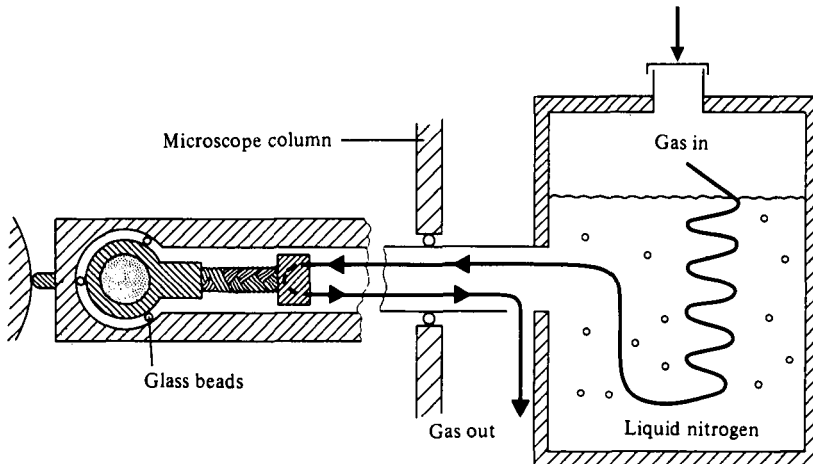


Fig. 36. Schematic view of the gas-cooled cryospecimen holder of the type Philips PW/6591. For a better representation in the drawing, the tip of the holder is rotated by 90° in respect of the liquid-nitrogen recipient. For explanation, see text.

materials act against good thermal isolation of the specimen. A smart system has been designed in the Gatan cryoholder. It consists of suppressing boiling in the liquid nitrogen by excellent isolation of the container. This minimizes evaporation once the equilibrium temperature is reached. The internal wall of the recipient vessel is made of thick conductive material to spread the heat along the surface in contact with the liquid nitrogen. The small amount of heat, flowing from the rod is then exchanged at the surface of the liquid nitrogen, which evaporates without visible boiling. The disadvantage of the system is a consequence of its excellent isolation; it takes a long time to reach equilibrium.

7.7 Other side-entry cryospecimen holders

Side-entry specimen holders can also be cooled by a flow of cold gas. This is the case for the old Philips system PW/6591 (Philips, Eindhoven, The Netherlands), which is unfortunately no longer commercially available. It is schematized in Fig. 36. In this system the liquid nitrogen is boiling in a container outside the electron microscope, thus building up pressure for blowing cold nitrogen gas through a thin pipe to a heat exchanger close to the specimen. The specimen itself is mounted in a small copper support fixed by three glass beads into the tip of the specimen holder. This system has two specific advantages. Firstly, the border between the cold and the warm region of the specimen is formed by the three glass beads placed symmetrically around the specimen. In principle, long-range thermal drift is therefore suppressed. Secondly, cooling by gas flow is very rapid because the mass and the size of the cold part is small. Good working conditions can therefore be reached within minutes of introduction. Cooling by gas flow has, however, the drawback of causing turbulences and therefore vibrations in the immediate vicinity of the specimen. Experience has shown that, with some precautions, this effect can be kept within acceptable limits.

An interesting idea developed recently consists in replacing the metal rod for

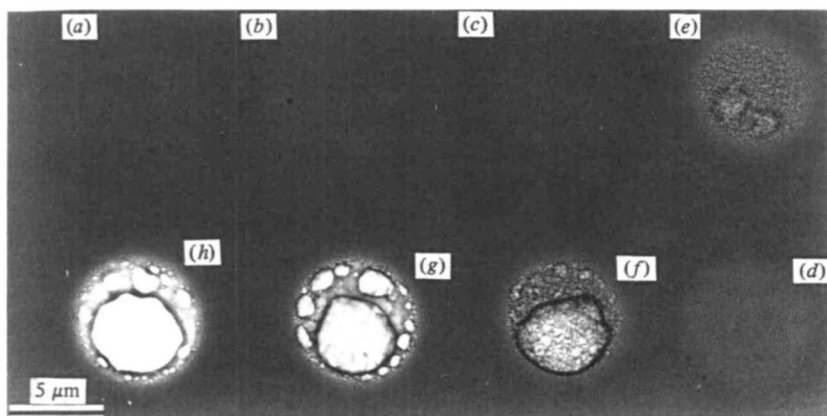


Fig. 37. Bubbling on a carbon-coated formvar film c. 10 nm thick, covered with a layer of condensed vitreous water. Fields (a)–(h) correspond to irradiations by 5, 20, 40, 80, 120, 240, 340 and 450 keV/nm² respectively. The total thickness of the specimen is 160 nm.

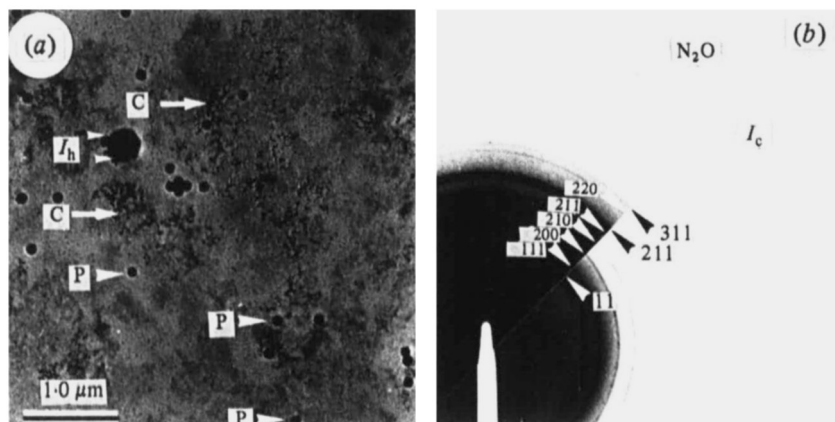


Fig. 38. Beam-induced formation of nitrous oxide crystals from a carbon-coated collodion film covered with a layer of cubic ice. The dose given is 4 keV/nm² and the temperature is –160 °C. (a) Direct image. C, Crystals of N₂O; P, polystyrene spheres; I_h, contaminating hexagonal ice crystal. (b) Electron diffractogram of the same field showing a powder diffractogram with the ring of cubic ice and N₂O. The (211) reflection of cubic ice I_c corresponds to 0.224 nm. (From Dubochet *et al.* 1982a, with permission.)

thermal conduction by a heat pipe (Jakubowski, 1985). This device transfers heat in closed circuit by capillary flow of a liquid cryogen from a cold source, where the liquid is condensed from the gas phase, to the warm source where it evaporates. As compared to the copper rod of equal sections, a heat pipe is in principle capable of a 600-fold increased thermal conduction. Thermal stability could then be reached very rapidly in the specimen.

7.8 Top entry

A number of top-entry cryospecimen holders have been designed and built. Several are still operating with success. An excellent review is found in Heide

(1982b). Compared to side-entry systems, they have the advantage of an inherently symmetrical temperature gradient and therefore should not be affected by thermal drift. In some systems it is only the specimen cartridge which is actively cooled and it is thermally isolated from the rest of the electron microscope. In other cases – as, for example, in the system installed since 1983 on Zeiss electron microscopes – it is the whole specimen table which is cooled. The cartridge is kept at low temperature by contact with the cold table. This system offers excellent conditions for minimizing thermal drift, and also the effect of external vibration is easy to avoid because of the large mass and rigidity of the cold part.

8. IMAGE FORMATION

A general description of image formation in electron microscopy can be found in several textbooks (Heidenreich, 1964; Reimer, 1984; Saxton, 1978). Short but excellent presentations are also found in articles (Erickson & Klug, 1971; Amos *et al.* 1982). The wave theory of image formation requires a knowledge of optics which can be gained from a standard textbook (Born & Wolf, 1975) or in an easy and didactical form in the Lectures on Physics by Feynman *et al.* (1965). The case of image formation by amplitude contrast has been treated in view of quantitative measurements on hydrated specimens (Eusemann *et al.* 1982).

A basic concept of quantum mechanics is that an electron is a particle or a wave, depending on the experiment in which it is participating. A typical experiment in which the electron is a particle is schematized in Fig. 39(a). It consists in removing all the electrons that are scattered by more than a given angle, θ_0 . In the electron microscope the objective aperture is used for that purpose and θ_0 is the objective aperture angle. Contrast arises by the fact that some regions of the specimen scatter more electrons than others and, consequently, less electrons arrive in the corresponding region of the image.

Completely different is the image in which the electron is a wave. It is then diffracted in the specimen and made to interfere with the undiffracted part of the wave in the image plane by the optical system. In this mode of image formation, schematized in Fig. 39(b), all the electrons crossing the specimen participate in the image. Contrast results from the interference of all the individual electrons. It should be noted that interferences can equally well be obtained with electrons that have lost energy in the specimen as with those that have not, but the image is focused in a different plane.

8.1 Amplitude contrast

Amplitude-contrast bright-field image formation is the dominant mode when large specimens are observed in focus with a small objective aperture. The contrast results from the scattering of the electrons by the atom of the specimen. Each atom has its own scattering amplitude. These complex values are tabulated in the literature (Schäfer *et al.* 1971). By chance, it so happens that, within a useful

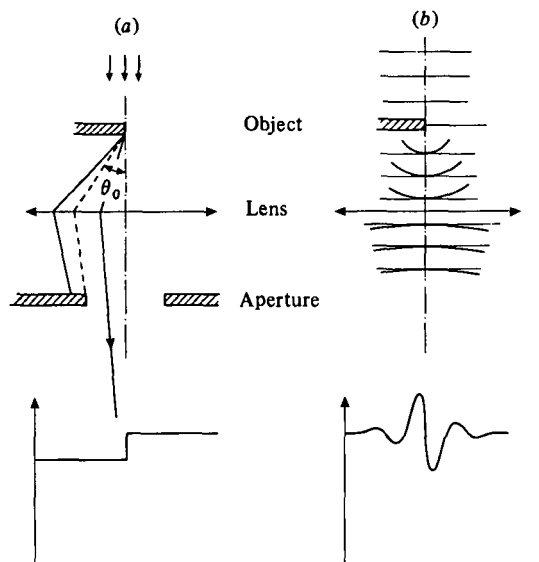


Fig. 39. Schematic representation of bright field image formation by (a) amplitude contrast in which the electron is a particle and (b) phase contrast in which it is a wave. The lower graph represents the intensity on the corresponding point of the image.

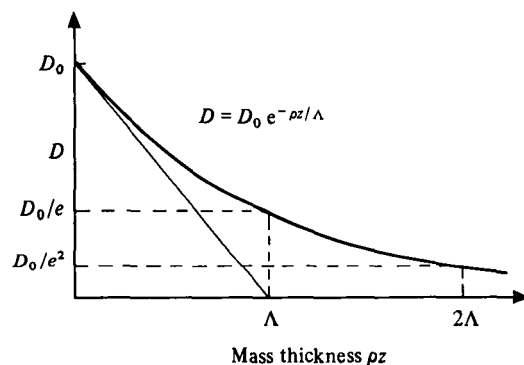


Fig. 40. Simplified relation between the optical density, D , of the micrograph and the mass thickness of the specimen, ρz , in the case of bright-field amplitude-contrast image formation, recorded in the range of optical density where the photographic film has a linear response to the electron dose. D_0 is the optical density of the photographic film in regions where there is no specimen. ρ is the density of the specimen element and z its thickness. Λ is the free mass thickness characterizing the operating conditions of the microscope (acceleration voltage, objective aperture angle).

approximation, the total scattering of an element of biological matter increases proportionally to the mass increment. Another simplifying fact is that, under the conditions generally used in electron microscopy, the optical density of the photographic film is proportional to the dose received (Valentine, 1966; Hahn, 1980). Consequently, the number of electrons arriving on an image element and the optical density on the micrograph decrease exponentially with increasing mass

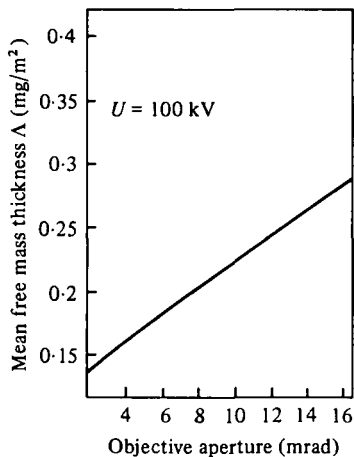


Fig. 41. Mean free mass thickness, Λ , expressed as a function of the objective aperture angle, θ_0 , for bright-field image formation with 100 kV electrons. One mg/m² corresponds to a thickness of 1 nm at a density of 1 g/cm³. (From Eusemann *et al.* (1982), with modifications.)

thickness, ρz , of the specimen, in which ρ is the density and z the thickness. This relation is drawn in Fig. 40. The characteristic parameter, Λ , is the mean free mass thickness, corresponding to the mass thickness producing, on average, one scattering event per electron. The value of Λ , expressed as a function of the objective aperture angle, θ_0 , is given in Fig. 41, for 100 keV electrons. For other energy it varies with the square root of the voltage. All these data are very approximate and they apply only to cases where phase contrast is negligible, which is not easy to ascertain when small specimens are observed. They are, however, useful for rapid estimation of specimen thickness or particle mass. They can also be used to estimate the density of large particles and even the hydration of specimens, by comparing the mass thickness before and after freeze drying. Practical examples are given in Dubochet *et al.* (1982*a, b*).

8.2 Phase contrast

Phase-contrast image formation relies on the phase shift, $\Delta\phi$, between the diffracted and the undiffracted wave. The first contribution to the phase shift, $\Delta\phi_1$, is introduced by the specimen itself. It is normally close to $\pi/2$. The second component, $\Delta\phi_2$, is due to the optical system itself, where defocus, Δz , and spherical aberration, C_s , both contribute to the shift of the wave of wave length λ , according to the equation (Scherzer, 1949).

$$\Delta\phi_2 = 2\pi\lambda^{-1}(\Delta z\theta^2/2 - C_s\theta^4/4).$$

However, in order to be best expressed in terms of contrast, the additional phase shift, $\Delta\phi_2$, must also be $\pi/2$ or, more generally, any value like $(2n-1)\pi/2$, in which n is an integer so that the scattered wave is brought into or out of phase with the unscattered wave, and can thus best interfere. For other values, the contrast is less

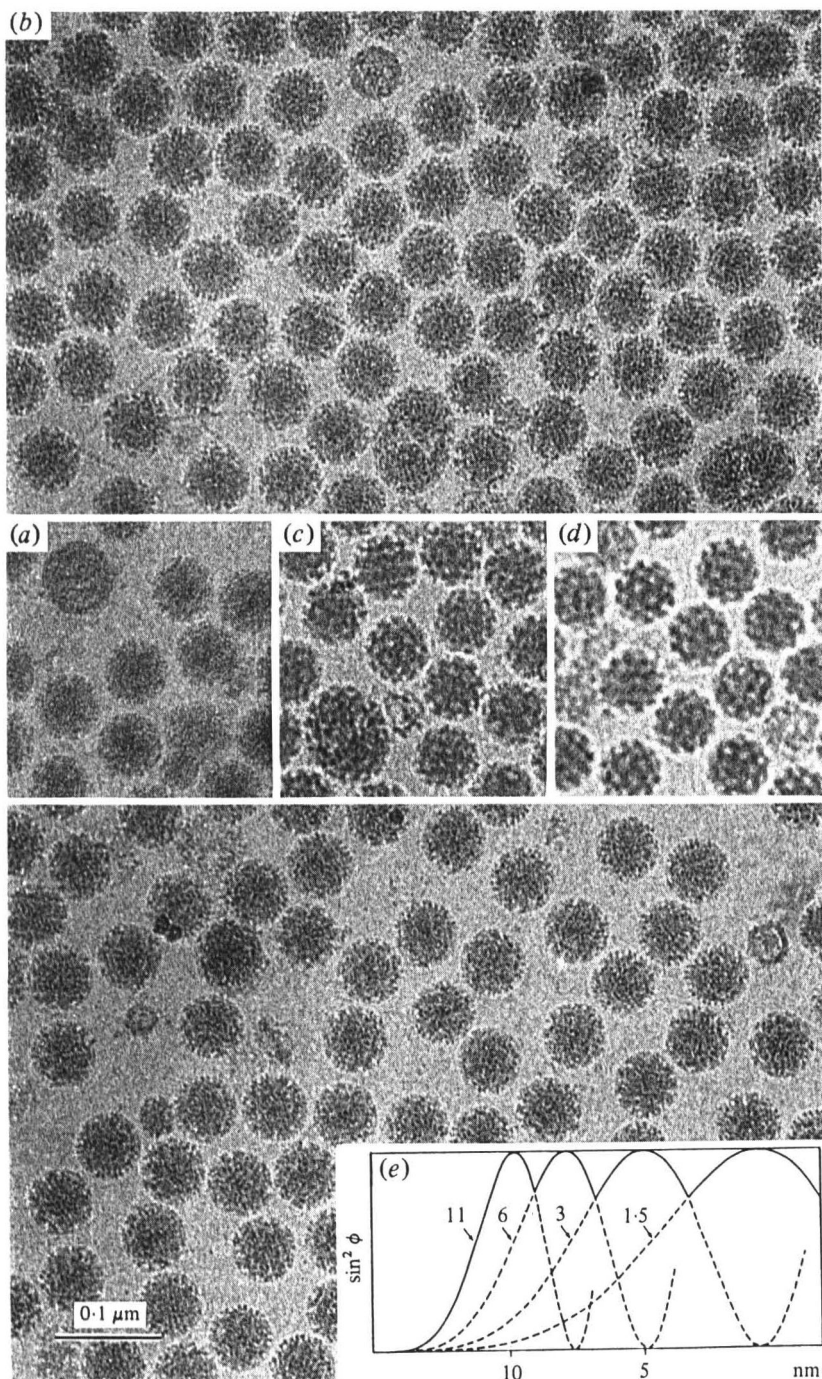


Fig. 42. Focus series of a vitrified solution of Semliki forest virus recorded at 1.5, 3, 6 and 11 μm underfocus for (a)–(d) respectively. (e) Corresponding phase-contrast transfer function.

strong, or even completely suppressed for phase shift of $n\pi$. The contrast transfer function, $\sin \Delta\phi_2$, expresses this property. Examples are represented in Fig. 42(e), for some values of Δz . From these properties, it becomes evident that phase contrast is an efficient mode of image formation for observing thin structures which produce only small amplitudes for the diffracted waves. Besides this, a phase image does not contain the whole information spectrum picked-up by the electron beam in the specimen. At least two micrographs are needed to fill the gaps of the transfer function and the long-range information is always missing.

8.3 Real image

In practice, both amplitude and phase-contrast contribute to image formation. The situation is especially favourable in typical negatively stained specimens. They can be imaged in a slightly underfocused situation, in such a way as to produce good phase contrast for the smallest structures that one can reasonably hope to observe. Amplitude contrast complements this information for larger dimensions where the phase-contrast transfer function becomes very small. It is thus possible to obtain in a single micrograph a good representation of all the information provided by the specimen. This favourable situation does not hold true for specimens that can be studied at very high resolution (Erickson & Klug, 1971) for unstained crystalline objects (Unwin & Henderson, 1975) or, even worse, for hydrated unstained specimens. In the latter case the contribution of amplitude contrast is so small that, for most structures, image formation relies exclusively on phase contrast up to dimensions around 10 or 20 nm. Indeed, structures like bacterial pilis (diameter = 6 nm), intermediate filaments (diameter = 10 nm) and even TMV or small spherical viruses (20 and 25 nm respectively) are essentially invisible on precisely focused micrographs, whereas even a single double-strand DNA molecule can be seen if enough phase contrast is produced by a strong defocusing. This effect has been tested quantitatively in T-layers of *B. brevis* (Lepault & Pitt, 1984), on TMV (Lepault, 1985) and on the tail of the bacteriophage T4 (Lepault & Leonard, 1985). There is a point, however, where amplitude contrast can no longer be neglected, in particular when unperiodic objects are observed, for which correction of the transfer function has to be made up to the origin. In the past the problem has been solved by adding a more or less arbitrarily chosen low-frequency component to the transfer function (Erickson & Klug, 1971; Unwin, 1972). In principle it could also be solved by using the complex values of the scattering coefficients, as they are calculated by the scattering theory (Schäfer *et al.* 1971). There are also methods to measure them directly in the electron microscope (Typke & Radermacher, 1982). It seems probable, and this is confirmed by preliminary work on DNA-containing particles, that the problem of quantitative processing of images of unperiodic, unstained, hydrated biological samples will require a more precise approach.

As a consequence of the low contribution of amplitude contrast to image formation of unstained, hydrated specimens, the retrieval of all the information

contained in the electron beam relies much more on phase contrast than with conventional, dry, stained specimens. Even for observations limited to a resolution of several nanometres, two or more micrographs need to be recorded for each specimen. The process is easy to optimize in this range of resolution because the whole information spectrum is concentrated in the very small values of the diffraction angle θ . The term in θ^4 becomes negligible in the Scherzer equation and the first maximum of the transfer function corresponds to a dimension d such as $d^2 = 2\lambda\Delta z$, whereas the first zero corresponds to $d^2 = \lambda\Delta z$. Increasing Δz by a factor of two brings the zero of the first image in coincidence with the first maximum of the second image, thus optimally extending the retrieval of the long-range information. As illustrated in Fig. 42, the process can be extended over several micrographs. Obviously it should not be done in the reverse order, because beam damage will have destroyed the high-resolution information before the micrograph has been recorded.

Another difference between the image formation in stained and unstained specimens comes from the high proportion of inelastically scattered electrons. In a thin specimen stained by heavy atoms, an image may be formed predominantly be elastically scattered electrons. This is not the case in unstained hydrated specimens as the mean free mass thickness for inelastic scattering, corresponding to $c. 130$ nm, is typically three times smaller than that for elastic scattering and is generally in the order of the thickness t of the specimen. The energy of the electrons participating in the image therefore forms a broad distribution, the centre of which can roughly be estimated to correspond to an energy loss of $\Delta V = 20$ eV $\times (t/130)$. This change in the average electron energy also reduces the focal length of the objective and places the specimen in a more underfocused position by $\Delta z = C_e \Delta V / 2V$, in which V is the acceleration voltage of the microscope and C_e is the coefficient of chromatic aberration (typically = 2 mm). In practice this effect is not seen easily, probably because it is hidden by a more severe one, the loss of resolution with increasing specimen thickness, caused in part by the delocalization of the inelastic scattering events, and by the chromatic aberration due to the energy spread of the scattered electrons. The newly developed electron microscope with energy filter could help reduce this latter effect.

9. BEAM DAMAGE

The electron beam deposits energy in the specimen and causes it to deteriorate. Excellent general reviews of this subject have been written (Isaacson, 1977; Coslett, 1978), but for the specific case of hydrated specimens at low temperature the results are still scattered in many different articles (Glaeser & Taylor, 1978; Talmon *et al.* 1979, 1986; Dubochet *et al.* 1982 *a, b*; Talmon, 1982, 1984; Lepault *et al.* 1983 *a, b*; Jeng & Chiu, 1984).

9.1 Electron scattering

Elastically scattered electrons carry valuable information about the specimen, but for acceleration voltage up to 100 kV few of them leave enough energy to displace even weakly bound atoms. Inelastically scattered electrons are those causing most of the damage. They leave a large amount of energy in the specimen, amounting to 5–80 eV for 97 % of the events (Wall *et al.* 1974). On average, the energy loss, expressed in electronvolts, can be approximated by $\Delta E \approx 6Z$, where Z is the atomic number of the scattering atom (Eusemann *et al.* 1982). For water the average energy loss per inelastic event is thus *c.* 20 eV. The ratio of elastic to inelastic scattering events can be approximated by the simple equation $\sigma_e/\sigma_i \approx Z/19$ (Lenz, 1954; Crewe, 1973). This means that whereas there are about three elastic for 1 inelastic event in a specimen stained with uranium, the ratio is in general about 1 to 3 for water or biological specimens. A crude estimation of the cross-section for inelastic scattering is also given by the simple equation: $\sigma_i \approx 9Z^3/V$ in which V is the accelerating voltage (Lenz, 1954; Crewe, 1973). At 100 kV this gives the value of $1.6 \times 10^{-4} \text{ nm}^2$ for carbon and $3.6 \times 10^{-4} \text{ nm}^2$ for a water molecule, and the average distance between two inelastic scattering events in water ($\rho = 0.92 \text{ g/cm}^3$) is calculated to be about 90 nm, which agrees reasonably well with the value of 132 nm given by a more careful analysis (Eusemann *et al.* 1982).

9.2 The forms of beam damage

Heating. The electron beam heats the specimen. This effect was dramatic in early microscopes but it is marginal in modern instruments with well-controlled illumination limited to the field of observation. This is particularly true for dry biological specimens observed at low beam current (Isaacson, 1977). Water is a poor heat conductor and vitrified specimens can therefore warm up more easily. Experiment and calculation show, however, that in this case also, heating is generally negligible (Talmon & Thomas, 1977 *a, b*, 1978, 1979). This can easily be confirmed by observing that the evaporation rate of water is the same in the immediate vicinity of the irradiated beam as in any other place. Beam heating effects are, however, expected when the temperature is close to liquid helium (Kohl *et al.* 1981) or around liquid nitrogen temperature, when the thermal contact between specimen and holder is bad. This happens frequently for large contaminating ice crystals lying on the specimen, sometimes for whole cryosections and rarely for a whole grid when it is thermally isolated from the holder by contaminating ice crystals.

Devitrification into cubic ice can be induced by the electron beam at a temperature where it would not take place naturally (Dubochet *et al.* 1982 *c*). The dose for inducing this effect increases when the temperature decreases below the natural devitrification temperature T_v . It is about 100 ke/nm^2 at -160°C . At still lower temperature all the water in the specimen has generally sublimated before it has time to crystallize.

Contamination. This is another effect caused by the electron beam at room temperature. It is due to the calcination of adsorbed carbonaceous molecules diffusing, on the specimen surface, into the irradiated area (Hart *et al.* 1970). It is essentially suppressed when the adsorbed molecules are immobilized by cooling the specimen and, in general, this already takes place as soon the temperature is some tens of degrees below zero °C (Leisegang, 1954; Wall *et al.* 1977). Consequently, beam-induced contamination generally has a negligible effect on vitrified specimens.

Mass loss is also considerably reduced at low temperature (Hall & Gupta, 1974; Dubochet, 1975, Freeman *et al.* 1980). For *dry* specimens it seems to have the low value expected from knock-on processes in which surface atoms are directly ejected by the collision with the electron (Dietrich *et al.* 1978). In practice, it is negligible for observations under low dose conditions around liquid-nitrogen temperature. The situation is different for *hydrated* specimens, where beam-induced sublimation and bubbling combine to cause mass loss.

Pure water sublimates under the beam at the approximate rate of 1 molecule for every 100 electrons (Talmon *et al.* 1979; Dubochet *et al.* 1982c). This represents a loss of 1 nm for a dose of about 3 ke/nm², corresponding to a typical observation. Sublimation is independent of the thickness of the water layer. It is similar in vitreous, cubic or hexagonal ice. It is only marginally influenced by the temperature since the measurement between -264 and -183 °C gives only a 2.5 reduction of the sublimation rate (Heide, 1982a). Also the flux of the electron beam seems of little influence, even in the STEM, where it is typically five orders of magnitude larger than in the CTEM. All these properties suggest that sublimation is the result of the ejection of surface atoms or small molecules each time they suffer an inelastic scattering event. An alternative proposal, the pre-knock-on process (Symons, 1982b), hypothesises that the shock-wave produced by elastic scattering inside the specimen may free some atoms when it reaches the surface.

Bubbling. As its name indicates, bubbling is an effect which makes hydrated organic specimens appear to boil under irradiation by the electron beam. It was first observed on frozen negatively stained specimens (Heide & Grund, 1974), then on catalase crystals in hexagonal ice (Glaeser & Taylor, 1978) and on plastic films covered with water (Talmon *et al.* 1979). Quantitative studies were made on organic solutions (Dubochet *et al.* 1982c), whereupon the name of bubbling was introduced, and on various biological particles (Lepault *et al.* 1983a, b or c) and polymers (Talmon, 1984; Talmon *et al.* 1986). Fig. 37 illustrates the development of bubbling on a carbon-coated plastic film covered with condensed vitreous water. In this case the bubbles appear after an irradiation of c. 10 ke/nm². At first they are numerous and small, but soon they fuse together and continue to grow, causing a large deformation to the specimen. The bubbles break when they reach the surface and mass loss becomes more rapid. In the presence of only a small amount of organic material it may happen that further irradiation makes the bubbles disappear again. Observing the development of the bubbles gives a good idea of the activity that takes place in the specimen during irradiation. The reality

of the bubbles is also impressively demonstrated in stereopairs of specimens in an advanced stage of bubbling.

Bubbling appears in vitrified samples of organic material and also between hexagonal ice crystals, where the organic material is concentrated. Specimens in which the water is crystallized into cubic ice are resistant to bubbling. It has also been observed in pure water but for very high irradiation and especially along crystal defects (Unwin & Muguruma, 1971, 1972). In biological specimens it generally starts after an irradiation of 2–10 ke/nm². This value depends on the size of the biological particle and on its density. For example, small viruses (TBSV) take longer to bubble than larger ones (SFV) and in T4 bacteriophages the dense DNA starts bubbling before the less-dense protein capsid. In vitrified sections of whole cells it is generally along the membranes and in the nucleus that bubbling starts. Bubbling seems to depend only marginally on the dose rate, and measurements in the STEM give the same value as in the CTEM (W. Tichelaar, Heidelberg, private communication). It is reduced at very low temperature but even at 4 K it does not seem to be suppressed. If this observation is confirmed, it would imply that the gas forming the bubbles has truly strange properties.

Drift. This is not usually considered as a form of beam damage but in cryo-electron microscopy and, in particular, for hydrated specimens, the trouble caused by beam-induced displacements in the specimens is so disturbing that it cannot be ignored. The usual syndrome is drifted micrographs. They give rise to a characteristic optical diffractogram in which the information is present in one direction but lost in all the others. Beam-induced drift is due to the forces created by the accumulation of charges in the poorly conducting specimen. As opposed to the drift caused by a displacement in the specimen holder, it varies rapidly in time and over the illuminated area. It is more severe in the absence of a conducting supporting film. Minimum dose imaging in which the micrograph is taken with the first electrons crossing the specimen is especially prone to drift as the specimen has no opportunity to stabilize beforehand. With a well-centered illumination this results in a typical pattern of radial drift increasing with the distance to the centre of the micrograph. The drift pattern is also generally influenced by the large electron dose which was applied during focusing in the immediate vicinity and just before recording the image.

There is no foolproof recipe to prevent beam-induced drift but much can be done to reduce it by careful use of the electron beam. It is obviously an advantage if the beam is kept as low as possible during observation and that the specimen is left for a period without irradiation before image recording. Most important is that the operator always knows where the beam is applied during low-dose operation in order to choose the optimal place to focus before recording. It is also of an advantage that the illuminated area is kept as small as possible. Extrapolating on this observation, it has also been hypothesized that drift could be overcome by combining a large number of partial images, each recorded in sequence, on the same micrograph, with a very small illuminated area (R. Henderson, private communication). Another approach may be derived from the well-known observation that specimens break much more readily in the absence than in the

presence of an objective aperture. Similarly, we have observed that the fork used as an anticontaminator has a favourable effect in reducing drift. This is probably due to back-scattered electrons forming a neutralizing cloud around the specimen. In the future it will perhaps be possible to prevent drift by neutralizing most of the charges of the specimen directly in the electron microscope.

9.3 Mechanisms of beam damage

The mechanisms leading to beam damage are complex and not well understood. They are discussed in some general reviews (Glaeser, 1975; Reimer, 1975; Isaacson, 1977). Several particular cases are treated in terms of radiochemistry (Box, 1975; Hüttermann, 1982*a, b*; Symons, 1982*a*) but the doses used in electron microscopy are so high that it is always difficult to understand the basic mechanisms under conditions where many phenomena overlap. More informative in this respect are some of the daily observations made on frozen specimens. Bubbling is one of them; two more examples are presented below.

Bubbling can be explained as the consequence of the formation of small molecules during radiolytic processes. In dry specimens they can escape by evaporation or surface diffusion and this causes the important mass loss observed at room temperature. In some cases (for example, in a thick layer of dry sucrose irradiated at high flux at room temperature) the molecules do not have time to diffuse away before their accumulation bursts into bubbles. An equal dose applied at lower flux causes the same mass loss without, however, producing bubbles, because the molecules have time to escape before they accumulate. The displacement of the molecules is very much slowed down at low temperature but accumulation still does not take place in dry specimens, probably because they are porous. The same may hold true for specimens in which water is in cubic crystals. The radiolytic fragments are, however, blocked in vitrified specimens, including the regions of concentrated material between hexagonal crystals. When their concentration is high enough, the fragments nucleate into a bubble which can then easily grow further in the plastic environment of vitreous water. As was shown on model systems, the deformation is smaller in the presence of hexagonal ice (Talmon *et al.* 1986).

Water also plays a direct role in the chemistry of beam damage. For example, a carbon film irradiated in the presence of water is etched more rapidly than in a dry environment (Heide, 1982*a*). The same holds true for organic materials (Talmon, 1982). This effect is not of great importance, however, in structural studies, because it only becomes significant for doses much higher than those compatible with high-resolution observations. However, it becomes essential in EXAF or EDAX studies, in which the electron dose required for normal observation produces the complete perforation of the specimen before a spectrum can be obtained.

Cellulose nitrate is frequently used, under the name of collodion, to make thin supporting films for electron microscopy. When irradiated at room temperature, it loses about half of its mass after a dose of 10 ke/nm². This mass loss is nearly

suppressed and nothing seems to happen when the dry film is irradiated at low temperature. As illustrated in Fig. 38, and as reported previously (Dubochet *et al.* 1982*a*), the situation is very different when the film is in water: during irradiation, a large number of small crystals grow into imbricated thread-like structures; they reach a maximum size and number after some ke/nm² and disappear slowly with further increasing dose. In the absence of irradiation, the crystals are stable at low temperature but they sublime without remains above c. -150 °C. Because of this low sublimation temperature it can be deduced that the substance forming the crystals must be of relatively low molecular weight. It can be identified from its electron diffractogram with the help of tables characterizing the crystal parameters of substances. One such table has been prepared for the special purpose of cryo-electron microscopy (Tatlock, 1982). It reveals that the crystals formed on irradiated collodion are made of nitrous oxide N₂O. Obviously, the process leading to the formation of these crystals is complex; molecules of N₂O must first be formed from the cellulose nitrate and they must then diffuse on the specimen until they are trapped on a growing N₂O crystal. The role of water in the process is not clear, but without it no crystals are formed.

Pure ice seems to be stable when it is irradiated between liquid-nitrogen temperature and that at which its natural sublimation becomes significant; its crystalline structure remains unchanged while the crystals slowly sublime under the effect of the beam. Below c. -200 °C the situation is very different; the structure of the ice crystal is destroyed and it is transformed into an amorphous mass after an irradiation of only 0.5–2 ke/nm² (Lepault *et al.* 1983*c*; Dubochet & Lepault, 1984). However, this amorphous substance retains some 'memory' of its history; upon rewarming above the devitrification temperature, it reforms the original crystal even if it was hexagonal. If the irradiation is larger, corresponding to a dose of more than 2 ke/nm², the 'memory' is lost and the usual transition, from vitreous to cubic, takes place at the usual temperature, T_v . This seemingly contradictory property, namely that the sensitivity of ice to the electron beam increases with decreasing temperature, can be explained by a so-called restoration mechanism: at very low temperature, ice is normally sensitive to beam damage, as are also any biological crystals, and each inelastic scattering event is likely to produce structural damage. The crystals are therefore destroyed for a dose in the range of 1 ke/nm²; at a higher temperature, however, the unstable structure induced by the inelastic event in ice is reactive enough for further transformation, but the only stable arrangement it can find is the initial state of the undamaged crystal.

9.4 Structural damage

For the electron microscopist all these considerations about mass loss, gas formation or radiochemistry are of indirect interest. The only essential point is structural damage, but of course this is difficult to measure directly at high resolution since any direct micrograph only provides the post-damage observation but never the initial state (Unwin, 1974). Electron diffraction of crystals is therefore the avenue of choice for measuring structural beam damage to organic

specimens (Kobayashi & Sakaoku, 1965; Glaeser, 1971). It has also been applied to vitrified biological specimens (Taylor & Glaeser, 1976; Lepault *et al.* 1983*a*; Lepault & Dobochet, 1986*b*; Jeng & Chiu, 1984). Altogether, the results can be expressed quite simply by the following rules. (1) beam damage is reduced by a factor of 2–6 around liquid-nitrogen temperature, (2) there is no significant difference whether the specimen is hydrated or not, (3) the resolution δ (nm) obtainable on a vitrified specimen around liquid-nitrogen temperature is related to the total electron dose D (e/nm²) by the relation $\delta = D/1000$. This, somewhat optimistic, rule of thumb, which is valid for a dose smaller than that inducing bubbling, is deduced from the few quantitative studies made by electron diffraction on protein crystals. It also fits our observations made on viruses or their components. In practice it means that, under usual recording conditions (1 optical density unit, speed = 1 μm^{-2}), the first micrograph recorded without preirradiation at 30000 times magnification ($D = 1 \text{ ke/nm}^2$) could record information down to about 1 nm resolution. For each subsequent micrograph of the same field, the expected resolution is reduced by 1 nm.

Whether the very low temperature of 4 K, approached in some helium-cooled cryo-electron microscopes, further reduces structural damage has been the subject of a heated debate (Siegel, 1972; Dietrich *et al.* 1979; Knapek & Dubochet, 1980; Lamvik *et al.* 1983; Lepault *et al.* 1983*b*; Wade, 1984). With the conclusion of the study made in common by all the groups involved (International Study Group, 1986), it now seems to be demonstrated that, under the present working conditions, there is not much to be gained by liquid-helium cooling, at least as far as beam damage is concerned. The possibility that other observation procedures, specimen preparation methods, microscopes or, still better cooling (Fujiyoshi *et al.* 1986) may have a favourable effect is still open for discussion, but such claims will have to be strongly substantiated before becoming accepted in the future.

10. HOW TO OPERATE

This section describes practical methods to prepare and manipulate vitrified specimens. The procedures have been chosen because they have been abundantly tested in our laboratory and because of their simplicity. Experience has shown that none of the operations described in this chapter is difficult in itself. The quality of the final results depends, however, on their smooth and rapid succession and they should be practised accordingly. The reader will adapt them to his own convenience and to match the specificity of his laboratory and specimens. Complementary information is found in the instruction manual of the commercial instruments. A list of suppliers has been compiled by Robards & Sleytr (1985).

10.1 Safety

Frost-bite. Liquid propane or ethane are chosen as cryogens because they are much more efficient than liquid nitrogen. Whereas it is possible to plunge the hand rapidly into boiling nitrogen without harm, the same is out of the question with

the cryogens used for vitrification. Even a small drop falling on naked skin will produce a blister. The same in the eye would probably cause a serious injury. Such an accident could easily occur during the preparation of liquid ethane, if the gas flow is too violent. A particularly dangerous situation may develop when a recipient with liquid ethane is completely immersed in liquid nitrogen. A pellicle of ethane solidifies at the surface and seals the residual liquid, which bursts when the interior further expands into a solid. This sometimes results in violent projections. Beginners must therefore perform the whole freezing operation with eye protection.

Liquid nitrogen becomes dangerous when it cannot flow away from the skin. This is the case when clothes are soaked or when it accumulates in the shoes. The best way to avoid this type of accident is to have a practical system for pouring liquid nitrogen at the work place. A tip-up container on a mobile support was found to be useful.

Fire. Ethane has nearly the same density as air, and propane is heavier. Both form an explosive mixture in proportions ranging from 2 to 20 vol. %. The explosion can be triggered by electrical apparatus, including a lamp. In most countries there are legal requirements concerning the use of these gases. In our laboratory we require that all the work is done in a hood.

Suffocation. Large quantities of liquid nitrogen are frequently used for freezing and for cryo-ultramicrotomy. Each litre of the liquid produces 700 litres of gas. There is a risk of suffocation when oxygen concentration in the air is reduced by half its normal value. This can take place in a small and poorly ventilated room, as microtomy locals frequently are.

Poisoning. Alkylamines used for the treatment of carbon film by glow discharge are violently poisonous for lungs and skin. The maximum permitted concentration is 5 ppm, corresponding to about 20 mg/m³ for amylamine. Consequently the exhaust of the glow discharge machine must be outside the laboratory. Fortunately, the smell of these compounds is so nauseous that they cannot accumulate unnoticed.

10.2 Bulk specimens

10.2.1 Freezing

Material. The freezing apparatus developed at EMBL is a simple plunger – versatile, portable and easily assembled, not to mention inexpensive. It is shown in Fig. 43(a). A slightly more elaborate model, for which the plans are available upon request, is depicted in Fig. 43(b). The plunger is formed by a weighted, friction-reduced rod, propelled with elastic bands. A shock adsorbing foam cone receives the rod as the specimen enters the cryogen. Cryogen is prepared in a 20 ml flat-bottomed metal cap sitting in a polystyrene container of liquid nitrogen. It is stirred with a 1 cm magnet, driven by a water-propelled (because of explosion risk) magnetic stirrer mounted on an adjustable support. The specimen holder is fixed on the plunger rod in the same manner as a disposable

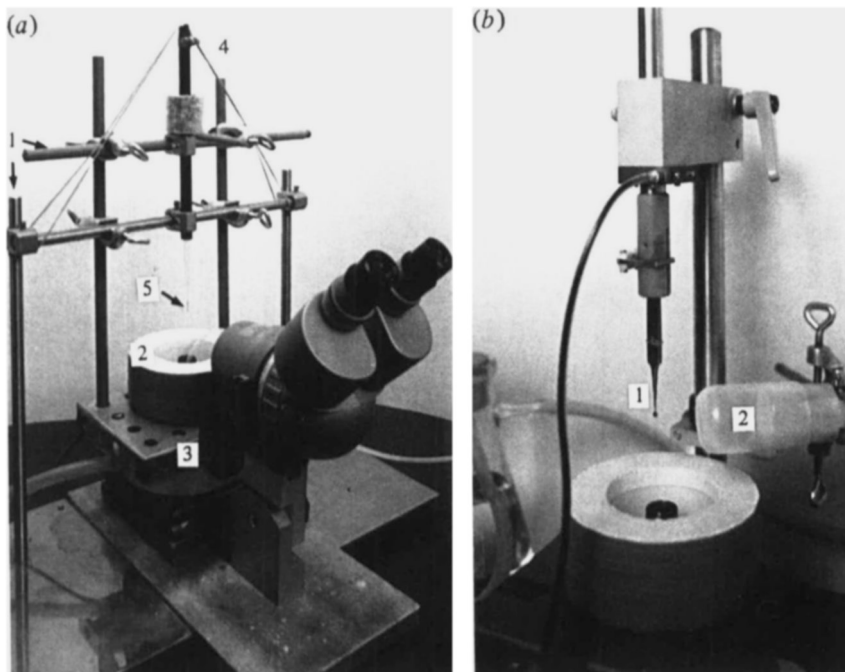


Fig. 43. Plunger for freezing. (a) Simple apparatus equipped here for freezing bulk specimens. (1) Retort stand clamps; (2) liquid nitrogen and ethane dewars; (3) water-driven magnet; (4) plunger with elastic band propulsion; (5) specimen support. (b) A more elegant freezing apparatus equipped for preparing thin vitrified layers of suspensions. (1) Tweezer holding the specimen support grid; (2) humidified air outlet.

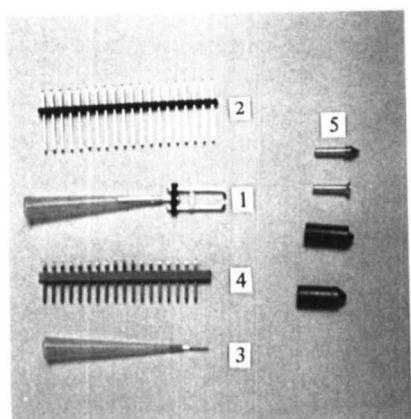


Fig. 44.

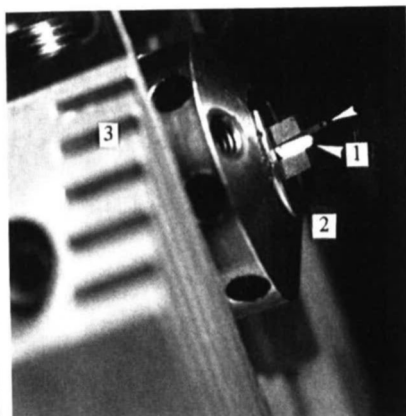


Fig. 45.

Fig. 44. Specimen supports for cooling bulk samples for cryosectioning. (1) Parallel pins suitable for mounting fibres; (2) pin source; electronic wrapping strips; (3) single pins for pelleted suspensions; (4) pin source; electronic wrapping strips; (5) other commercially produced specimen supports.

Fig. 45. Specimen pin mounted in microtome chuck. (1) Clamped specimen support is embedded in indium metal base plate. (2) Chuck head. (3) Microtome bridge.

hypodermic needle. A binocular helps in viewing the specimen pin and sample mounting. The plunger is released by removal of the locating pin (Fig. 43*a*).

The specimen support must be easy to mount and to remove. For cryosections, it must also be compatible with the cryo-ultramicrotome. A simple system consists of electronic wrapping pins pushed in the tip of a disposable micropipette (Fig. 44 (3)). The tip of the pin is flattened in order to form a surface of 100–500 µm diameter, suitable for receiving a microdrop of a viscous sample. Alternatively, two parallel pins can be used to mount a stretched fibre.

Operation. Before starting the operation make sure that (*a*) the sample pin is in the field of view of the binocular; (*b*) the pin is in line with the cryogen pot; (*c*) there is enough cryogen (liquid ethane or propane) in the cap, maintained in a semi-solid state by vigorous stirring (we use freshly made ethane, although it is not important that the cryogen is kept very clean and free of contaminating ice, as the surface of the sample block will be removed during sectioning); (*d*) after releasing the plunger rod the specimen pin reaches the cryogen and stays in it; (*e*) the pin is loose enough to be easily removed from the micropipette tip in the cryogen.

Bulky suspensions of cells, of large particles or the like, can be pelleted by centrifugation into a sealed disposable micropipette tip. After partially slicing off the extremity of the tip, a very small volume of the semi-solid sample can be applied directly to the pin. It must be kept in mind that most specimens are vitrified only to a depth of some 10 µm and that all the residual volume is waste. Any excess supernatant remaining on the specimen is removed at the last moment before the plunger is released. After freezing, the specimen holder is removed from the plunger and transferred to liquid nitrogen. At this stage it is advisable to check the aspect of the specimen with a good stereo-microscope, but still keeping it under liquid nitrogen. It frequently happens that the specimen is displaced during immersion and is not suitable for further processing. The specimens on the metal pins can be stored for indefinite periods, in small bottles, not tightly closed, immersed in liquid nitrogen.

Fibrous bulk samples (as, for example, isolated muscle, collagen fibres or highly viscous liquids) can be mounted on a double support (Fig. 44(1)) and kept in a buffered solution. It is transferred at the very last moment to the freezing apparatus, where the excess solution is removed before plunging.

Tissues or large bulk samples are best frozen by projection on a cold metal block. The practical aspects of the method are described elsewhere (Sitte *et al.* 1987).

10.2.2 Sectioning

Material. The cryo-ultramicrotome must be capable of operating in a thermally stable mode, with specimen, knife and chamber atmosphere at a temperature < −140 °C. The cryo-chamber must be large enough for comfortable manipulation of accessories, such as the grid-holding device, knife assembly, grid press, sample bottles and an anti-static device. The working chamber must be illuminated by a strong and adjustable light which should not produce heat.

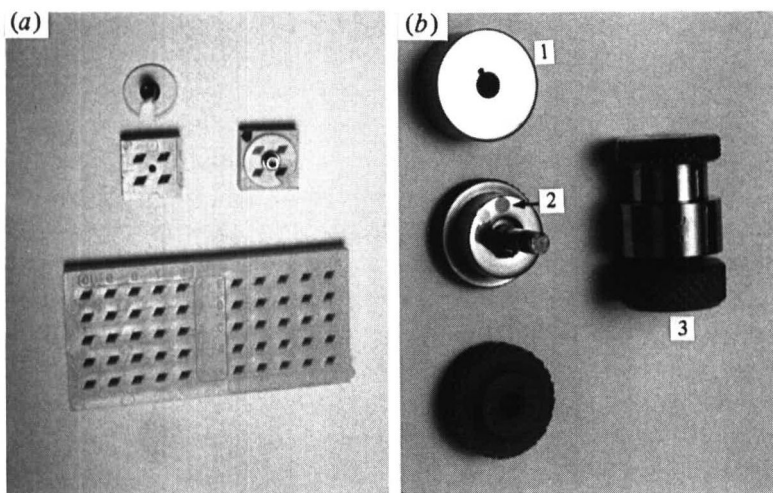


Fig. 46. (a) Modified grid boxes for long-term storage under liquid nitrogen of grids containing vitrified specimens. (b) Cryosection press. (1) Polished inside surfaces; (2) specimen grids; (3) screw top on assembled unit.

The knives can be diamond or glass. The former must be mounted on a special holder capable of withstanding the stress of frequent and rapid temperature changes. These special knives are commercially available. The sharpness of glass knives is of the utmost importance and their preparation requires great care. We found that the method of balance-breaking of Tokuyasu & Okamura (1959) and Griffiths *et al.* (1983) gave the best results. Tungsten coating of the freshly prepared knives greatly improves their quality and life expectancy (Roberts, 1975).

Specimen-supporting grids must be of small mesh size. We use hexagonal or square 600- to 1000-mesh grids, coated with carbon, floated from freshly cleaved mica. The grids are held with a special holder, as close as possible to the knife edge. A grid-press in which two polished metal surfaces can be pressed together with a screw (Fig. 46b(3)) is also put in the cryo-chamber. Grid boxes are adapted for long-term storage in liquid nitrogen for grids and sections (Fig. 46a).

Operation. Before starting, the cryo-chamber must be carefully dried to minimize water contamination. The chamber, together with the various tools which will be used subsequently, are cooled and left to equilibrate at the working temperature (typically -160°C). The pin holding the specimen is then brought into the chamber in a cup filled with liquid nitrogen. With cooled forceps the pin is inserted in the microtome-head and firmly screwed against the indium plate (Fig. 45(1)). Other types of supports are available for cryo-microtomes (Fig. 44(5)). In general they are suitable for larger specimens than those which can be vitrified.

Trimming of the specimen should be avoided, as only the very surface is vitrified and trimming removes the best frozen volume. In general, it is not necessary if the sample was well concentrated and free of liquid excess.

Slow cutting speed ($0.2\text{--}0.4$ mm/s) gives good results but the strokes must be done in rapid succession in order to counteract any irregular advance of the microtome. This irregularity means that cutting should be done only during the most stable phase of the cooling cycle (not during or shortly after liquid-nitrogen refilling) and that the section thickness setting is not representative of the actual section thickness. It is best adjusted during cutting, according to the aspect of the sections. It is therefore of advantage to start cutting by manual movement until decent sections start to appear, after which the instrument may be switched to the automatic mode. One or a few groups of sections are accumulated on the knife edge before they are collected. Normally a 15 min period of cutting provides sufficient sections for 1–2 grids. The filling cycle of liquid nitrogen can be activated while the sections are collected.

To assist in section collection the field of view seen through the binocular should include the specimen, the knife edge and the grid. Sections are transported to the central area of the grid with a fine pointed hair mounted on a flexible plastic applicator (a plastic straw) which is kept outside the cryo-chamber until it is used. The aim is to collect the sections using only the tip of the hair. Difficulty will be experienced if the sections attach away from the tip of the hair. In the event that sections are repelled from the hair by static charges, an air-ionizing instrument may be used to modify static charges in the area of the grids and sections. In general, the sections attach correctly to the hair tip if it has just been introduced into the cryo-chamber.

When sufficient sections have been transferred, the grids are retracted from the knife edge. The top half of the press is removed exposing the ice-free polished surface of the lower platform, where the grids are placed. The top half of the press is relocated without disturbing the grids. For short-term storage the complete press and grids may be kept in liquid nitrogen ready for direct transfer to the microscope cryo-holder. Otherwise grids with sections can be stored for longer periods in liquid nitrogen, in modified grid boxes (Fig. 46*a*).

10.3 Thin layer of vitrified suspension

Material. The concentration of the suspension observed in unsupported thin films must be high so that sufficient particles are present in the small volume of film. This range is typically between 1 and 10 mg/ml but it can vary considerably, depending on the particles and on the surface properties of the film and its interaction with the particles.

The plunger for preparing thin layers of vitrified suspension on a perforated supporting film is similar to that shown in Fig. 43*b*. It differs from the one used for freezing bulky specimens by the fact that a much smaller volume of liquid ethane is used and that the specimen is mounted on a grid held by tweezers (Fig. 43*b(1)*). The latter must be treated (Teflonated) in order to prevent the solution from rising by capillary action and it can be fixed by a rapid clamping system to the plunger rod.

A perforated supporting film can be prepared by the method of Fukami & Adachi (1965) and Fukami *et al.* (1972) which gives a thin perforated plastic film of c. 5 μm average hole size. The preparation must take place in a very humid atmosphere (80 %) and the plastic solution must be sufficiently diluted (e.g. 0.1–0.4 % in ethylacetate). The thickness of the plastic must be small compared to the hole size in order to form clean holes. The plastic film is coated on one side with a thick layer (c. 20 nm) of evaporated carbon. Most of the plastic is then removed by dissolution but some residue, bubbling under the beam, is useful for focusing. It is advisable to control the perforated film with some stereomicrographs.

Liquid ethane is prepared from the gas in a 2 ml aluminium recipient inserted in a styrofoam container of liquid nitrogen. Liquid ethane must be very pure and free of water because a small amount of cryogen usually remains on the specimen where it evaporates, either during transfer or in the microscope. This would leave any impurity as a contaminant on the specimen. It is therefore convenient to prepare liquid ethane fresh for each specimen.

Operation. A drop of suspension (2–5 μl) is put on the grid. Liquid ethane is prepared by flowing a stream of ethane gas through a thin plastic pipe (diam. 2 mm) into the liquid nitrogen cooled recipient. This operation requires precautions and some training: too little pressure results in a block of solid ethane that obstructs the pipe; too much pressure blows all the cryogen away and may be dangerous. When the undercooled ethane is close to becoming solid and is therefore ready for vitrification, most of the drop of suspension is removed from the specimen by pressing it firmly, by hand, between two double layers of blotting paper (Whatman no. 1, qualitative) for 1–2 s and immediately releasing the guillotine. With the geometry shown in Fig. 43b) the free falling time is 10^{-1} s and the vitrification time probably around 10^{-4} s. The specimen is then raised slowly, leaving time for liquid ethane to flow away from the tweezers and grid, but not enough to rewarm it, and it is reimmersed in the liquid nitrogen of the surrounding recipient. The grid is detached from the tweezers to which it is fixed by frozen solution, by forcing a piece of cold metal (tweezer tip or scalpel) into the tweezers. The specimen is left to fall in a recipient (a small bottle cup) in the liquid nitrogen. The container for liquid ethane and the tweezers are removed and left to warm and dry. The specimen can be transported in liquid nitrogen, covered for protection against water contamination, or it can be put in a special grid box (Fig. 46a) for indefinite storage in clean liquid nitrogen.

Partial evaporation of the water in the thin film can be reduced by minimizing the time the thin liquid film is left in contact with air. More efficient is to bring a stream of air, humidified by bubbling in water, slowly flowing from a large pipe (diam. 3 cm), directly on to the grid. (Fig. 43b(2)).

Surface forces, acting in the thin film, on the particles of the specimen, can be controlled to a large extent by coating the surface with a lipid layer (Schultz *et al.*, in preparation). For this purpose, a 2 mg/ml solution of polydisperse liposomes of neutral lipids (phosphatidyl choline) is prepared by simple dissolution of the pure

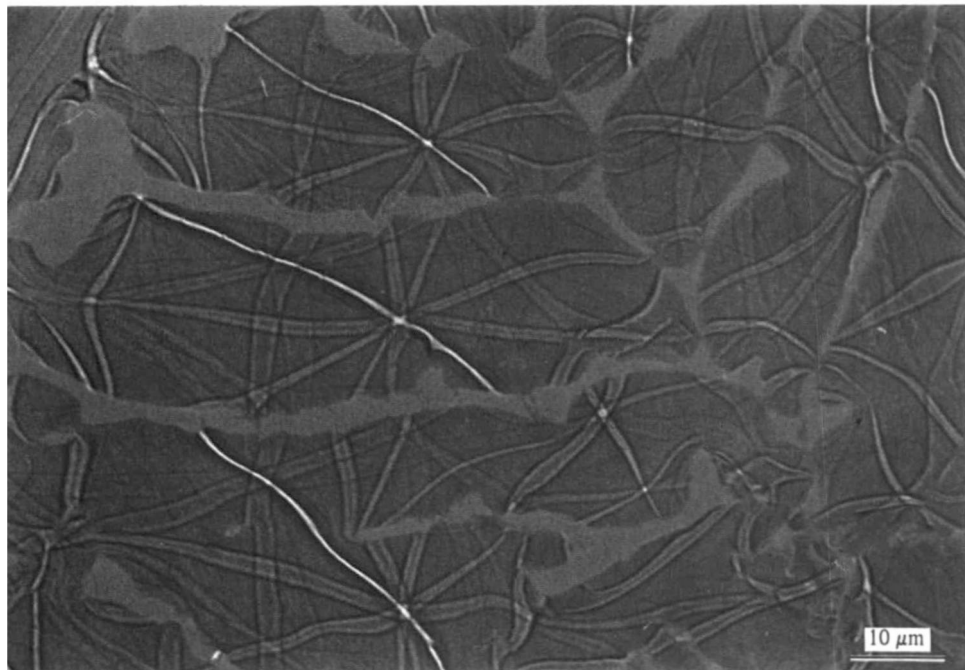


Fig. 47. Thin crystal of hexagonal ice obtained by freezing of a water drop while it was spreading on the partially hydrophilic carbon support. Bend contours due to Bragg reflexions of the deformed crystal are clearly seen.

lipid in the desired buffer. An equal volume of this solution is added to the drop on the grid. The negative lipid phosphatidyl glycerol can also be used to produce special surface effects, as for example repulsion of negatively charged particles.

An alternative preparation procedure is the 'bare grid method' (Adrian *et al.* 1984) in which the unsupported liquid film is prepared over the holes of a clean 200- or 400-mesh grid in absence of any supporting film. Instead of using blotting papers, most of the liquid of the drop is removed with a pipette. The moment at which the guillotine is released is best determined, after some experience, by observing the forming film with a binocular. The bare-grid method increases the possibilities for interactions between particles in the liquid layer but is prone to concentration-induced artifacts due to the partial evaporation of the water in the thin film.

Vitrified specimens can also be prepared on a continuous supporting film rendered hydrophilic by glow discharge in air or, for more reproducible results, treated by glow discharge in amylamine (10 s at 100 V/cm in 10 Pa). After adsorption of the material to the support, most of the liquid is removed with a blotting paper, as for negative staining, and the guillotine immediately released. This method does not allow the particles of the suspension to interact in the liquid film and causes some flattening artifacts due to adsorption to the supporting film. On the other hand, it generally allows one to work with lower concentrations of biological material than with specimens which are prepared without support.



Fig. 48. Thin layer of nearly pure water in which hexagonal (h) and cubic (c) ice coexist with vitreous water (v). The thinnest region of the film is vitreous whereas the thicker regions, close to the grid bars, are crystallized.

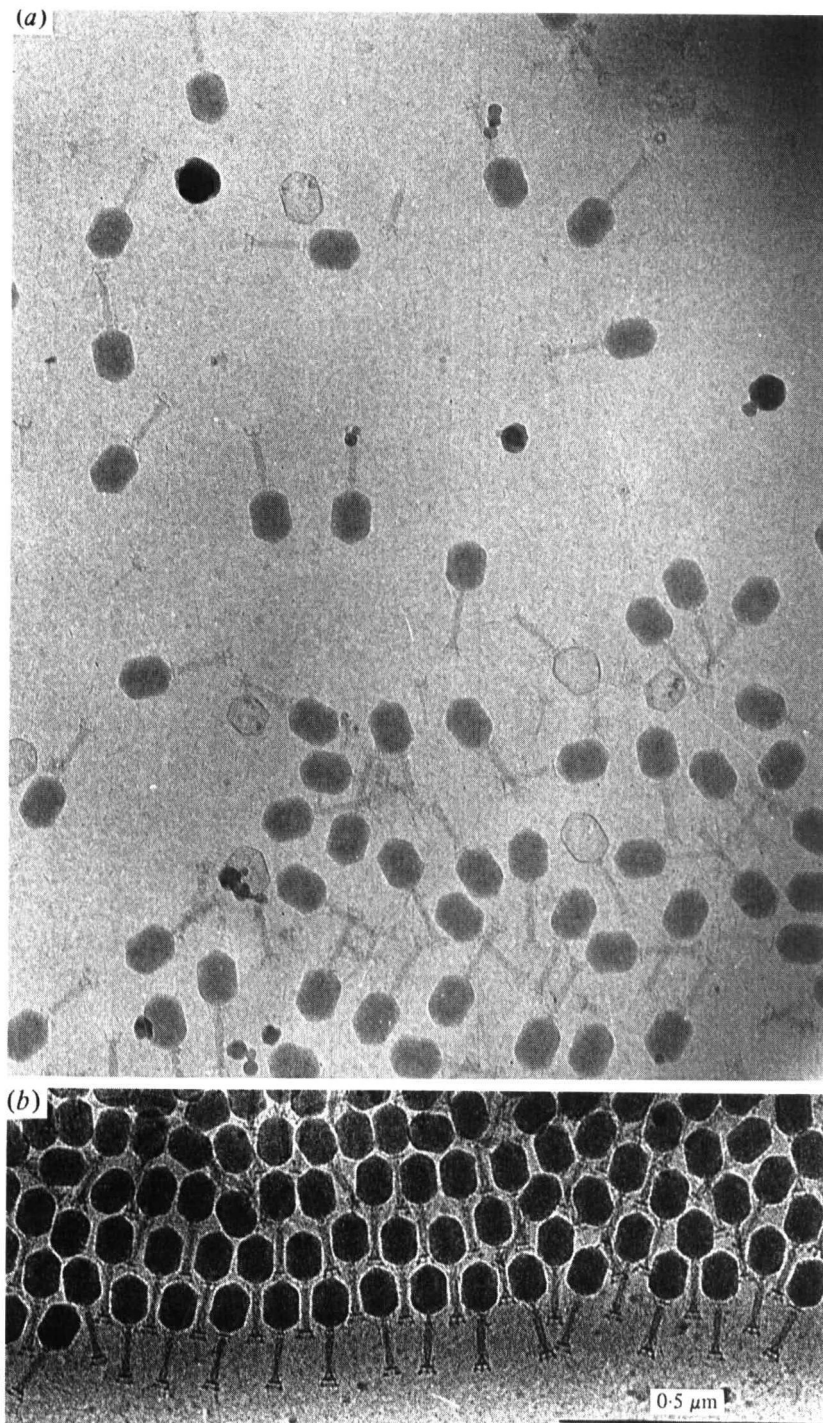


Fig. 49. (a) Thin vitrified layer of a heterogeneous T4 bacteriophage solution. Because the shape of the head is well preserved in water, such micrographs could be used to determine its exact geometry (Kellenberger *et al.* in preparation). (b) Arrangement of the bacteriophages in the thin film. The latter specimen was prepared by the bare-grid method; the bacteriophages were expelled from the centre of the grid hole when the film became thinner than their head; they were therefore concentrated in the surrounding region, where they packed in the densest possible arrangement. The whole process took in the order of 1 s.

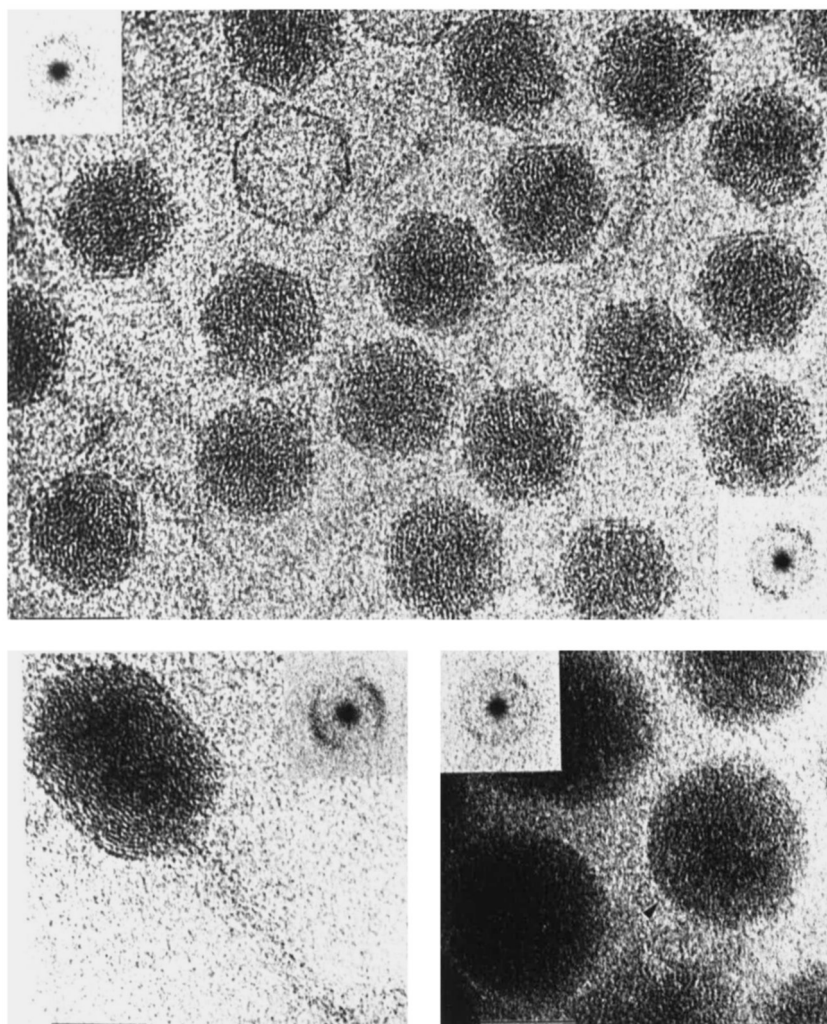


Fig. 50. λ bacteriophage imaged under conditions best revealing the packaging of the DNA in the head. Small, randomly orientated domains are visible in which the DNA seems to be arranged with crystalline order.

10.4 Transfer and observation

Commercial cryo-specimen holders are equipped with a device for transferring the frozen specimen into the electron microscope without undue rewarming and contamination. Complete protection would, however, require a counter-productive heavy and complicated system. It is of advantage to look for a compromise in which simplicity of the transfer procedure requires that it is made rapidly and under clean conditions. To achieve this it is important that all the material used for the transfer is carefully dried before starting. In particular, all the liquid nitrogen which may come in contact with the specimen and the specimen rod must be free from ice crystals. Also, contact of any cold surface with

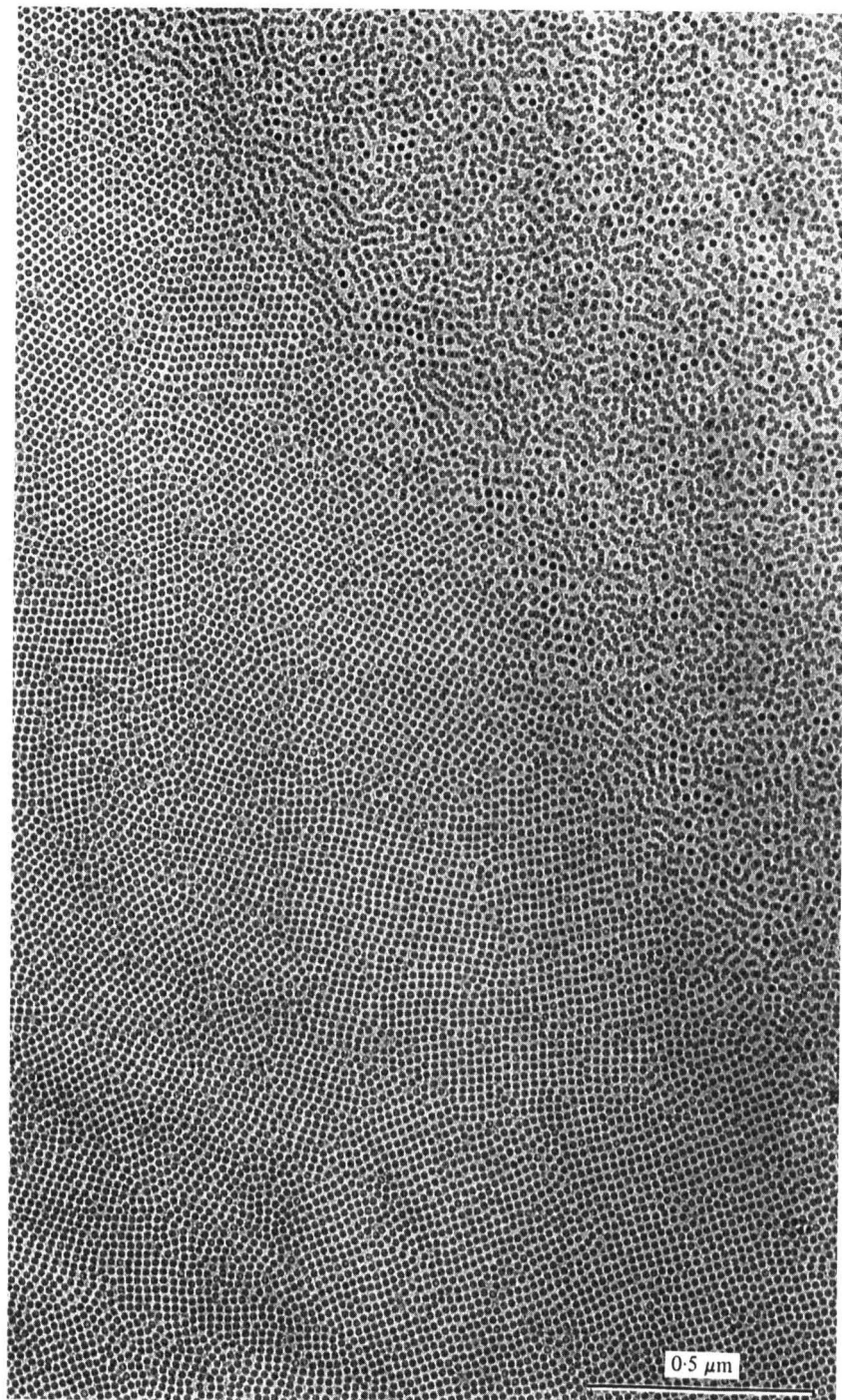


Fig. 51. Thin layer of brome grass virus prepared by the bare-grid method. The packing of the virus becomes more ordered as the layer thins from top right to bottom left of the image.

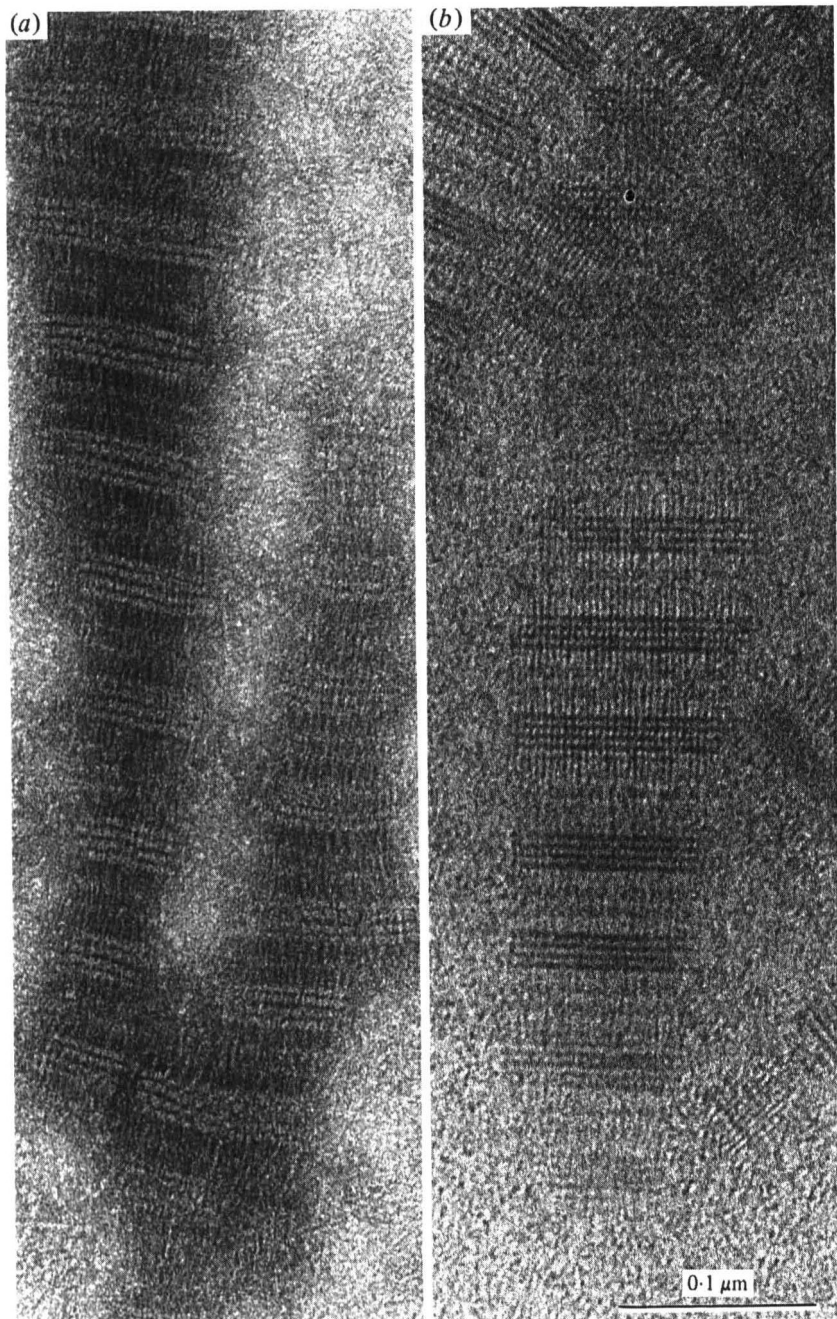


Fig. 52. Crystal of the N-terminal cleaved fibre protein of adenovirus type 2. (a) Conventional negative staining with uranyl acetate. (b) Vitrified layer prepared by the perforated grid method. (Material: courtesy Ch. Devaux, Grenoble.)

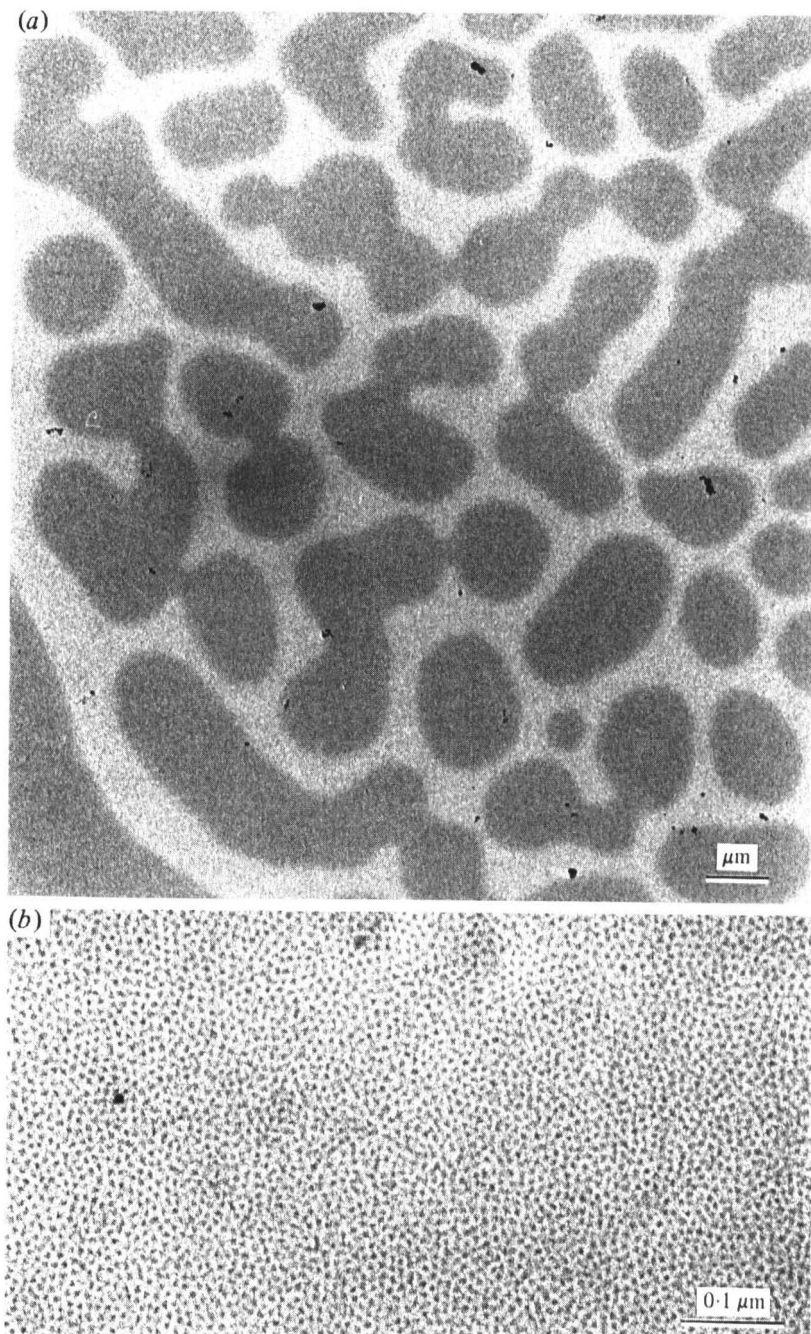


Fig. 53. Micro-emulsion of O-xylene, Tween 80, propylene glycol and water prepared by the perforated grid method. (a) Low-magnification image showing the distribution of the microdroplets. The less-dense areas correspond to regions where they are arranged into a single disordered layer within the liquid film. Darker areas correspond to regions where two superimposed layers are formed. (b) High-magnification image showing the microdroplets of c. 5 nm diameter arranged into a monolayer. (Material: courtesy A. Angell, Purdue university.)

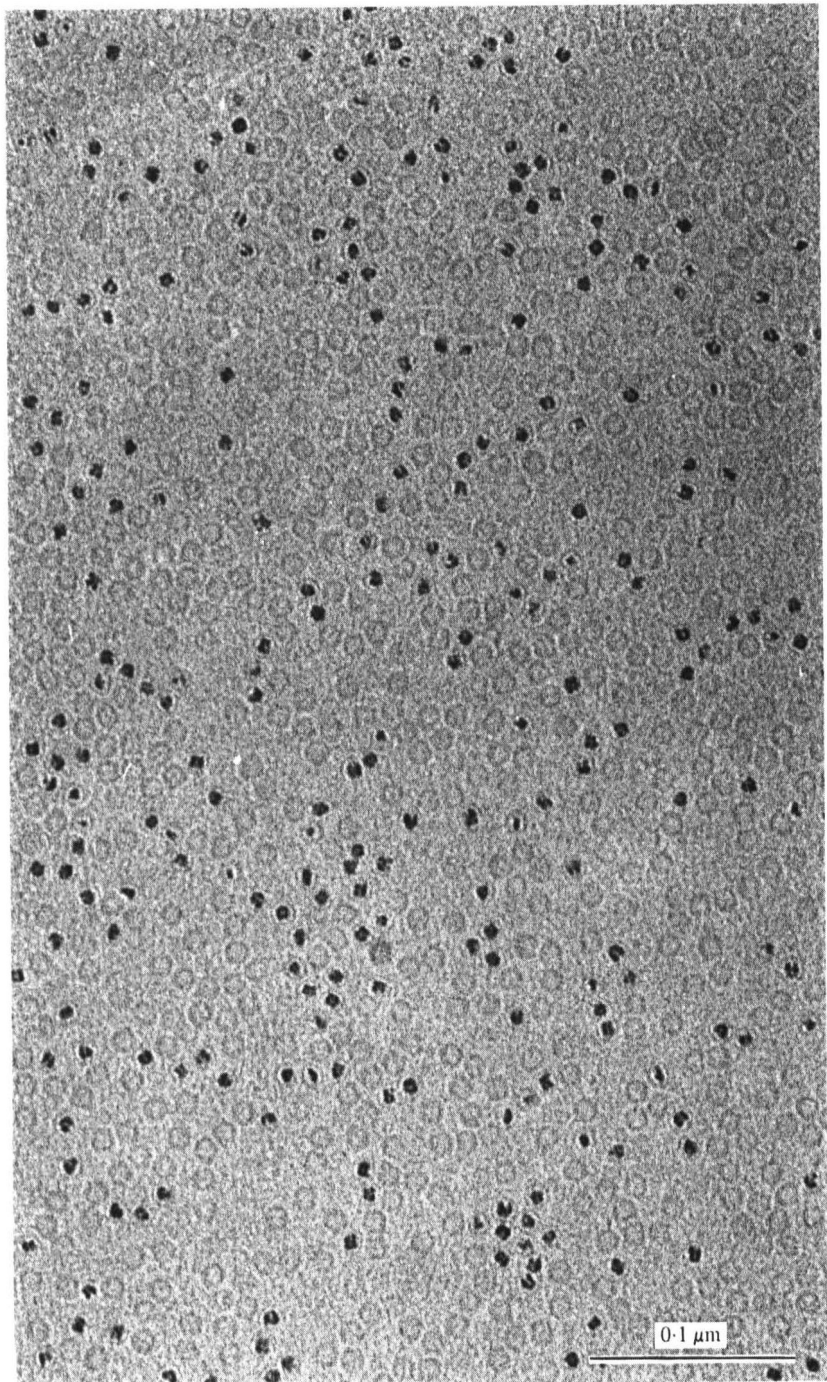


Fig. 54. Ferritin and apoferitin prepared by the perforated-film method. (Material: courtesy W. H. Massover, Newark.)

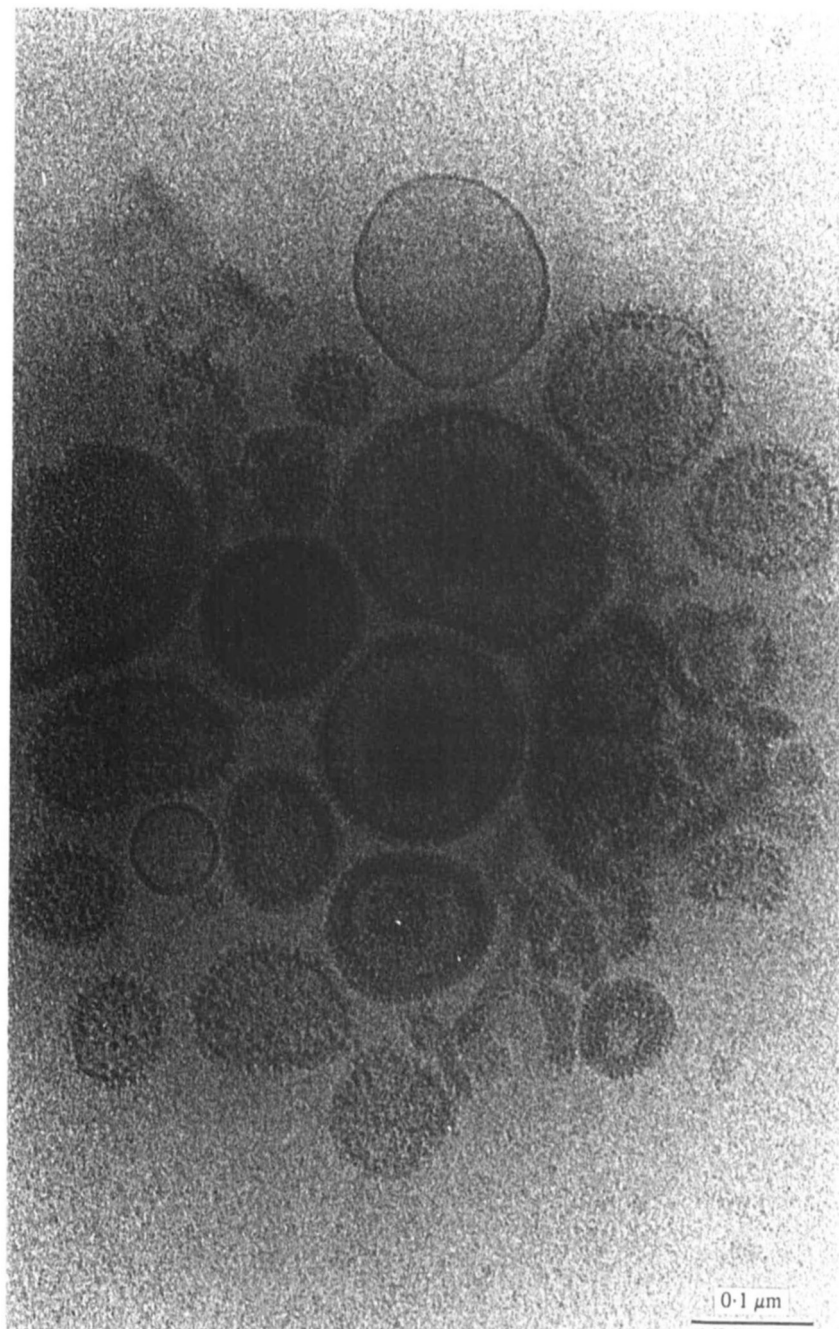


Fig. 55. Virosomes formed by lipid vesicles containing spike proteins of vesicular stomatitis virus (Material: courtesy K. Metsikkö, Heidelberg.)

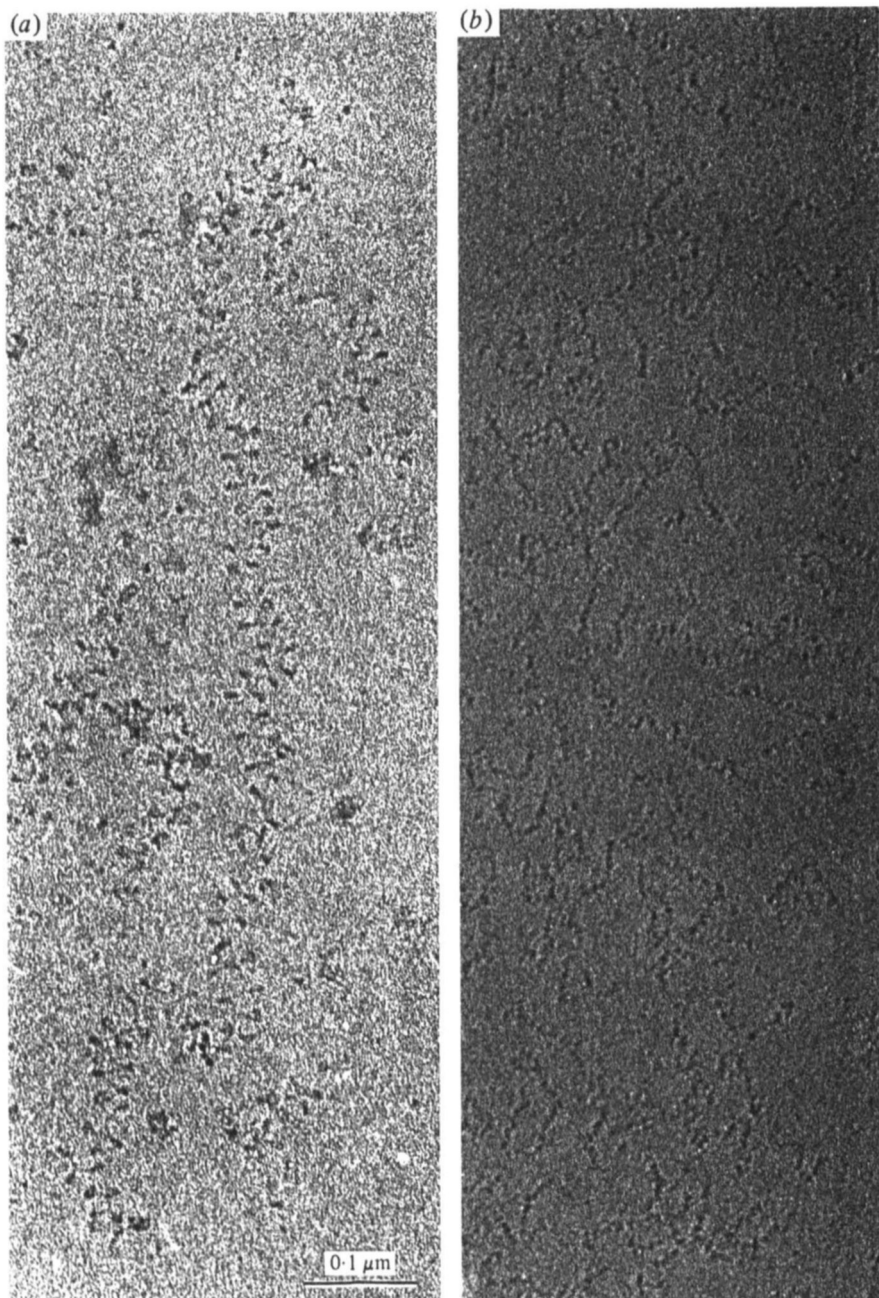


Fig. 56. (a) Chicken erythrocyte chromatin prepared by the perforated-grid method in 10 mM-NaCl. The individual nucleosomes are clearly visible along the zig-zaging filaments. (b) Turnip yellow mosaic virus RNA prepared by the perforated-film method in 125 mM-NaCl. (Material: courtesy J. Witz, Strasbourg.)

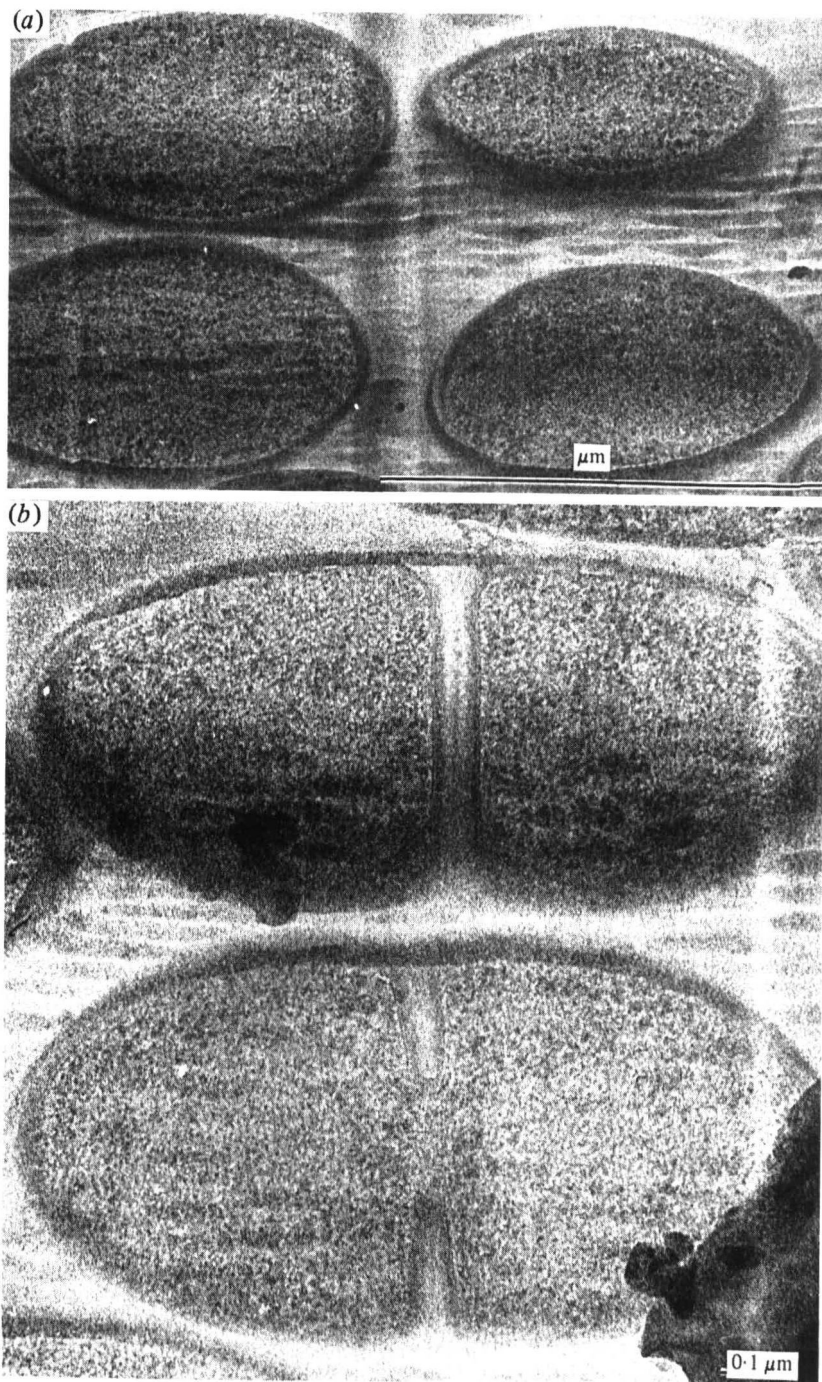


Fig. 57. (a) Unfixed, unstained, vitrified cryosection of a pellet of the Gram-positive bacterium *Staphylococcus aureus*. (b) Dividing bacteria displaying 5.5 nm inner cytoplasmic membrane. (Material: courtesy K. Lickfeld, Essen.)

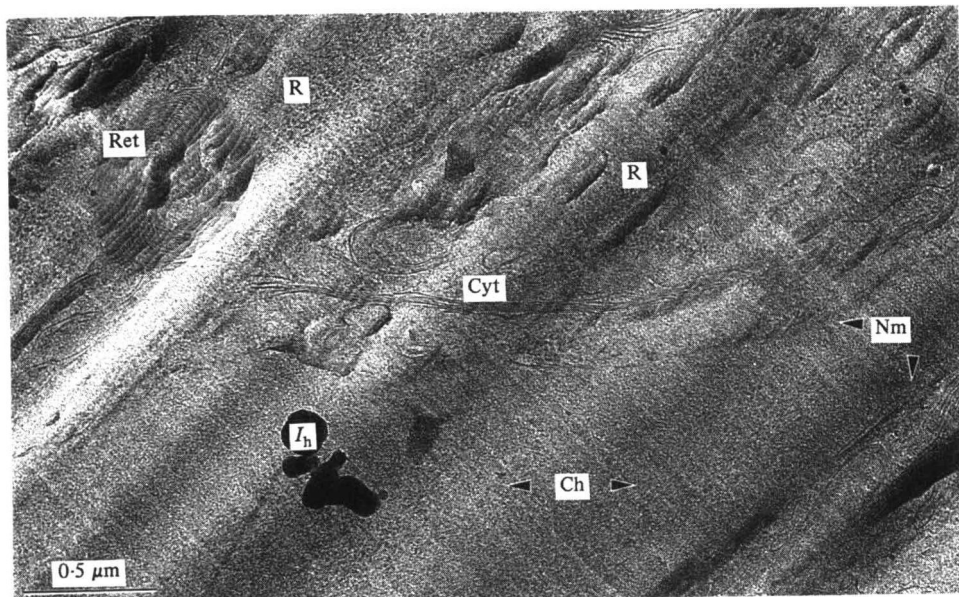


Fig. 58. Unfixed, unstained, vitrified cryosection of culture cells (normal rat kidney). Nm, nuclear membrane; Ch, chromatin; Cyt, cytoskeleton; R, ribosomes; Ret, reticular structure, I_h , hexagonal ice contaminant.

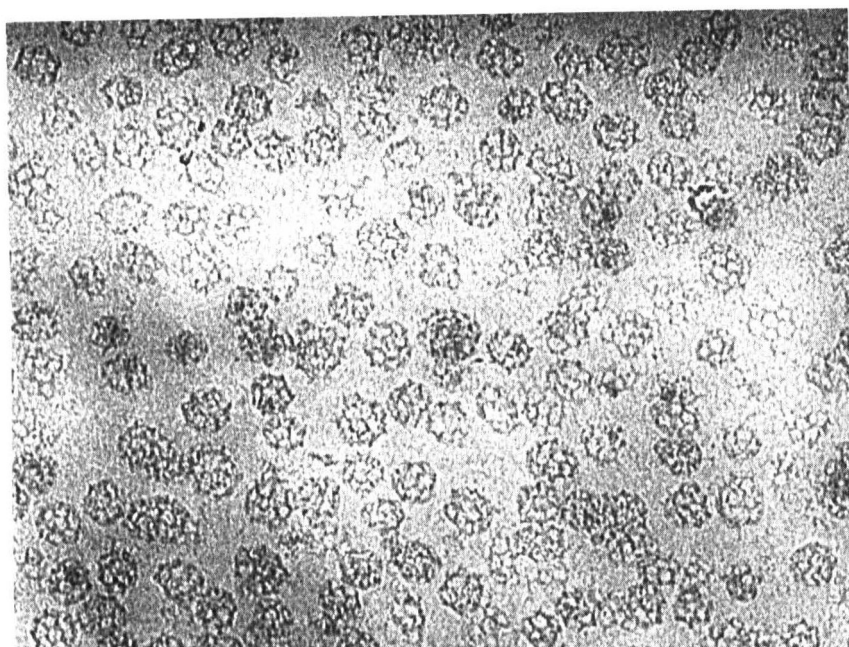


Fig. 59. Purified clathrin cages in vitreous ice. (Courtesy G. Vigers, Boulder, Colorado.)

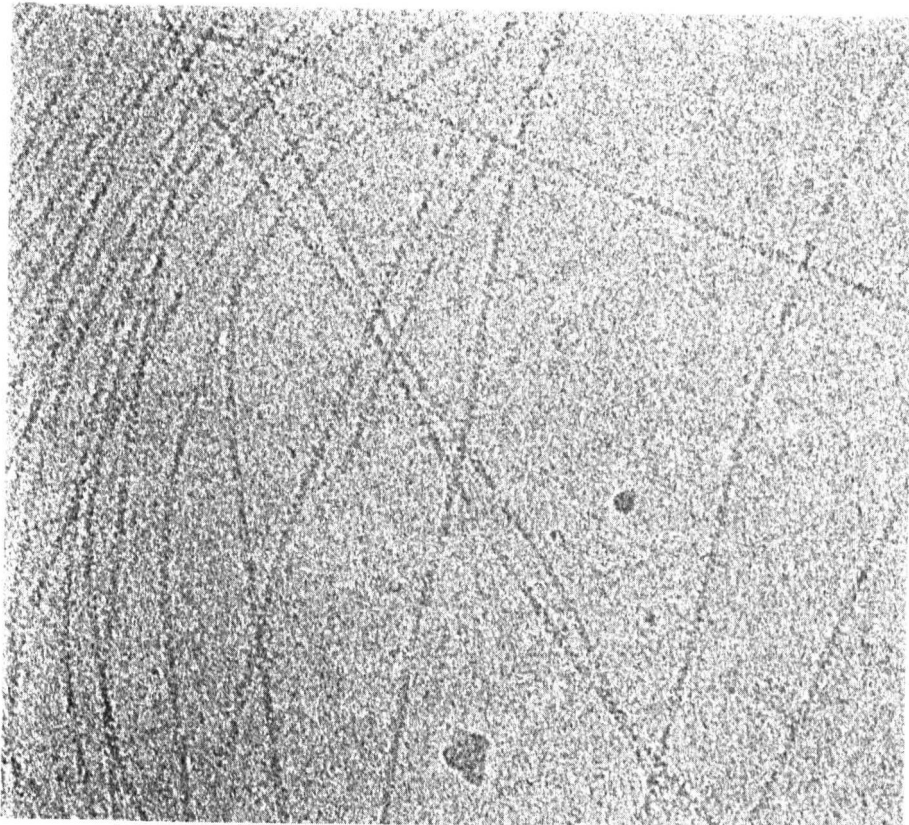


Fig. 6o. Actin filaments in vitreous ice (courtesy R. Milligan, San Diego).

the humid air of the laboratory must be minimized. Covering liquid-nitrogen surfaces and the wearing of a breathing mask may help. The rule that the quality of a transfer is inversely proportional to its duration has been abundantly confirmed by experience. The successful microscopist plans his movements accordingly.

Once the specimen is in the microscope it is best to protect it, as much as possible, from the evaporating water introduced during the transfer. The shield installed on most commercial systems is efficient for this purpose. It should only be open when the water pressure, judged from the contamination speed on the specimen, is negligible.

The specimen drifts and vibrates as long as the temperature of the cryo-specimen holder is not stabilized. This effect can be observed directly at high magnification on the carbon film, after the water layer has been removed by a strong irradiation and, with some experience, the moment when the specimen is ready for recording high-resolution micrographs can be determined.

Low-dose image recording is essential with vitrified specimens and this should be done in such a way as to minimize beam-induced drift of the specimen. For this purpose it is advantageous to focus at a relatively large distance from the recorded area – for example, in an adjacent hole. In most modern electron microscopes, the built-in method for low-dose image recording is not designed for independent and

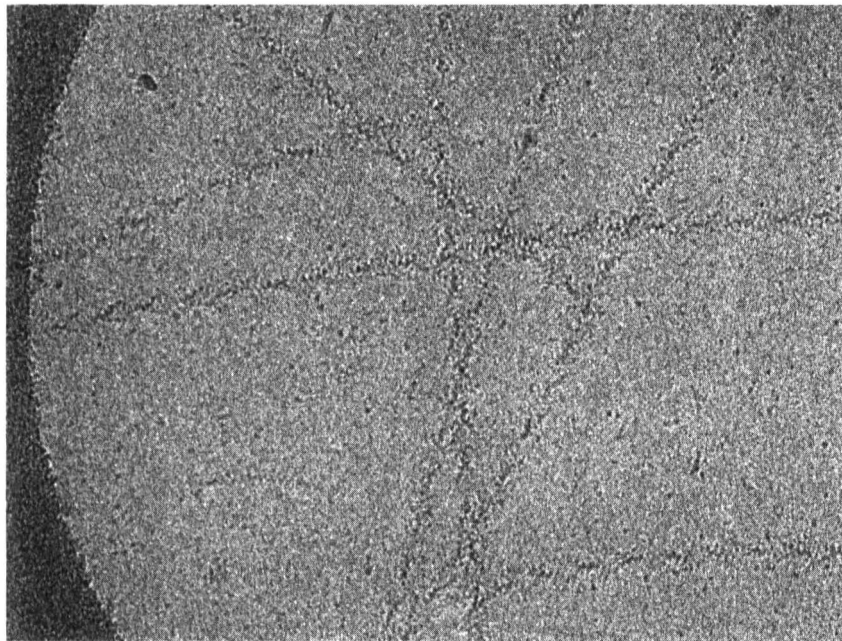


Fig. 61. Actin filaments labelled with S1 myosin molecules, often referred to as 'decorated' actin, embedded in vitreous ice. (Courtesy R. Milligan, San Diego.)

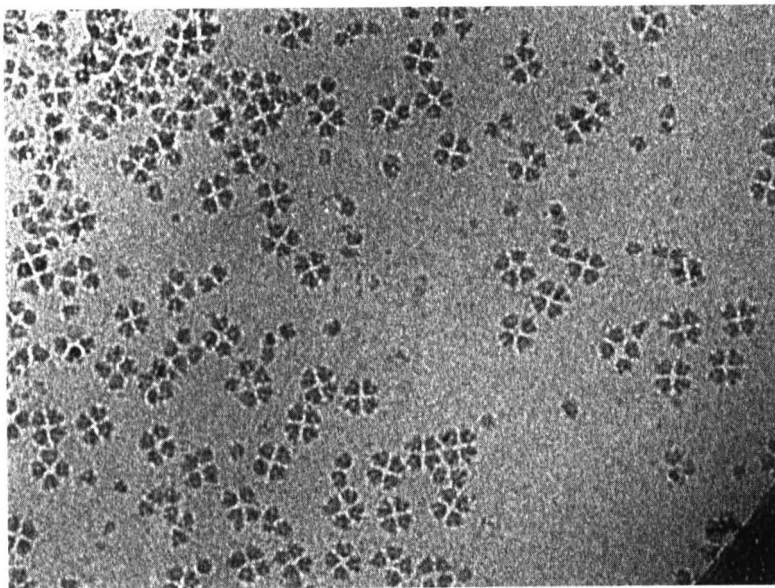


Fig. 62. Eukaryotic ribosome tetramers in vitreous ice. (Courtesy R. Milligan, San Diego.)

rapid selection of both the place to record and the place to focus. The following method was found to be useful by many users:

(a) After the operator has decided the magnification and the exposure time for recording the micrograph, he defines two positions of the condenser setting, R and S. R provides the correct illumination for recording the image at the chosen

magnification and exposure time. In order to minimize the stress induced on the specimen by the electron beam, the total beam current is also chosen for only illuminating the recorded area. In the other setting, S, the beam is spread in such a way as to provide the minimum illumination necessary for localizing the selected region. In general this corresponds to a 20- to 100-fold smaller flux than for recording the image.

(b) The area to be recorded and an adjacent area for focusing are selected at low magnification.

(c) The image is focused on the selected area in such a way that the first maximum of the transfer function corresponds to the expected significant resolution.

(d) Illumination is put on S and the specimen is moved to the area selected for recording.

(e) The beam is blanked for some seconds in order to let the specimen stabilize and the micrograph is recorded without further pre-irradiation.

(f) Another or more micrographs with a defocus two or three times larger can be recorded for a better retrieval of the long-range information of the image.

11. SOME RESULTS

Fig. 47 to 62 are selected illustrations of the possibilities of the method.

12. REFERENCES

- ADRIAN, M., DUBOCHET, J., LEPAULT, J. & McDOWALL, A. W. (1984). Cryo-electron microscopy of viruses. *Nature* **308**, 32–36.
- AMOS, L. A., HENDERSON, R. & UNWIN, P. N. T. (1982). Three-dimensional structure determination by electron microscopy of two-dimensional crystals. *Prog. Biophys. molec. Biol.* **39**, 183–231.
- ANGELL, C. A. (1983). Supercooled water. *A. rev. phys. Chem.* **34**, 593–630.
- ANGELL, C. A. & CHOI, Y. (1986). Crystallization and vitrification in aqueous systems. *J. Microsc.* **141**, 251–261.
- BELLARE, J. R., DAVIS, H. T., SCRIVEN, L. E. & TALMON, Y. (1986). An improved controlled-environment vitrification system (CEVS) for cryofixation of hydrated TEM samples. In *Proc. XIth Int. Conf. Elec. Microsc.*, Kyoto, vol. II (ed. T. Imura, S. Maruse and T. Suzuki), pp. 367–368.
- BERNAL, J. D. & FOWLER, R. H. (1933). A theory of water and ionic solution with particular reference to hydrogen and hydroxyl ions. *J. chem. Phys.* **1**, 515–548.
- BERNHARD, W. (1965). Ultramicrotomie à basse température. *Année biol.* **4**, 5–19.
- BERRY, R. S., RICE, S. A. & ROSS, J. (1980). *Physical Chemistry*. New York: Wiley.
- BORN, M. & WOLF, E. (1975). *Principles of Optics*, 5th ed. Oxford: Pergamon Press.
- BOX, H. C. (1975). Cryoprotection of irradiated specimens. In *Physical Aspects of Electron Microscopy and Microbeam Analysis* (ed. B. M. Siegel and D. R. Beaman), pp. 279–285. New York: Wiley.
- BRACK, C. (1981). DNA electron microscopy. *Crit. Rev. Biochem.* **10**, 113–169.
- BRÜGGLER, P. & MAYER, E. (1980). Complete vitrification in pure liquid water and dilute aqueous solutions. *Nature* **288**, 569–571.

- BURTON, E. F. & OLIVER, W. F. (1935). The crystal structure of ice at low temperature. *Proc. R. Soc. Lond. A* **153**, 166–172.
- CANTOR, C. R. & SCHIMMEL, R. P. (1980). *Biophysical Chemistry*, vol. 1–3. San Francisco: Freeman.
- CHANG, C.-F., OHNO, T. & GLAESER, R. M. (1985). The fatty acid monolayer technique for preparing frozen hydrated specimens. *J. elec. Microsc. Techn.* **2**, 59–65.
- CHANG, J.-J., McDOWALL, A. W., LEPAULT, J., FREEMAN, R., WALTER, C. A. & DUBOCHET, J. (1983). Freezing, sectioning and observation artefacts of frozen hydrated sections for electron microscopy. *J. Microsc.* **132**, 109–123.
- CHIU, W. (1982). High resolution electron microscopy of unstained hydrated protein crystals. In *Electron Microscopy of Proteins*, vol. 2 (ed. J. R. Harris), pp. 233–259. London: Academic Press.
- CHIU, W. (1986). Electron microscopy of frozen, hydrated biological specimens. *A. Rev. Biophys. Chem.* **15**, 237–257.
- CHRISTENSEN, A. K. (1971). Frozen thin sections of fresh tissue for electron microscopy, with a description of pancreas and liver. *J. Cell Biol.* **51**, 772–804.
- CLEGG, J. S. (1982). Alternative views on the role of water in cell function. In *Biophysics of Water* (ed. F. Franks and S. Mathias), pp. 365–383. Chichester: Wiley.
- COSLETT, V. E. (1978). Radiation damage in the high resolution electron microscopy of biological materials: a review. *J. Microsc.* **113**, 113–129.
- CREW, A. V. (1973). Considerations of specimen damage for the transmission electron microscope, conventional versus scanning. *J. molec. Biol.* **80**, 315–325.
- DAVIDSON, D. W. (1973). Clathrate hydrates. In *Water: A Comprehensive Treatise*, vol. 2, (ed. F. Franks), pp. 115–234. New York: Plenum Press.
- DAVY, J. D. & BRANTON, D. (1970). Subliming ice surfaces: freeze-etch electron microscopy. *Science* **163**, 1216–1218.
- DIETRICH, I., FORMANEK, H., FOX, F., KNAPEK, E. & WEYL, R. (1979). Reduction of radiation damage in an electron microscope with superconducting lens system. *Nature* **277**, 380–381.
- DIETRICH, I., FOX, F., HEIDE, H. G., KNAPEK, E. & WEYL, R. (1978). Radiation damage due to knock-on processes on carbon foils cooled to liquid helium temperature. *Ultramicroscopy* **3**, 185–189.
- DOWELL, L. G. & RINFRET, A. P. (1960). Low-temperature forms of ice as studied by X-ray diffraction. *Nature* **188**, 1144–1148.
- DUBOCHET, J. (1975). Carbon loss during irradiation of T4 bacteriophages and *E. coli* bacteria in electron microscopes. *J. Ultrastruct. Res.* **52**, 276–288.
- DUBOCHET, J., ADRIAN, M., LEPAULT, J. & McDOWALL, A. W. (1985). Cryo-electron microscopy of vitrified biological specimens. *Trends in Biochem. Sci.* **10**, 143–146.
- DUBOCHET, J., ADRIAN, M., SCHULTZ, P. & OUDET, P. (1986). Cryo-electron microscopy of vitrified SV40 minichromosomes. The liquid drop model. *EMBO J.* **5**, 519–528.
- DUBOCHET, J., ADRIAN, M., TEIXEIRA, J., KADIYALI, R. K., ALBA, C. M., MACFARLANE, D. R. & ANGELL, C. A. (1984). Glass-forming microemulsions: vitrification of simple liquids and electron microscope probing of droplet packing modes. *J. phys. Chem.* **88**, 6727–6732.
- DUBOCHET, J., ADRIAN, M. & VOGEL, R. H. (1983a). Amorphous solid water obtained by vapour condensation or by liquid cooling: a comparison. *Cryo-Letters* **4**, 233–240.
- DUBOCHET, J., CHANG, J.-J., FREEMAN, R., LEPAULT, J. & McDOWALL, A. W. (1982a). Frozen aqueous suspensions. *Ultramicroscopy* **10**, 55–62.
- DUBOCHET, J., GROOM, M. & MÜLLER, NEUTEBOOM, S. (1982b). The mounting of

- macromolecules for electron microscopy. In *Advances in Optical and Electron Microscopy*, vol. 8 (ed. V. E. Cosslett and R. Barer), pp. 107–135. London: Academic Press.
- DUBOCHET, J. & KELLENBERGER, E. (1972). Selective adsorption of particles to the supporting film and its consequences on particle counts in electron microscopy. *Microscopica Acta* **72**, 119–130.
- DUBOCHET, J. & LEPAULT, J. (1984). Cryo-electron microscopy of vitrified water. *J. Physics* **45**, C7/85–94.
- DUBOCHET, J., LEPAULT, J., FREEMAN, R., BERRIMAN, J. A. & HOMO, J.-CL. (1982c). Electron microscopy of frozen water and aqueous solutions. *J. Microsc.* **128**, 219–237.
- DUBOCHET, J. & McDOWALL, A. W. (1981). Vitrification of pure water for electron microscopy. *J. Microsc.* **124**, RP3–4.
- DUBOCHET, J. & McDOWALL, A. W. (1984a). Frozen hydrated sections. In *Science of Biological Specimen Preparation*, pp. 147–152. Chicago: SEM Inc., AMF O'Hare.
- DUBOCHET, J. & McDOWALL, A. W. (1984b). Cryo-ultramicrotomy: study of ice crystals and freezing damage. In *Proc. 8th Eur. Congr. Elec. Microsc., Budapest* (ed. A. Csanady, P. Röhlich and D. Szabo), vol. 2, pp. 1407–1410. Budapest: Progr. Committee.
- DUBOCHET, J., McDOWALL, A. W., MENGE, B., SCHMID, E. N & LICKFELD, K. G. (1983b). Electron microscopy of frozen-hydrated bacteria. *J. Bact.* **155**, 381–390.
- EISENBERG, D. & CROTHERS, D. (1979). *Physical Chemistry with Applications to the Life Sciences*. Menlo Park, CA.: Benjamin/Cumming.
- EISENBERG, D. & KAUFMANN, W. (1969). *The Structure and Properties of Water*. Oxford University Press.
- ERICKSON, H. P. & KLUG, A. (1971). Measurement and compensation of defocusing and aberrations by Fourier processing of electron micrographs. *Phil. Trans. R. Soc. Lond. B* **261**, 105–118.
- ESCAIG, J. (1982a). New instruments which facilitate rapid freezing at 83 K and 6 K. *J. Microsc.* **126**, 221–229.
- ESCAIG, J. (1982b). Ultra-rapid freezing of cells and cellular material: a review of methods. In *Proc. 10th Int. Congr. Elec. Microsc., Hamburg*, vol. 3, pp. 169–176. Frankfurt: Deutsche Ges. für Elektronenmikroskopie, e.V.
- EUSEMANN, R., ROSE, H. & DUBOCHET, J. (1982). Electron scattering in ice and organic materials. *J. Microsc.* **128**, 239–249.
- FAHY, G. M., MACFARLANE, D. R., ANGELL, C. A. & MERYMAN, H. T. (1984). Vitrification as an approach to cryo-preservation. *Cryobiology* **21**, 407–426.
- FERNANDEZ-MORAN, H. (1960). Low temperature preparation techniques for electron microscopy of biological specimens based on rapid freezing with liquid helium II. *Ann. N. Y. Acad. Sci.* **85**, 689–713.
- FERNANDEZ-MORAN, H. (1966). High-resolution electron microscopy with superconducting lenses at liquid helium temperatures. *Proc. Natn. Acad. Sci. U.S.A.* **56**, 801–808.
- FERNANDEZ-MORAN, H. (1985). Cryo-electron microscopy and ultramicrotomy: Reminiscences and reflections. In *Advances in Electronics and Electron Physics*, supplement 16, pp. 167–223. New York: Academic Press.
- FEYNMAN, R. P., LEIGHTON, R. B. & SANDS, M. (1965). *Lectures on Physics*, vol. I–III. Reading, Massachusetts: Addison-Wesley.

- FINNEY, J. L. (1986). The role of water perturbations in biological process. In *Water and Aqueous Solutions* (ed. G. W. Neilson and J. E. Enderby), pp. 227–244. Bristol: Hilger.
- FRANK, H. S. (1970). The structure of ordinary water. *Science* **169**, 635–641.
- FRANKS, F. (1972–82). *Water: A Comprehensive Treatise*, vol. 1–7 (ed. F. Franks). New York: Plenum Press.
- FRANKS, F. (1982). The properties of aqueous solutions at subzero temperatures. In *Water: A Comprehensive Treatise*, vol. 7 (ed. F. Franks), pp. 215–338. New York: Plenum Press.
- FREDERIK, P. M., BUSING, W. M. & PERSSON, A. (1982). Concerning the nature of the cryosectioning process. *J. Microsc.* **125**, 167–175.
- FREDERIK, P. M., BUSING, W. M. & PERSSON, A. (1984). Surface defects on thin cryosections. In *Scanning Electron Microscopy*, vol. 1, pp. 433–443. Chicago: SEM Inc., AMF O'Hare.
- FREEMAN, R., LEONARD, K. R. & DUBOCHET, J. (1980). The temperature dependence of beam damage to biological samples in the scanning transmission electron microscope (STEM). *Proc. 7th. Eur. Congr. Elec. Microsc., The Haag*, vol. 2 (ed. P. Brederoo and G. Boom), pp. 640–641. Leiden: The 7th. Eur. Congr. Foundation.
- FUJIYOSHI, Y., UYEDA, N., YAMAJISHI, H., MORIKAWA, K., MIZUSAKI, T., AOKI, Y., KIHARA, H. & HARADA, Y. (1986). Biological macromolecules observed with high resolution cryo-electron microscope. In *Proc. XIth Int. Cong. Elec. Microsc., Kyoto*, vol. III (ed. T. Imura, S. Maruse and T. Susuki), pp. 1829–1832. Tokyo: Jap. Soc. Elec. Microsc.
- FUKAMI, A. & ADACHI, K. (1965). A new method of preparation of a self-perforated micro-plastic grid and its application. *J. Elec. Microsc. (Japan)* **14**, 112–118.
- FUKAMI, A., ADACHI, K. & KATOH, M. (1972). Micro grid techniques (continued) and their contribution to specimen preparation techniques for high resolution work. *J. Elec. Microsc. (Japan)* **21**, 99–108.
- FULLER, S. D. (1987). The $T = 4$ envelope of Sindbis virus is organized by interactions with a complementary $T = 3$ capsid. *Cell* **48**, 923–934.
- FULLER, S. D. & ARGOS, P. (1987). Is Sindbis a simple picornavirus with an envelope? *EMBO J.* **26**, 1503–1511.
- GEIGER, A., MAUSBACH, P. & SCHNITKER, J. (1986). Computer simulation study of the hydrogen-bond network in metastable water. In *Water and Aqueous Solutions* (ed. G. W. Neilson and J. E. Enderby), pp. 31–40. Bristol: Adam Hilger.
- DE GENNES, P. G. (1984). Comment s'étaie une goutte. *Pour la Science* **79**, 88–96.
- DE GENNES, P. G. (1985). Wetting: statistics and dynamics. *Rev. mod. Phys. (USA)* **57**, 827–863.
- GHORMLEY, J. A. & HOCHANADEL, C. J. (1971). Amorphous ice: density and reflectivity. *Science* **171**, 62–64.
- GLAESER, R. M. (1971). Limitation to significant information in biological electron microscopy as a result of radiation damage. *J. Ultrastruct. Res.* **36**, 466–482.
- GLAESER, R. M. (1975). Radiation damage and biological electron microscopy. In *Physical Aspects of Electron Microscopy and Microbeam Analysis* (ed. B. M. Siegel and D. R. Bearman), p. 205. New York: Wiley.
- GLAESER, R. M. & TAYLOR, K. A. (1978). Radiation damage relative to transmission electron microscopy of biological specimens at low temperature: a review. *J. Microsc.* **112**, 127–138.

- GRIFFITHS, G., McDOWALL, A. W., BACK, R. & DUBOCHET, J. (1984). On the preparation of cryosections for immunocrytochemistry. *J. Ultrastruct. Res.* **89**, 65–78.
- GRIFFITHS, G., SIMONS, K., WARREN, G. & TOKUYASU, K. T. (1983). Immunoelectron microscopy using thin, frozen sections: application to studies of the intracellular transport of Semliki forest virus spike glycoproteins. *Meth. Enzymol.* **96**, 435–450.
- GUPTA, B. L. & HALL, T. A. (1981). The X-ray microanalysis of frozen-hydrated sections in scanning electron microscopy: an evaluation. *Tissue Cell* **13**, 623–643.
- HAHN, M. (1980). Properties of commercial films for electron microscopy. In *Electron Microscopy and Molecular Dimensions* (ed. W. Baumesiter and W. Vogell), pp. 200–207. Heidelberg: Springer-Verlag.
- HALL, T. A. & GUPTA, B. L. (1974). Beam-induced loss of organic mass under electron microscope conditions. *J. Microsc.* **100**, 177–188.
- HANDLEY, D. A., ALEXANDER, J. T. & CHIEN, S. (1981). The design and use of a simple device for rapid quench-freezing of biological samples. *J. Microsc.* **121**, 273–282.
- v. HARREVELD, A., TRUBATCH, J. & STEINER, J. (1974). Rapid freezing and electron microscopy for the arrest of physiological processes. *J. Microsc.* **100**, 189–198.
- HART, R. K., KASSNER, T. F. & MAURIN, J. K. (1970). Contamination of surfaces during high-energy electron radiation. *Phil. Mag.* **21**, 453–467.
- HAYAT, M. A. (1970). *Principles and Techniques of Electron Microscopy. Biological Applications*, vol. 1. London: Van Nostrand Reinhold.
- HAYWARD, S. B., GRANO, D. A., GLAESER, R. M. & FISHER, K. A. (1978). Molecular orientation of bacteriorhodopsin within the purple membrane of halobacterium halobium. *Proc. natn. Acad. Sci. U.S.A.* **75**, 4320–4324.
- VAN HEEL, M. & FRANK, J. (1981). Use of multivariate statistics in image analysing the images of biological macromolecules. *Ultramicroscopy* **6**, 187–194.
- HEIDE, H. G. (1982a). On the irradiation of organic samples in the vicinity of ice. *Ultramicroscopy* **7**, 299–300.
- HEIDE, H. G. (1982b). Design and operation of cold stages. *Ultramicroscopy* **10**, 125–154.
- HEIDE, H. G. & GRUND, S. (1974). Eine Tiefkühlkette zum Überführen von wasserhaltigen biologischen Objekten im Elektronenmikroskop. *J. Ultrastruct. Res.* **48**, 259–268.
- HEIDE, H. G. & ZEITLER, E. (1985). The physical behaviour of solid water at low temperatures and the embedding of electron microscopical specimens. *Ultramicroscopy* **16**, 151–160.
- HEIDENREICH, R. R. (1964). *Fundamentals of Transmission Electron Microscopy*. New York: Interscience Publ.
- HEUSER, J. E., REESE, T. S., DENNIS, M. J., JAN, Y., JAN, L. & EVANS, L. (1979). Synaptic vesicle exocytosis captured by quick freezing and correlated with quantal transmitter release. *J. Cell Biol.* **81**, 275–300.
- HIROMI, K. (1979). *Kinetics of Fast Enzyme Reactions. Theory and Practice*. Kodansha Scientific Books. New York: Wiley.
- HOBBS, P. V. (1974). *Ice Physics*. Oxford: Clarendon Press.
- HOMO, J.-CL., BOOY, F., LABOUESSE, P., LEPAULT, J. & DUBOCHET, J. (1984). Improved anticontaminator for cryo-electron microscopy with Philips EM 400. *J. Microscopy* **136**, 337–340.
- HUTCHINSON, T. E., BACANER, M., BRODHURST, J. & LILLEY, J. (1974). Electron microscopy of frozen biological tissue. *Rev. scient. Instrum.* **45**, 252–255.

- HUTTERMANN, J. (1982a). Physical mechanisms of electron interaction with organic solids. *Ultramicroscopy*. **10**, 7–14.
- HUTTERMANN, J. (1982b). Solid-state radiation chemistry of DNA and its constituents. *Ultramicroscopy*. **10**, 25–40.
- INTERNATIONAL EXPERIMENTAL STUDY GROUP (1986). Cryoprotection in electron microscopy. *J. Microsc.* **141**, 385–391.
- ISAACSON, M. S. (1977). Specimen damage in the electron microscope. In *Principles and Techniques of Electron Microscopy. Biological Applications*, vol. 7 (ed. M. A. Hayat), pp. 1–78. New York: Van Nostrand Reinhold.
- JAFFE, J. S. & GLAESER, R. M. (1984). Preparation of frozen-hydrated specimens for high resolution electron microscopy. *Ultramicroscopy* **13**, 373–378.
- JAKUBOWSKI, U. (1985). Can heat pipes solve the problems of drift and vibration of cryoholders? *Ultramicroscopy*. **17**, 379–382.
- JENG, T.-W. & CHIU, W. (1984). Quantitative assessment of radiation damage in a thin protein crystal. *J. Microsc.* **136**, 35–44.
- JESIOR, J.-CL. (1987). How to avoid compression. II. The influence of sectioning conditions. *J. Ultrastruct. Res.* (In the Press.)
- JOHARI, G. P. (1977). On the heat capacity, entropy and glass transition of vitreous ice. *Phil. Mag.* **35** (4), 1077–1090.
- KELLENBERGER, E. (1987). The response of biological macromolecules and supramolecular structures to the physics of cryo-specimen preparation. In *Cryotechniques in Biological Electron Microscopy* (ed. R. A. Steinbrecht and K. Zierold, pp. 35–63. Heidelberg: Springer-Verlag).
- KELLENBERGER, E., CARLEMALM, E. & VILLIGER, W. (1986b). Physics of the preparation and observation of specimens that involve cryoprocedure. In *Science of Biological Specimen Preparation* (ed. M. Müller, R. Becker, A. Boyde and J. Wolosewick), pp. 1–20. Chicago: SEM Inc., AMF O'Hare.
- KELLENBERGER, E., HÄNER, M. & WURTZ, M. (1982). The wrapping phenomenon in air-dried and negatively stained preparations. *Ultramicroscopy*. **9**, 139–150.
- KELLENBERGER, E. & KISTLER, J. (1979). The physics of specimen preparation. In *Advances in Structure Research by Diffraction Methods*, vol. viii (ed. W. Hoppe and R. Mason), pp. 49–79. Wiesbaden: Friedr. Vieweg.
- KISTLER, J. & KELLENBERGER, E. (1977). Collapse phenomena in freeze-drying. *J. Ultrastruct. Res.* **59**, 70–75.
- KLEINSCHMIDT, A. K. & ZAHN, R. K. (1959). Über Deoxyribonucleinsäure-Molekülen in Protein-Mischfilmen. *Z. Naturf.* **14b**, 770–779.
- KNAPEK, E. & DUBOCHET, J. (1980). Beam damage to organic crystals is considerably reduced in cryo-electron microscopy. *J. molec. Biol.* **141**, 147–161.
- KOBAYASHI, K. & SAKAOKU, K. (1965). Irradiation changes in organic polymers at various acceleration voltages. *Lab. Investigation* **14**, 1097–1114.
- KÖNIG, H. (1943). Eine kubische Eismodification. *Z. Kristallogr.* **105**, 279–286.
- KOHL, H., ROSE, H. & SCHNABL, H. (1981). Dose-rate effect at low temperatures in FBEM and STEM due to object-heating. *Optik* **58**, 11–24.
- LANGER, J. S. (1980). Growth of ice crystals. *Rev. mod. Phys.* **52**, 1–28.
- LAMVIK, M. K., KOPF, D. A. & ROBERTSON, J. D. (1983). Radiation damage in L-valine at liquid helium temperature. *Nature* **301**, 332–334.
- LEISEGANG, S. (1954). Zur Erwärmung elektronenmikroskopischer Objekte bei kleinem Strahlquerschnitt. In. *Proc. 3rd Int. Conf. Elec. Microsc., London*, pp. 176–188.

- LENZ, S. (1954). Zur Streuung mittelschneller Elektronen in kleinste Winkel. *Z. Naturf.* **9a**, 185–204.
- LEPAULT, J. (1985). Cryo-electron microscopy of helical particles TMV and T4 polyheads. *J. Microsc.* **140**, 73–80.
- LEPAULT, J., BOOY, F. P. & DUBOCHET, J. (1983a). Electron microscopy of frozen biological suspensions. *J. Microsc.* **129**, 89–102.
- LEPAULT, J. & DUBOCHET, J. (1980). Freezing, fracturing and etching artefacts in particulate suspensions. *J. Ultrastruct. Res.* **72**, 223–233.
- LEPAULT, J. & DUBOCHET, J. (1986a). Electron microscopy of frozen hydrated specimens: preparation and characteristics. In *Meth. Enzymol.* **127**, 719–730.
- LEPAULT, J. & DUBOCHET, J. (1986b). Beam damage and frozen-hydrated specimens. In *Proc. XIth Int. Congr. Elec. Microsc., Kyoto*, vol. 1 (ed. T. Imura, S. Maruse and T. Suzuki), pp. 25–28. Tokyo: Japanese Society for Electron Microscopy.
- LEPAULT, J., DUBOCHET, J., BASCHONG, W. & KELLENBERGER, E. (1987). Organization of double-stranded DNA in bacteriophages: a study by cryo-electron microscopy of vitrified samples. *EMBO J.* **6**, 1507–1512.
- LEPAULT, J., DUBOCHET, J., DIETRICH, I., KNAPEK, E. & ZEITLER, E. (1983b). Amendment to: Electron beam damage to organic specimens at liquid helium temperature. *J. molec. Biol.* **163**, 511.
- LEPAULT, J., FREEMAN, R. & DUBOCHET, J. (1983c). Electron beam induced ‘vitrified ice’. *J. Microsc.* **132**, RP3–RP4.
- LEPAULT, J. & LEONARD, K. (1985). Three-dimensional structure of unstained frozen-hydrated extended tails of bacteriophage T4. *J. molec. Biol.* **182**, 431–441.
- LEPAULT, J., PATTUS, F. & MARTIN, N. (1985). Cryo-electron microscopy of artificial biological membranes. *Biochim. biophys. Acta* **820**, 315–318.
- LEPAULT, J. & PITTS, T. (1984). Projected structure of unstained, frozen-hydrated T-layer of *Bacillus brevis*. *EMBO J.* **3**, 101–105.
- LICKFELD, K. G. (1985). Ein Beitrag zur Frage welche Kräfte und Faktoren Dünnschneiden bewirken. *J. Ultrastruct. Res.* **93**, 101–115.
- LUYET, B. J. & GEHENIO, P. M. (1940). *Life and Death at Low Temperatures*. Normandy, Missouri: Biodynamica.
- MACKENZIE, A. P. (1977). Non equilibrium freezing behaviour of aqueous systems. *Phil. Trans. R. Soc. Lond. B* **278**, 167–189.
- MADDOX, J. (1983). Snowflakes are far from simple. *Nature* **306**, 13.
- MANDELKOW, E.-M., RAPP, R. & MANDELKOW, E. (1986). Microtubule structure studied by quick freezing: cryo-electron microscopy and freeze fracture. *J. Microsc.* **141**, 361–373.
- MAYER, E. (1985). Vitrification of pure liquid water. *J. Microsc.* **140**, 3–15.
- MAYER, E. & BRÜGGLER, P. (1982). Vitrification of pure liquid water by high pressure jet freezing. *Nature* **298**, 715–718.
- MAYER, E. & BRÜGGLER, P. (1983). Devitrification of glassy water. Evidence for a discontinuity of states. *J. phys. Chem.* **87**, 4744–4749.
- MAYER, E. & HALLBRUCKER, A. (1987). Cubic ice from liquid water. *Nature* **325**, 601–602.
- MAZUR, P. (1970). Cryobiology: the freezing of biological systems. *Science* **168**, 939–949.
- MAZUR, P. (1984). Freezing of living cells: Mechanisms and implications. *Am. J. Physiol.* **247**, C125–C142.

- McDOWALL, A. W., CHANG, J.-J., FREEMAN, R., LEPAULT, J., WALTER, C. A. & DUBOCHET, J. (1983). Electron microscopy of frozen hydrated sections of vitreous ice and vitrified biological samples. *J. Microsc.* **131**, 1-9.
- McDOWALL, A. W., HOFMANN, W., LEPAULT, J., ADRIAN, M. & DUBOCHET, J. (1984). Cryo-electron microscopy of vitrified insect flight muscle. *J. molec. Biol.* **178**, 105-111.
- McDOWALL, A. W., SMITH, J. M. & DUBOCHET, J. (1986). Cryo-electron microscopy of vitrified chromosomes *in situ*. *EMBO J.* **5**, 1395-1402.
- MENCO, B. P. M. (1986). A survey of ultra-rapid cryofixation methods with particular emphasis on applications to freeze-fracturing, freeze-etching, and freeze-substitution. *J. Elec. Microsc. Techn.* **4**, 177-240.
- MILLIGAN, R. & FLICKER, J. (1987). *J. Cell Biol.* **105**, 29-39.
- MISHIMA, O., CALVERT, L. D. & WHALLEY, E. (1984). 'Melting ice' I at 77 K and 10 Kbar: a new method of making amorphous solids. *Nature* **310**, 393-395.
- MOOR, H. (1987). Theory and practice of high pressure freezing. In *Cryotechniques in Biological Electron Microscopy* (ed. A. Steinbrecht and K. Zierold). Heidelberg: Springer Verlag, (in the Press).
- MÜLLER, M., MEISTER, N. & MOOR, H. (1980). Freezing in a propane jet and its application in freeze-fracturing. *Mikroskopie (Vienna)* **36**, 129-140.
- MÜLLER, M. & MOOR, H. (1984). Cryofixation of thick specimens by high pressure freezing. In *Science of Biological Specimen Preparation*, vol. 2 (ed. J.-P. Revel, T. Barnard and G. H. Haggis), pp. 131-138. Chicago: SEM Inc., AMF O'Hare.
- NARTEN, A. H. & LEVY, H. A. (1969). Observed diffraction pattern and proposed models of liquid water. *Science* **165**, 447-454.
- NEILSON, G. W. & ENDERBY, J. E. (eds.) (1986). *Water and Aqueous Solutions*. Bristol & Boston: A. Hilger.
- NITTMANN, J. & STANLEY, H. E. (1986). Tip splitting without interfacial tension and dendritic growth patterns arising from molecular anisotropy. *Nature* **321**, 663-668.
- PARSEGIAN, V. A. (1975). Long range van der Waals forces. In *Physical Chemistry: Enriching Topics from Colloid and Surface Science* (ed. H. V. Olphen & K. J. Mysels), pp. 27-72. Série IUPAC.
- PARSONS, D. F. (1974). Structure of wet specimens in electron microscopy. *Science* **186**, 407-414.
- PAULING, L. (1970). *General Chemistry*, 3rd ed. San Francisco: Freeman.
- PLATTNER, H. & BACHMANN, L. (1982). Cryofixation: A tool in biological ultrastructural research. *Int. Rev. Cytol.* **79**, 237-304.
- PLATTNER, H. & KNOLL, G. (1984). Cryofixation of biological materials for electron microscopy by the methods of spray-, sandwich-, cryogen-jet- and sandwich-cryogen-jet-freezing: A comparison of techniques. In *Science of Biological Specimen Preparation*, vol. 2 (ed. J.-P. Revel, T. Barnard and G. H. Haggis), pp. 139-146. Chicago: SEM Inc., AMF O'Hare.
- POLGE, C., SMITH, A. U. & PARKES, A. S. (1949). Revival of spermatozoa after vitrification and dehydration at low temperatures. *Nature* **164**, 666-667.
- POLIAN, A. & GRIMSDITCH, M. (1984). New high pressure phase of H₂O: Ice X. *Phys. Rev. Lett.* **52**, 1312-1314.
- RACHEL, R., JAKUBOWSKI, U., TIETZ, H., HEGERL, R. & BAUMEISTER, W. (1986). Projected structure of the surface protein of deinococcus radiodurans determined to 8 Å resolution by cryomicroscopy. *Ultramicroscopy*, **20**, 305-316.

- RAHMAN, A., & STILLINGER, F. H. (1971). Molecular dynamics study of liquid water. *J. chem. Phys.* **55**, 3336–3359.
- RASMUSSEN, D. H. (1982). Ice formation in aqueous systems. *J. Microsc.* **128**, 167–174.
- RASMUSSEN, D. H. & MACKENZIE, A. P. (1973). Clustering in supercooled water. *J. chem. Phys.* **59**, 5003–5013.
- REIMER, L. (1975). Review of the radiation damage problem of organic specimens in electron microscopy. In *Physical Aspects of Electron Microscopy and Microbeam Analysis* (ed. B. M. Siegel and D. R. Beaman), pp. 231–245. New York: Wiley.
- REIMER, L. (1984). *Electron microscopy*. Heidelberg: Springer Verlag.
- RIEHLER, U. (1968). Schnellgefrieren organischer Präparate für die Elektronen-Mikroskopie. *Chemie-Ing. Techn.* **40**, 213–218.
- RIEHLER, U. & HOCHLI, M. (1973). The theory and technique of high pressure freezing. In *Freeze-Etching Techniques and Applications* (ed. E. L. Benedetti and P. Farvard), pp. 31–61. Paris: Société Française de Microscopie Electronique.
- ROBARDS, A. W. & SLEYTR, U. B. (1985). *Low Temperature Methods in Biological Electron Microscopy*. New York: Elsevier.
- ROBERTS, I. M. (1975). Tungsten coating – a method of improving glass microtome knives for cutting ultrathin sections. *J. Microsc.* **103**, 113–119.
- SANDER, C. M. (1986). Fractal growth processes. *Nature* **322**, 789–793.
- SAXTON, W. O. (1978). *Computer Techniques for Image Processing in Electron Microscopy*. Academic Press.
- SCEATS, M. G. & RICE, S. A. (1982). Amorphous solid water and its relationship to liquid water: A random network model for water. In *Water: A Comprehensive Treatise* (ed. F. Franks), pp. 83–214. New York: Plenum Press.
- SCHÄFER, L., YATES, A. C., BONHAM, R. A. (1971). New values for the partial wave electron scattering factor for the elements $1 \leq Z \leq 57$ and $72 \leq Z \leq 90$ for incident electron energies of 10, 40, 70 and 100 keV. *J. chem. Phys.* **55**, 3055–3056.
- SCHERZER, O. (1949). The theoretical resolution limit of the electron microscope. *J. appl. Phys.* **20**, 20–29.
- SIEGEL, G. (1972). The influence of very low temperature on the radiation damage of organic crystals irradiated by 100 kV electrons. *Z. Naturf. A* **27**, 325–332.
- SITTE, H., EDELMANN, L. & NEUMANN, K. (1987). Cryofixation without pretreatment at ambient pressure. In *Cryotechniques in Biological Electron Microscopy* (ed. R. A. Steinbrecht and K. Zierold), pp. 87–113. Heidelberg: Springer Verlag.
- SITTE, H. & NEUMANN, K. (1983). Beitrag 1. 1. 2. In *Methodensammlung der Elektronenmikroskopie* (ed. G. Schimmel and W. Vogell), pp. 1–248. Stuttgart: Wiss. Verlag GmbH.
- SITTE, H., NEUMANN, K., HÄSSIG, H., KLEBER, H. & KAPPL, G. (1980). FC4 cryochamber for Reichert OmU4-ultramicrotome Ultracut. In *Proc. 7th Eur. Congr. Elec. Microsc., The Hague*, vol. 2 (ed. P. Brederoo and G. Boom), pp. 540–541. Leiden: Eur. Congr. Fundation.
- SLEYTR, U. B. & ROBARDS, A. W. (1977). Plastic deformation during freezing-cleavage: a review. *J. Microsc.* **110**, 1–25.
- STANLEY, H. E. & TEIXEIRA, J. (1980). Interpretation of the unusual behaviour of H_2O and D_2O at low temperatures: tests of a percolation model. *J. chem. Phys.* **73**, 3404–3422.
- STEWART, M. & VIGERS, G. (1986). Electron microscopy of frozen-hydrated biological material. *Nature* **319**, 631–636.

- STILLINGER, F. H. (1980). Water revisited. *Science* **309**, 451–457.
- STILLINGER F. H. & WEBER, T. A. (1984). Packing structures and transitions in liquids and solids. *Science* **225**, 983–989.
- SYMONS, M. C. R. (1982a). Chemical aspects of electron beam interactions in the solid state. *Ultramicroscopy* **10**, 15–24.
- SYMONS, M. C. R. (1982b). The pre knock-on concept. *Ultramicroscopy* **10**, 41–44.
- TALMON, Y. (1982). Thermal and radiation damage to frozen hydrated specimens. *J. Microsc.* **125**, 227–237.
- TALMON, Y. (1984). Radiation damage to organic inclusions. *Ultramicroscopy* **14**, 305–316.
- TALMON, Y., ADRIAN, M. & DUBOCHET, J. (1986). Electron beam damage to organic inclusions in vitreous, cubic and hexagonal ice. *J. Microsc.* **141**, 375–384.
- TALMON, Y., DAVIS, H. T., SCRIVEN, L. E. & THOMAS, E. L. (1979). Mass loss and etching of frozen hydrated specimens. *J. Microsc.* **117**, 321–332.
- TALMON, Y. & THOMAS, E. L. (1977a). Beam heating of a moderately thick cold stage specimen in the SEM/STEM. *J. Microsc.* **111**, 151–164.
- TALMON, Y. & THOMAS, E. L. (1977b). Temperature rise and sublimation of water from this frozen hydrated specimens in cold stage microscopy. *Scanning Elec. Microsc.* **1**, 265–272.
- TALMON, Y. & THOMAS, E. L. (1978). Electron beam heating temperature profiles in moderately thick cold stage STEM/SEM specimens. *J. Microsc.* **113**, 69–75.
- TALMON, Y. & THOMAS, E. L. (1979). Open system microthermometry – a technique for the measurement of local specimen temperature in the electron microscope. *J. Mater. Sci.* **14**, 1647–1650.
- TANFORD, C. (1961). *Physical Chemistry of Macromolecules*. New York: Wiley.
- TATLOCK, G. J. (1982). Solid gases. *Ultramicroscopy* **10**, 87–96.
- TAYLOR, K. A. (1978). Structure determination of frozen, hydrated, crystalline biological specimens. *J. Microsc.* **112**, 15–125.
- TAYLOR, K. A. & GLAESER, R. M. (1974). Electron diffraction of frozen, hydrated protein crystals. *Science* **106**, 1036–37.
- TAYLOR, K. A. & GLAESER, R. M. (1976). Electron microscopy of frozen hydrated biological specimens. *J. Ultrastruct. Res.* **55**, 448–456.
- TAYLOR, K. J., CHANZY, H. & MARCHESSAULT, R. H. (1975). Electron diffraction for hydrated crystalline biopolymers: Nigeran. *J. molec. Biol.* **92**, 165–167.
- TEIXEIRA, J., STANLEY, E., BOTTINGA, Y. & RICHET, P. (1983). Application of a percolation model to supercooled liquids with a tetrahedral structure. *Bull. Minéral.* **106**, 99–105.
- THORNBURY, W. & MENGERS, P. E. (1957). An analysis of frozen section techniques. I. Sectioning of fresh-frozen tissues. *J. Histochem. Cytochem.* **5**, 47–52.
- TOKUYASU, K. T. (1973). A technique for ultracryotomy of cell suspensions and tissues. *J. Cell Biol.* **57**, 551–565.
- TOKUYASU, K. T. (1980). Immunochemistry of ultrathin frozen sections. *Histochem. J.* **12**, 381–403.
- TOKUYASU, K. T. & OKAMURA, S. (1959). A new method for making glass knives for thin sectioning. *J. Biophys. Biochem. Cytol.* **6**, 305–308.
- TRINICK, J., COOPER, J., SEYMOUR, J. & EGELMAN, E. H. (1986). Cryo-electron microscopy and three-dimensional reconstruction of actin filaments. *J. Microsc.* **141**, 349–360.

- TYPKE, D. & RADERMACHER, M. (1982). Determination of the phase of complex atomic scattering amplitudes from light-optical diffractograms of electron microscope images. *Ultramicroscopy* **9**, 131–138.
- UNWIN, P. N. T. (1972). Electron microscopy of biological specimens by means of an electrostatic phase plate. *Proc. R. Soc. London A* **329**, 327–359.
- UNWIN, P. N. T. (1974). Electron microscopy of the stacked dish aggregate of Tobacco Mosaic Virus protein. II. The influence of electron irradiation on the stain distribution. *J. molec. Biol.* **87**, 657–670.
- UNWIN, P. N. T. & HENDERSON, R. (1975). Molecular structure determination by electron microscopy of unstained crystalline specimens. *J. molec. Biol.* **94**, 425–440.
- UNWIN, P. N. T. & MUGURUMA, J. (1971). Transmission electron microscopy of ice. *J. appl. Phys.* **42**, 3640–3641.
- UNWIN, P. N. T. & MUGURUMA, J. (1972). Electron microscope observations on the defect structure of ice. *Physica status solidi (a)* **14**, 207–216.
- VALENTINE, R. C. (1966). Response of photographic materials to electrons. In *Advances in Optical and Electron Microscopy*, vol. 1 (ed. R. Barer and V. E. Cosslett), pp. 180–202. London: Academic Press.
- VIGERS, G. P. A., CROWTHER, R. A. & PEARSE, B. M. F. (1986a). Three-dimensional structure of clathrin cages in ice. *EMBO J.* **5**, 529–534.
- VIGERS, G. P. A., CROWTHER, R. A. & PEARSE, B. M. F. (1986b). Location of the 100kD–50kD accessory proteins in clathrin coats. *EMBO J.* **5**, 2079–2085.
- VOGEL, R. H., PROVENCHER, S. W., VON BONSDORFF, C.-H., ADRIAN, M. & DUBOCHET, J. (1986). Envelope structure of Semliki forest virus reconstructed from cryo-electron micrographs. *Nature* **320**, 533–535.
- WADE, R. H. (1984). The temperature dependence of radiation damage in organic and biological material. *Ultramicroscopy* **14**, 265–270.
- WALL, J., BITTNER, J. W. & HAINFELD, J. (1977). Contamination at low temperature. In *Proc. 35th Ann. EMSA Meeting, Boston*, pp. 558–559.
- WALL, J., ISAACSON, M. & LANGMORE, J. (1974). The collection of scattered electrons in dark-field electron microscopy. II. Inelastic scattering. *Optik* **39**, 359–374.
- WILSON, D. (1979). *Supercold: An Introduction to Low Temperature Technology*, London & Boston: Faber & Faber.
- ZIEROLD K. (1982). Preparation of biological cryosections for analytical electron microscopy. *Ultramicroscopy* **10**, 45–54.
- ZIEROLD, K. (1984). The morphology of ultrathin cryosections. *Ultramicroscopy* **14**, 201–209.
- ZIEROLD, K. (1987). Cryoultramicrotomy. In *Cryotechniques in Biological Electron Microscopy* (ed. A. Steinbrecht and K. Zierold, pp. 132–148). Heidelberg: Springer Verlag.